

AD-A047 958

DEFENSE COMMUNICATIONS AGENCY ARLINGTON VA  
DETERMINATION OF EFFECTIVE IONOSPHERIC ELECTRON DENSITY PROFILE--ETC(U)  
JAN 76

F/G 17/2.1

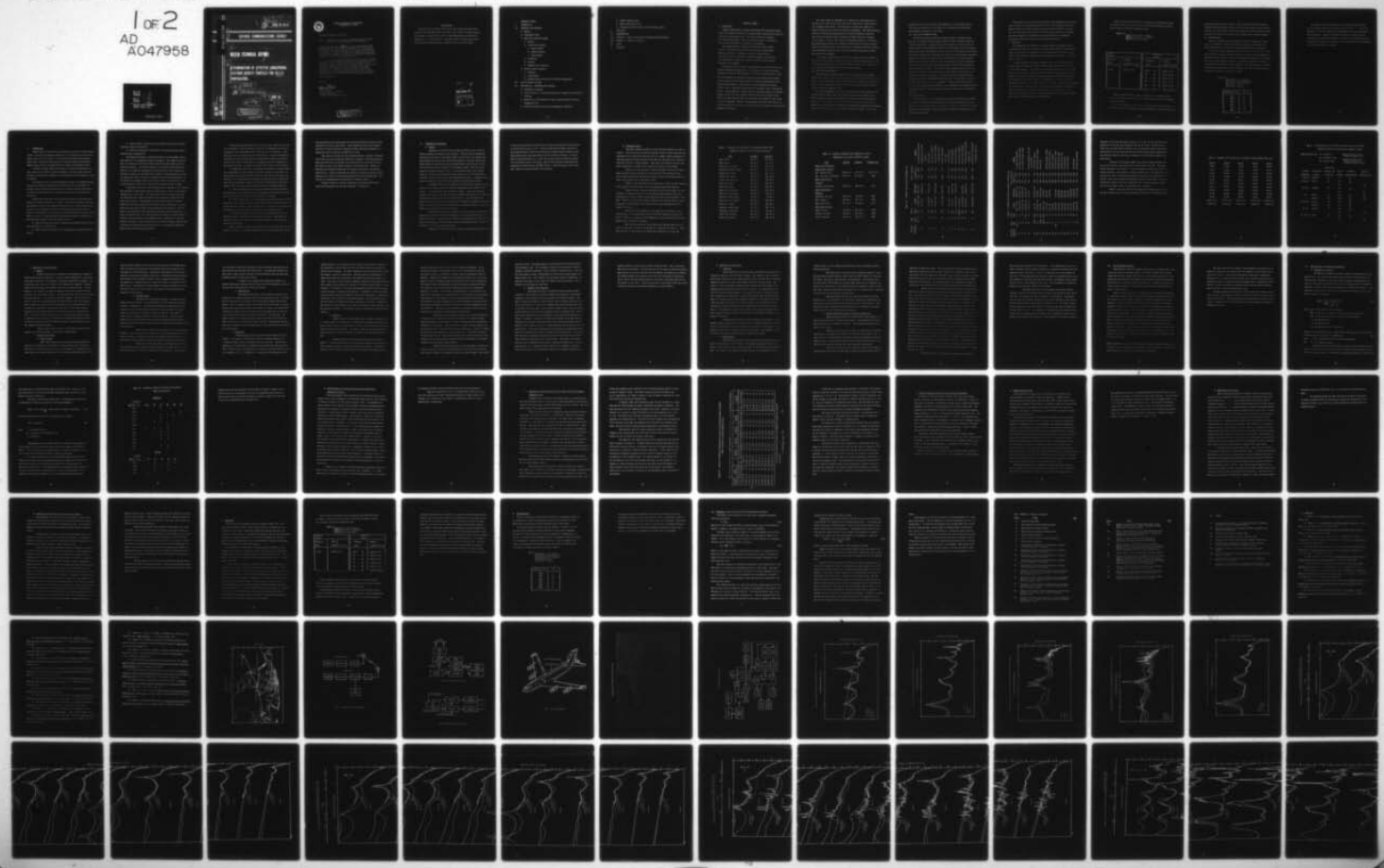
UNCLASSIFIED

1 OF 2  
AD  
A047958

DCA-C650-TP-76-4

SBIE-AD-E100 008

NL



AD No.

DDC FILE COPY

AD A047958

AD-E 100 008

(14) DCA-

(2) C650-TP-76-4



## DEFENSE COMMUNICATIONS AGENCY

### MEECN TECHNICAL REPORT.

DETERMINATION OF EFFECTIVE IONOSPHERIC  
ELECTRON DENSITY PROFILES FOR VLF/LF  
PROPAGATION.

(18) FBI E

(19) AD-E 100 008

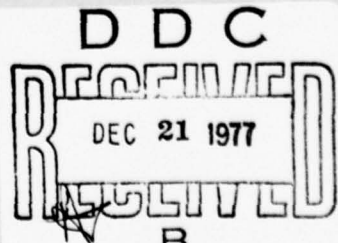
(11)

1 JAN 76

(12) 118 p.

DISTRIBUTION STATEMENT A

Approved for public release;  
Distribution Unlimited



107150



DEFENSE COMMUNICATIONS AGENCY  
WASHINGTON, D. C. 20305

TECHNICAL PUBLICATION C650 -TP-76-4

TITLE: Determination of Effective Ionospheric Electron Density Profiles for VLF/LF Propagation at Midlatitudes

ABSTRACT: This document is <sup>one</sup> another of a series of reports issued by the DCA/MEECN System Engineer which are directed at definitive prediction of the time availability of VLF/LF radio system included in the MEECN. The studies described in this report are critical to VLF/LF system performance. The Tri-Service Propagation Program was established by the MEECN System Engineer to improve the accuracy and reliability of VLF/LF link integrity analyses.

This report presents experimental data derived from field strengths of VLF/LF signals between 9 and 56 kHz measured on several mid-latitude paths. Comparisons between experimental data and theoretical predictions are shown for several flights, both in daytime and in nighttime, over the path from Hawaii to southern California. The comparisons show that an essentially constant exponential electron density profile describes the data for all the frequencies in the above range for daytime; whereas at night, the best fit exponential profile gradient increases with frequency.

FOR THE DIRECTOR:

OFFICIAL

*Warren G. Reed*

WARREN G. REED  
Deputy Director for Systems  
Systems Directorate  
Command Control Technical Center

DISTRIBUTION STATEMENT A

Approved for public release;  
Distribution Unlimited

#### ACKNOWLEDGMENT

The VLF/LF data described in this report were recorded for DCA by NELC, primarily aboard the RADC KC-135 aircraft, as part of the Tri-Service Propagation Program. This particular series of data measurements are reported and analyzed by D. G. Morfitt of NELC. The author wishes to express appreciation for assistance provided by the participants of the Tri-Service Program.

MISSION for	
1.3	White Section <input checked="" type="checkbox"/>
1.3	Dark Section <input type="checkbox"/>
2.0 INCHES	
3.0 INCHES	
4.0 INCHES	
5.0 INCHES	
6.0 INCHES	
7.0 INCHES	
8.0 INCHES	
9.0 INCHES	
10.0 INCHES	
11.0 INCHES	
12.0 INCHES	
13.0 INCHES	
14.0 INCHES	
15.0 INCHES	
16.0 INCHES	
17.0 INCHES	
18.0 INCHES	
19.0 INCHES	
20.0 INCHES	
21.0 INCHES	
22.0 INCHES	
23.0 INCHES	
24.0 INCHES	
25.0 INCHES	
26.0 INCHES	
27.0 INCHES	
28.0 INCHES	
29.0 INCHES	
30.0 INCHES	
31.0 INCHES	
32.0 INCHES	
33.0 INCHES	
34.0 INCHES	
35.0 INCHES	
36.0 INCHES	
37.0 INCHES	
38.0 INCHES	
39.0 INCHES	
40.0 INCHES	
41.0 INCHES	
42.0 INCHES	
43.0 INCHES	
44.0 INCHES	
45.0 INCHES	
46.0 INCHES	
47.0 INCHES	
48.0 INCHES	
49.0 INCHES	
50.0 INCHES	
51.0 INCHES	
52.0 INCHES	
53.0 INCHES	
54.0 INCHES	
55.0 INCHES	
56.0 INCHES	
57.0 INCHES	
58.0 INCHES	
59.0 INCHES	
60.0 INCHES	
61.0 INCHES	
62.0 INCHES	
63.0 INCHES	
64.0 INCHES	
65.0 INCHES	
66.0 INCHES	
67.0 INCHES	
68.0 INCHES	
69.0 INCHES	
70.0 INCHES	
71.0 INCHES	
72.0 INCHES	
73.0 INCHES	
74.0 INCHES	
75.0 INCHES	
76.0 INCHES	
77.0 INCHES	
78.0 INCHES	
79.0 INCHES	
80.0 INCHES	
81.0 INCHES	
82.0 INCHES	
83.0 INCHES	
84.0 INCHES	
85.0 INCHES	
86.0 INCHES	
87.0 INCHES	
88.0 INCHES	
89.0 INCHES	
90.0 INCHES	
91.0 INCHES	
92.0 INCHES	
93.0 INCHES	
94.0 INCHES	
95.0 INCHES	
96.0 INCHES	
97.0 INCHES	
98.0 INCHES	
99.0 INCHES	
100.0 INCHES	
101.0 INCHES	
102.0 INCHES	
103.0 INCHES	
104.0 INCHES	
105.0 INCHES	
106.0 INCHES	
107.0 INCHES	
108.0 INCHES	
109.0 INCHES	
110.0 INCHES	
111.0 INCHES	
112.0 INCHES	
113.0 INCHES	
114.0 INCHES	
115.0 INCHES	
116.0 INCHES	
117.0 INCHES	
118.0 INCHES	
119.0 INCHES	
120.0 INCHES	
121.0 INCHES	
122.0 INCHES	
123.0 INCHES	
124.0 INCHES	
125.0 INCHES	
126.0 INCHES	
127.0 INCHES	
128.0 INCHES	
129.0 INCHES	
130.0 INCHES	
131.0 INCHES	
132.0 INCHES	
133.0 INCHES	
134.0 INCHES	
135.0 INCHES	
136.0 INCHES	
137.0 INCHES	
138.0 INCHES	
139.0 INCHES	
140.0 INCHES	
141.0 INCHES	
142.0 INCHES	
143.0 INCHES	
144.0 INCHES	
145.0 INCHES	
146.0 INCHES	
147.0 INCHES	
148.0 INCHES	
149.0 INCHES	
150.0 INCHES	
151.0 INCHES	
152.0 INCHES	
153.0 INCHES	
154.0 INCHES	
155.0 INCHES	
156.0 INCHES	
157.0 INCHES	
158.0 INCHES	
159.0 INCHES	
160.0 INCHES	
161.0 INCHES	
162.0 INCHES	
163.0 INCHES	
164.0 INCHES	
165.0 INCHES	
166.0 INCHES	
167.0 INCHES	
168.0 INCHES	
169.0 INCHES	
170.0 INCHES	
171.0 INCHES	
172.0 INCHES	
173.0 INCHES	
174.0 INCHES	
175.0 INCHES	
176.0 INCHES	
177.0 INCHES	
178.0 INCHES	
179.0 INCHES	
180.0 INCHES	
181.0 INCHES	
182.0 INCHES	
183.0 INCHES	
184.0 INCHES	
185.0 INCHES	
186.0 INCHES	
187.0 INCHES	
188.0 INCHES	
189.0 INCHES	
190.0 INCHES	
191.0 INCHES	
192.0 INCHES	
193.0 INCHES	
194.0 INCHES	
195.0 INCHES	
196.0 INCHES	
197.0 INCHES	
198.0 INCHES	
199.0 INCHES	
200.0 INCHES	
201.0 INCHES	
202.0 INCHES	
203.0 INCHES	
204.0 INCHES	
205.0 INCHES	
206.0 INCHES	
207.0 INCHES	
208.0 INCHES	
209.0 INCHES	
210.0 INCHES	
211.0 INCHES	
212.0 INCHES	
213.0 INCHES	
214.0 INCHES	
215.0 INCHES	
216.0 INCHES	
217.0 INCHES	
218.0 INCHES	
219.0 INCHES	
220.0 INCHES	
221.0 INCHES	
222.0 INCHES	
223.0 INCHES	
224.0 INCHES	
225.0 INCHES	
226.0 INCHES	
227.0 INCHES	
228.0 INCHES	
229.0 INCHES	
230.0 INCHES	
231.0 INCHES	
232.0 INCHES	
233.0 INCHES	
234.0 INCHES	
235.0 INCHES	
236.0 INCHES	
237.0 INCHES	
238.0 INCHES	
239.0 INCHES	
240.0 INCHES	
241.0 INCHES	
242.0 INCHES	
243.0 INCHES	
244.0 INCHES	
245.0 INCHES	
246.0 INCHES	
247.0 INCHES	
248.0 INCHES	
249.0 INCHES	
250.0 INCHES	
251.0 INCHES	
252.0 INCHES	
253.0 INCHES	
254.0 INCHES	
255.0 INCHES	
256.0 INCHES	
257.0 INCHES	
258.0 INCHES	
259.0 INCHES	
260.0 INCHES	
261.0 INCHES	
262.0 INCHES	
263.0 INCHES	
264.0 INCHES	
265.0 INCHES	
266.0 INCHES	
267.0 INCHES	
268.0 INCHES	
269.0 INCHES	
270.0 INCHES	
271.0 INCHES	
272.0 INCHES	
273.0 INCHES	
274.0 INCHES	
275.0 INCHES	
276.0 INCHES	
277.0 INCHES	
278.0 INCHES	
279.0 INCHES	
280.0 INCHES	
281.0 INCHES	
282.0 INCHES	
283.0 INCHES	
284.0 INCHES	
285.0 INCHES	
286.0 INCHES	
287.0 INCHES	
288.0 INCHES	
289.0 INCHES	
290.0 INCHES	
291.0 INCHES	
292.0 INCHES	
293.0 INCHES	
294.0 INCHES	
295.0 INCHES	
296.0 INCHES	
297.0 INCHES	
298.0 INCHES	
299.0 INCHES	
300.0 INCHES	
301.0 INCHES	
302.0 INCHES	
303.0 INCHES	
304.0 INCHES	
305.0 INCHES	
306.0 INCHES	
307.0 INCHES	
308.0 INCHES	
309.0 INCHES	
310.0 INCHES	
311.0 INCHES	
312.0 INCHES	
313.0 INCHES	
314.0 INCHES	
315.0 INCHES	
316.0 INCHES	
317.0 INCHES	
318.0 INCHES	
319.0 INCHES	
320.0 INCHES	
321.0 INCHES	
322.0 INCHES	
323.0 INCHES	
324.0 INCHES	
325.0 INCHES	
326.0 INCHES	
327.0 INCHES	
328.0 INCHES	
329.0 INCHES	
330.0 INCHES	
331.0 INCHES	
332.0 INCHES	
333.0 INCHES	
334.0 INCHES	
335.0 INCHES	
336.0 INCHES	
337.0 INCHES	
338.0 INCHES	
339.0 INCHES	
340.0 INCHES	
341.0 INCHES	
342.0 INCHES	
343.0 INCHES	
344.0 INCHES	
345.0 INCHES	
346.0 INCHES	
347.0 INCHES	
348.0 INCHES	
349.0 INCHES	
350.0 INCHES	
351.0 INCHES	
352.0 INCHES	
353.0 INCHES	
354.0 INCHES	
355.0 INCHES	
356.0 INCHES	
357.0 INCHES	
358.0 INCHES	
359.0 INCHES	
360.0 INCHES	
361.0 INCHES	
362.0 INCHES	
363.0 INCHES	
364.0 INCHES	
365.0 INCHES	
366.0 INCHES	
367.0 INCHES	
368.0 INCHES	
369.0 INCHES	
370.0 INCHES	
371.0 INCHES	
372.0 INCHES	
373.0 INCHES	
374.0 INCHES	
375.0 INCHES	
376.0 INCHES	
377.0 INCHES	
378.0 INCHES	
379.0 INCHES	
380.0 INCHES	
381.0 INCHES	
382.0 INCHES	
383.0 INCHES	
384.0 INCHES	
385.0 INCHES	
386.0 INCHES	
387.0 INCHES	
388.0 INCHES	
389.0 INCHES	
390.0 INCHES	
391.0 INCHES	
392.0 INCHES	
393.0 INCHES	
394.0 INCHES	
395.0 INCHES	
396.0 INCHES	
397.0 INCHES	
398.0 INCHES	
399.0 INCHES	
400.0 INCHES	
401.0 INCHES	
402.0 INCHES	
403.0 INCHES	
404.0 INCHES	
405.0 INCHES	
406.0 INCHES	
407.0 INCHES	
408.0 INCHES	
409.0 INCHES	
410.0 INCHES	
411.0 INCHES	
412.0 INCHES	
413.0 INCHES	
414.0 INCHES	
415.0 INCHES	
416.0 INCHES	
417.0 INCHES	
418.0 INCHES	
419.0 INCHES	
420.0 INCHES	
421.0 INCHES	
422.0 INCHES	
423.0 INCHES	
424.0 INCHES	
425.0 INCHES	
426.0 INCHES	
427.0 INCHES	
428.0 INCHES	
429.0 INCHES	
430.0 INCHES	
431.0 INCHES	
432.0 INCHES	
433.0 INCHES	
434.0 INCHES	
435.0 INCHES	
436.0 INCHES	
437.0 INCHES	
438.0 INCHES	
439.0 INCHES	
440.0 INCHES	
441.0 INCHES	
442.0 INCHES	
443.0 INCHES	
444.0 INCHES	
445.0 INCHES	
446.0 INCHES	
447.0 INCHES	
448.0 INCHES	
449.0 INCHES	
450.0 INCHES	
451.0 INCHES	
452.0 INCHES	
453.0 INCHES	
454.0 INCHES	
455.0 INCHES	
456.0 INCHES	
457.0 INCHES	
458.0 INCHES	
459.0 INCHES	
460.0 INCHES	
461.0 INCHES	
462.0 INCHES	
463.0 INCHES	
464.0 INCHES	
465.0 INCHES	
466.0 INCHES	
467.0 INCHES	
468.0 INCHES	
469.0 INCHES	
470.0 INCHES	
471.0 INCHES	
472.0 INCHES	
473.0 INCHES	
474.0 INCHES	
475.0 INCHES	
476.0 INCHES	
477.0 INCHES	
478.0 INCHES	
479.0 INCHES	
480.0 INCHES	
481.0 INCHES	
482.0 INCHES	
483.0 INCHES	
484.0 INCHES	
485.0 INCHES	
486.0 INCHES	
487.0 INCHES	
488.0 INCHES	
489.0 INCHES	
490.0 INCHES	
491.0 INCHES	
492.0 INCHES	
493.0 INCHES	
494.0 INCHES	
495.0 INCHES	
496.0 INCHES	
497.0 INCHES	
498.0 INCHES	
499.0 INCHES	
500.0 INCHES	
501.0 INCHES	
502.0 INCHES	
503.0 INCHES	
504.0 INCHES	
505.0 INCHES	
506.0 INCHES	
507.0 INCHES	
508.0 INCHES	
509.0 INCHES	
510.0 INCHES	
511.0 INCHES	
512.0 INCHES	
513.0 INCHES	
514.0 INCHES	
515.0 INCHES	
516.0 INCHES	
517.0 INCHES	
518.0 INCHES	
519.0 INCHES	
520.0 INCHES	
521.0 INCHES	
522.0 INCHES	
523.0 INCHES	
524.0 INCHES	
525.0 INCHES	
526.0 INCHES	
527.0 INCHES	
528.0 INCHES	
529.0 INCHES	
530.0 INCHES	
531.0 INCHES	
532.0 INCHES	
533.0 INCHES	
534.0 INCHES	
535.0 INCHES	
536.0 INCHES	
537.0 INCHES	
538.0 INCHES	
539.0 INCHES	
540.0 INCHES	
541.0 INCHES	
542.0 INCHES	
543.0 INCHES	
544.0 INCHES	
545.0 INCHES	
546.0 INCHES	
547.0 INCHES	
548.0 INCHES	
549.0 INCHES	
550.0 INCHES	
551.0 INCHES	
552.0 INCHES	
553.0 INCHES	
554.0 INCHES	
555.0 INCHES	
556.0 INCHES	
557.0 INCHES	
558.0 INCHES	
559.0 INCHES	
560.0 INCHES	
561.0 INCHES	
562.0 INCHES	
563.0 INCHES	

## **EXECUTIVE SUMMARY**

### **I. INTRODUCTION**

### **II. EXPERIMENT AND PROCEDURE**

#### **A. General**

#### **B. Propagation Paths**

#### **C. NELC Multi-frequency Sounder**

##### **1. General**

##### **2. Transmitting Antennae**

###### **a. Hawaii Antenna**

###### **b. Sentinel Antenna**

###### **c. Thule Antenna**

##### **3. Transmitter**

##### **4. Receiver**

##### **5. Computer Data Processing**

#### **D. Aircraft Receive Antennas**

##### **1. Long Wire**

##### **2. Loop Assembly**

##### **3. Antenna-Preampl-Multicoupler Calibration Measurements**

### **III. VLF/LF PROPAGATION MODEL**

### **IV. DATA ANALYSIS - BACKGROUND AND PROCEDURE**

#### **A. Ionospheric Parameters**

#### **B. Field Strength vs. Distance Characteristics Computed from Exponential Profiles**

#### **C. Comparison of Predicted VLF/LF Signal Levels with Multi-frequency Propagation Data**

#### **D. Airborne Propagation Data from an Operational Transmitter**

- E. TACAMO Propagation Data
  - F. ABNCP Window Antenna Data
  - G. Continuous Ground Recording of VLF/LF Sounder Signals
- V. CONCLUSION
  - VI. RECOMMENDATIONS
  - VII. APPENDIX A - Notes on Calibration and Normalization Procedures
  - VIII. APPENDIX B - Figures 1 through 26.
  - IX. TABLES
  - X. REFERENCES

## EXECUTIVE SUMMARY

### I. INTRODUCTION

Tacamo aircraft (Navy), airborne command posts (Air Force) and certain fixed site transmitting facilities provide strategic communications capability in the very low frequency (VLF, 15 to 30 kHz) and the low frequency (LF, 30 to 60 kHz) ranges. These communication systems are considered to be the most survivable in a nuclear war environment.

The Minimum Essential Emergency Communications Network (MEECN) requires a high probability of correctly receiving a message during disturbed conditions. Therefore, an accurate knowledge and/or assessment of system capability, including propagation and associated link connectivity, is required in order for the MEECN System Engineer to develop a viable MEECN.

The purpose of the Tri-Service Propagation Program, as established by the Defense Communications Agency (DCA), is to develop a reliable and accurate propagation prediction capability that will allow the system engineer to plan for the deployment and operation of the above joint assets and to reliably assess communication performance through an increased understanding of the propagation environment. The accuracy of VLF/LF propagation prediction computer codes is sensitive to the ionospheric parameters used in the analytic process. These parameters: electron density, ionospheric height, and electron-neutral particle collision frequency cannot be specified by single valued functions, rather they are found to vary greatly with respect to time, season of year and geographic location. This phenomenon while not surprising to the ionospheric physicist has often been misleading to system planners when analyzing propagation predictions.

This report shows the development of a capability to make predictions of TM-mode signal levels during normal propagation conditions at midlatitudes and for frequencies below 60 kHz. The need exists to extend this capability to higher latitudes and to include the TE-mode of propagation. With these additional abilities for making accurate predictions realistic operational conditions, under which existing and future improved VLF/LF MECN links are to operate, can be assured. A task of the Tri-Service Propagation Program is to identify and mathematically describe the ionospheric electron density profiles and other geophysical parameters which, when used with the propagation prediction computer codes (references 25 and 26), will insure that reliable evaluation of system performance can be achieved.

This technical report describes part of the current Tri-Service efforts in the acquisition of VLF/LF propagation data over several propagation paths. The midlatitude geographic area is examined in detail in this report. Analysis of data recorded over other paths will be reported separately.

## II. EXPERIMENT AND PROCEDURE

The experimental measurements described in the present report include VLF/LF radio signals radiated by various sources. These consist of those radiated by airborne long-trailing wire antennas, fixed site operational communication systems and an experimental oblique incidence multi-frequency sounder used to provide "controlled condition" data.

Most of the propagation data were recorded onboard an RADC inflight KC-135 aircraft during flights: across the continental United States (CONUS); from CONUS to Alaska, Greenland and England; from Greenland to Alaska and England; and from Hawaii to California. Also, sounder transmissions were recorded at ground-based receivers placed at Glasgow AFB (Montana) and Saskatoon, Saskatchewan, Canada in order to obtain time variability of the VLF/LF signals. For commun-

ication from aircraft to aircraft, the importance of the horizontal electric field has been recognized as a possible means to enhance system performance and therefore is included in this effort.

### III. THE VLF/LF PROPAGATION MODEL

The VLF/LF propagation prediction computer programs (references 25 and 26), used to calculate predicted signal levels for MEECN evaluation obtain the fullwave solution for a waveguide whose upper boundary has arbitrary electron and ion density distributions with height, and an adjustable collision frequency profile; and whose lower boundary is an earth which is characterized by an adjustable surface conductivity. The model also allows for earth curvature, ionospheric and ground inhomogeneity and anisotropy (resulting from the earth's magnetic field). VLF/LF TM and TE fields at any altitude above the ground are computed for ground based and airborne transmitting systems with arbitrary orientation of the transmitting antenna. This model has been subject to much analysis and verification with the conclusion that it provides the best known tool for complete system performance analysis. For the present report, the profiles are assigned exponential relationships with height, and are identified by the terms  $\beta$  ( $\text{km}^{-1}$ ) and  $H'$  (km). Here  $\beta$  is a gradient or scale height parameter and  $H'$  is the approximate height of reflection. The exponential form of these profiles was chosen because in the past they have proved to provide very good agreement with data.

### IV. DATA ANALYSIS

The data analyzed in this report consist mainly of multi-frequency sounder measurements taken aboard the RADC inflight aircraft for transmissions across the Pacific Ocean between Hawaii and Southern California. TE field data recorded during one of the flights to Hawaii and other available TE field data are also presented and analyzed.

The procedure used to determine the effective long propagation path electron density profile is to compare measured data with fields computed using the propagation prediction computer program and various assumed ionospheric profiles. By a trial and error process, the profile which provides the closest agreement with the measurement is considered to be the one which best represents the propagation conditions existing during the measurement period.

#### V. CONCLUSION

For propagation at midlatitudes in a winter daytime environment, the use of approximately identical exponential electron density profiles at frequencies between 9 and 56 kHz will adequately predict the measured signal levels. The values of the "best-fit" exponential electron density profiles were  $\beta = 0.3 \text{ km}^{-1}$  and  $H' = 72\text{-}75 \text{ km}$ .

In order to best-fit the winter nighttime fields, it was found necessary that the value of the exponential electron density gradient parameter  $\beta (\text{km}^{-1})$  increase with frequency. The range of this parameter varied from 0.3 at 9.4 kHz to 0.7 or 1.2 at 56 kHz. The value of the  $H'$  parameter was determined to vary between 86 and 89 km, depending on frequency and the aircraft flight from which the experimental data were recorded. The variations in  $\beta$  from 0.7 to 1.2 at the higher frequencies on two different nights illustrates changes in the ionosphere for the two nights. The fact that different best-fit exponential profiles are obtained over the VLF/LF band at night suggests the possibility that a more general multi-parameter profile is needed to represent VLF/LF propagation rather than the two parameter exponential representation.

Based on the field strength levels recorded over the midlatitude Hawaii to Southern California transmission path the following exponential profiles most accurately describe the propagation data.

**Table ES-1:**

RECOMMENDED ELECTRON DENSITY  
PROFILES FOR USE IN PROPAGATION  
PREDICTIONS (midlatitude)

DAYTIME Winter		NIGHTTIME Winter	
Frequency (kHz)	Profile $\beta$ ( $\text{km}^{-1}$ ), $H'$ (km)	Frequency (kHz)	Profile $\beta$ ( $\text{km}^{-1}$ ), $H'$ (km)
9-60	$\beta=0.3$ , $H'=74$	below 10	$\beta=0.3$ , $H'=87$
		10 - 15	$\beta=0.4$ , $H'=87$
		15 - 25	$\beta=0.5$ , $H'=87$
		25 - 30	$\beta=0.6$ , $H'=88$
		30 - 40	$\beta=0.7$ , $H'=88$
		40 - 60	$\beta=0.8$ , $H'=88$

These ionospheric profiles result in predictions of signal amplitudes which on the average are within 2 dB for daytime and within 3 dB for nighttime of those amplitudes.

Horizontally polarized (TE) as well as vertically polarized (TM) electric fields are important for meeting the MECN requirement for a viable communication

system involving the airborne assets. Calculations made with the propagation prediction computer program, (reference 25), and which agree with measured data indicate that stronger signal levels can be obtained for the horizontal electric field than for the vertical electric field at operational aircraft altitudes.

#### VI. RECOMMENDATIONS

The use of exponential electron density profiles, as presented in Table ES-1, is recommended in analyses of deployment, operation and evaluation of VLF/LF MEECN assets involving mid-latitude propagation paths in the winter.

In a previous report, (reference 16), the profile  $\beta = 0.5 \text{ km}^{-1}$ ,  $H^* = 87 \text{ km}$  was determined to produce acceptable nighttime TM signal levels throughout the 10-30 kHz frequency band and its use was suggested for frequencies up to 60 kHz. Utilization of the nighttime profiles, as presented in Table ES-1, results in an improvement in predicting signal amplitudes. The improvements are a function of propagation range and the average improvement over the 4 Mm path from Hawaii to Southern California are shown in Table ES-2.

Table ES-2:  
IMPROVEMENTS IN THE ACCURACY  
OF PREDICTED SIGNAL LEVELS OVER  
THAT OBTAINED FROM PREVIOUSLY  
RECOMMENDED PROFILE  
(Midlatitude - Winter)

Frequency (kHz)	dB
28.0	1
37.4	3
40.5	4
46.7	5
52.9	9
56.0	9

As suggested earlier both seasonal and latitudinal variations occur in the ionospheric parameters and hence the values of the  $\beta$  and  $H'$  as presented in Table ES-1 apply only to propagation during the winter months for midlatitudes. Application to other conditions may yield as much as 6 dB variance in predicted performance. Therefore, the accuracy of the VLF/LF propagation procedure for other seasons of the year and for other geographical latitudes needs to be examined.

## I. INTRODUCTION

There is need for the Air Force and the Navy to maintain reliable communications in the very low frequency range (VLF, 17 to 30 kHz) and in the low frequency range (LF, 30 to 60 kHz). For this reason the Defense Communications Agency (DCA), through the Minimum Essential Emergency Communications Network (MEECN) Systems Office, has established the Tri-Service Propagation Program.

In order to design, deploy and maintain the essential communication circuits required by the MEECN, reliable knowledge of the radio signal amplitude and phase characteristics, together with the properties of the atmospheric noise, is required.

The purpose of the Tri-Service Propagation Program is to develop reliable and accurate propagation prediction techniques that will allow the MEECN to reliably assess communication performance and to examine possible improvements in systems performance through an increased understanding of the propagation environment.

Several books concerning VLF/LF propagation prediction theory have been written in the past (references 1, 2 and 3). The earliest prediction techniques used empirical formulas that represent the "best fit" to a large volume of data. In recent years, propagation theories have been developed that describe the physics of interaction of the radio wave with the earth and the ionosphere (references 4, 5, and 6). These have been used quite satisfactorily to describe most measured characteristics of the radio signal, such as:

- A. Phase velocity variation with frequency used by OMEGA and other VLF/LF radio navigation aids (reference 7).
- B. Modal interference pattern at all frequencies in the VLF band (reference 8).

C. Fields excited by ground-based and airborne vertical and horizontal radiating antennas (reference 9).

D. Effect of propagation on performance of wide-band coherent communication systems (reference 10).

The effective ionospheric conductivity profile is the parameter that is most uncertain in a propagation prediction procedure. This conductivity parameter is a function of the electron density and the electron-neutral particle collision frequency. A successful technique for determining the conductivity profile is to "sound the ionosphere" by measuring VLF/LF radio transmissions and then to compare the resulting field strengths to those predicted by analytical propagation models into which an assumed profile has been incorporated. If the measured and computed results do not agree, other trial profiles are tried in the propagation model until a "best fit" to the measured data is found.

In the past, much of the VLF/LF propagation data reported in the literature have consisted of measurements made at a single receiver site on one propagation frequency over a given path. This limited type of data has not proven useful for determining the conductivity profile of the ionosphere through which the radio wave must pass. Data recorded using the Naval Electronics Laboratory Center (NELC) oblique incidence multi-frequency sounder (reference 11), on the other hand, gave signal levels at many frequencies simultaneously. With this type of data acquisition, much more data are available at the termination of a single propagation path, and in the case where the receiver is placed aboard an inflight recording aircraft, multi-frequency data is obtained as a continuous function of distance. The availability of such multiple frequency data provides a facility for determining a more unique form of the ionospheric conductivity profile than has previously been possible.

The technique described above, for determining the conductivity profile of the ionosphere, has been applied successfully to propagation data measured on equatorial and low-latitude paths (references 12, 13, 14 and 15). These data were primarily obtained from VLF transmissions. A very limited amount of information and data has been available concerning the effective ionospheric profiles that support long-distance LF propagation and VLF/LF propagation in the higher latitudes; i.e., polar cap region, auroral zone and mid-latitudes.

To improve the reliability of propagation predictions for those frequencies and propagation regions where data has been limited or unavailable, the experimental data acquisition program, which is described in this report, was designed so that measurements were obtained for both VLF and LF transmissions over paths of operational interest to the Office of MEECN System Engineering (OMSE) of DCA. These paths were characterized by the following properties.

A. Paths involving primarily sea water at nearly constant geomagnetic latitude where the propagation paths may be assumed to be horizontally homogeneous, thus simplifying interpretation and analysis of the data.

B. High-latitude paths; i.e., those passing through the polar cap region and auroral zone. Paths which pass through these regions provide an opportunity to determine the ionospheric conductivity profiles as produced by solar-geophysical phenomena such as PCA events, solar flares and geomagnetic storms.

C. Paths which contain highly varying ground conductivities, such as propagation across Canada and over the Greenland ice cap. These paths are included to examine the utility of the prediction model in simulating these propagation conditions.

Once a sufficient amount of experimental data has been acquired, the ionospheric parameters; i.e., electron density profiles which describe the propaga-

tion environment, may be determined with sufficient accuracy to insure reliable predictions of VLF/LF signal levels. These predictions can be used, together with data on signal variability, atmospheric noise, and system parameters, to compute the time availability of MEECN VLF/LF links.

This report is divided into the following sections: Section II describes the Tri-Service VLF/LF propagation experiment in general; including propagation paths over which data was obtained, the characteristics of the VLF/LF transmit and receive systems, and comments related to the measured data. Section III describes the propagation model used for computer simulation of the recorded signal levels. Section IV describes the method of data analysis and the results obtained as to "best fit" electron density profiles to the recorded data. Conclusions and recommendations are presented in Sections V and VI.

A general summary of previous comparisons of predicted VLF/LF signal levels with propagation data has been presented in reference 16.

## **II. EXPERIMENT AND PROCEDURE**

### **A. General**

Acquisition of initial VLF/LF propagation data for use in the Tri-Service Propagation Program has been achieved. The experimental measurements described and utilized in the present report include VLF/LF radio signals that were radiated by airborne long-trailing wire antennas, fixed site operational communication and navigation systems and experimental transmitting facilities, such as the NELC oblique incidence multi-frequency sounder, that was used to provide "controlled condition" data. The transmitted signals were recorded aboard an inflight aircraft flying primarily radials to or from transmitters, at flight terminal points, and at some intermediate locations. Propagation data were also obtained at some fixed site locations on ground-based receivers.

In October 1973 and January-February 1974, primarily nighttime, propagation data were recorded onboard a Rome Air Development Center (RADC) KC-135 aircraft. The measurements were made during flights: across the continental United States (CONUS); from CONUS to Alaska, Greenland and England; from Greenland to Alaska and England; and from Hawaii to California. Also in October 1973, about three weeks of sounder transmissions were recorded at ground-based receivers placed at Glasgow AFB (Montana) and Saskatoon, Saskatchewan, Canada, in order to obtain time variability of the VLF/LF signals.

Signals monitored during the October and January-February propagation measurements included: the NELC 10-frequency VLF/LF sounder transmissions from Sentinel (Arizona), Thule (Greenland), and Hawaii; operational Navy and Air Force VLF/LF transmitters; and on 30 January, airborne transmissions from a TACAMO and an ABNCP aircraft during other MECN tests.

Although all operational receive antennas are vertically polarized, the

Tri-Service data acquisition program also includes an evaluation of the usefulness of the horizontal electric field. There has been recent evidence (reference 9) that these horizontal fields may be particularly important during nighttime propagation periods when the transmissions are from aircraft to aircraft. To record data of both polarizations (i.e., TM or the vertical electric field ( $E_z$ ) and the TE or horizontal electric field ( $E_y$ )), special loop receiving antennas were constructed and installed aboard the RADC aircraft. These were used as well as the usual long wire antenna available on the aircraft.

## B. Propagation Paths

The major propagation paths for which data were obtained are shown in figure 1. These are paths for which satisfactory levels of signal amplitude were recorded and are paths which yield most easily to present analysis procedures in that they generally follow the great circle path from the particular transmitter from which the data is being recorded. These paths also comprise the characteristic requirements as listed in the introduction section of this report.

Table I lists the location and the coordinates of the U.S. Air Force bases and other sites as related to the acquisition of the propagation data. All of those locations are related to the paths flown by the aircraft except two which are the location of fixed receiver sites.

Table II lists the location and coordinates, as well as radio frequency, of the VLF/LF transmitter sites from which propagation data were obtained.

Tables III and IV list the individual aircraft flight paths with identification of dates and times (U.T.) for which data were recorded, the origin and destination of each flight, and descriptive remarks of each particular flight path. Table III lists the data flights conducted during October 1973 on flights 1 through 13, while Table IV lists the data for January and February 1974 on flights 14 through 33.

The signal levels recorded for this experiment consisted of either transmissions from the operational VLF/LF transmitters located at various positions in CONUS and in Europe, or from transmissions from the NELC multi-frequency sounder placed at specific locations.

Data from the operational transmitters were recorded aboard the aircraft on three special TRACOR receivers and on a single URM-139 receiver. These data consisted of transmissions from OMEGA (North Dakota) on 10.2 kHz, GBR

TABLE I. LOCATIONS AND COORDINATES OF AIR BASES AND OTHER SITES  
RELATED TO AIRCRAFT FLIGHTS AND DATA ACQUISITION

<u>Site</u>	<u>Latitude</u>	<u>Longitude</u>
Adak, Alaska	51° 53' N	176° 39' W
Bodo, Norway	66° 26' N	13° 9' E
Castle AFB, California	37° 25' N	120° 25' W
Davis-Monthan AFB, Arizona	32° 12' N	111° 0' W
Eielson AFB, Alaska	64° 37' N	147° 0' W
Glasgow AFB, Montana	48° 21' N	106° 34' W
Griffiss AFB, New York	43° 14' N	75° 25' W
Hickam AFB, Hawaii	21° 23' N	157° 53' W
Luke AFB, Arizona	33° 30' N	112° 33' W
March AFB, California	33° 58' N	117° 16' W
McChord AFB, Washington	47° 05' N	122° 35' W
Mildenhall AFB, England	52° 22' N	0° 29' E
Minot AFB, North Dakota	48° 23' N	101° 40' W
Reykjavik, Iceland	63° 56' N	22° 24' W
Saskatoon, Saskatchewan	53° 0' N	107° 0' W
Sondrestrom, Greenland	67° 10' N	50° 30' W
Tinker AFB, Oklahoma	35° 25' N	97° 23' W
Thule AFB, Greenland	76° 21' N	69° 4' W

TABLE II. LOCATION, COORDINATES AND FREQUENCY OF VLF/LF  
TRANSMITTER SITES USED ON AIRCRAFT FLIGHTS

<u>Site</u>	<u>Latitude</u>	<u>Longitude</u>	<u>Frequency kHz</u>
<u>Naval VLF High-Powered</u>			
<u>Transmitting Stations:</u>			
NAA - Cutler, Maine	44° 38' N	67° 16' W	14.7, 17.8
NLK - Jim Creek, Washington	48° 12' N	121° 55' W	18.6
<u>OMEGA Transmitting</u>			
<u>Stations:</u>			
La Moure, North Dakota	46° 22' N	98° 20' W	10.2
<u>Other Transmitting</u>			
<u>Stations:</u>			
Forestport, New York	43° 27' N	75° 05' W	36.0
GBR - England	52° 22' N	01° 11' W	16.0
Hawes, California	35° 0' N	117° 30' W	37.2
<u>NELC VLF/LF Sounder:</u>			
Hawaii, Hawaii	19° 38' N	155° 36' W	9-56
Sentinel, Arizona	32° 49' N	113° 09' W	9-56
Thule, Greenland	76° 33' N	68° 37' W	9-56

TABLE III. AIRCRAFT FLIGHT PATHS FOR OCTOBER 1973

<u>Aircraft</u>	<u>Date</u>	<u>Julian</u>	<u>Origin</u>	<u>Destination</u>	<u>Times of Recorded</u>		<u>Remarks</u>		
					<u>Flight No.</u>	<u>1973</u>	<u>Day</u>	<u>Data (U.T.)</u>	
1	Oct 3	276	Griffiss AFB	March AFB		1408	-	2009	No usable data obtained.
2	4	277	March AFB	Glasgow AFB		1519	-	1956	Overflow Luke, circled Sentinel.
3	4	277	Glasgow AFB	McChord AFB		2141	-	2359	Overflow NLK.
4	6	279	On ground			0004	-	0239	On ground at McChord.
5	6	279	McChord AFB	Griffiss AFB		0248	-	0752	Overflow NLK, Glasgow, OMEGA North Dakota.
6	10	283	Griffiss AFB	March AFB		0236	-	1837	Overflow Forestport and Hawes.
7	11	284	March AFB	Luke AFB		1214	-	1415	Circled Sentinel.
8	11	284	Luke AFB	Eielson AFB		1604	-	2341	Overflow Sentinel.
9	13	286	Eielson AFB	Eielson AFB		0325	-	0958	Round trip to Adak.
10	13	286-287	On ground			1108	-	1200	On ground at Eielson.
11	15	288	Eielson AFB	March AFB		0323	-	1028	Overflow NLK, Sentinel.
12	16	289	March AFB	McChord AFB		0345	-	0934	Circled Sentinel, overflow Glasgow, NLK.
13	17	290	McChord AFB	Griffiss AFB		0220	-	0719	Overflow NLK, Glasgow and Forestport, New York.

TABLE IV. AIRCRAFT FLIGHT PATHS FOR JANUARY - FEBRUARY 1974

Aircraft Flight No.	Date 1974	Julian Day	<u>Origin</u>	<u>Destination</u>	Times of Recorded Data (U.T.)		<u>Remarks</u>
					0001	- 0719	
14	Jan 15	15	Griffiss AFB	Mildenhall Eng	0001	-	No usable data obtained.
15	16	16	Mildenhall Eng	Mildenhall Eng	0100	- 0830	Via Iceland and Bodo, Norway.
16	18	18	Mildenhall Eng	Mildenhall Eng	0213	- 0912	Via Iceland and Bodo, Norway.
17	18	18-19	Mildenhall Eng	Griffiss AFB	1957	- 0434	
18	22	22	Griffiss AFB	Thule AFB	0605	- 1321	Overflow Forestport, NY, NAA, circled Thule.
19	23-24	23-24	Thule AFB	Mildenhall AFB	1856	- 0014	Overflow GBR, England.
20	25	25	Mildenhall Eng	Thule AFB	0714	- 1235	Overflow GBR, GBZ, England.
21	26-27	26-27	Thule AFB	Griffiss AFB	1956	- 0139	Overflow NAA.
22	28-29	28-29	Griffiss AFB	Tinker AFB	2230	- 0145	
23	29	29	Tinker AFB	March AFB	0500	- 0741	Overflow Sentinel, Arizona.
24	30	30	March AFB	Hickam AFB	1030	- 1450	Overflow Pacific (night).
25	31	31	On ground		0000	- 1900	On ground at Hickam.
26	Feb 1	32	Hickam AFB	Castle AFB	0620	- 1100	Overflow Pacific (night).
27	2	33	March AFB	Hickam AFB	1830	- 2350	Overflow Pacific (day).
28	3	34	Hickam AFB	March AFB	1830	- 2320	Overflow Pacific (day).
29	5	36	March AFB	Minot AFB	0508	- 0918	Circled Sentinel.
30	6	37	Minot AFB	Thule AFB	0925	- 1410	Overflow Glasgow.
31	7	38	Thule AFB	Eielson AFB	1422	- 1835	
32	9	40	Eielson AFB	Sondrestrom	1450	- 2020	Overflow Thule.
33	10	41	Sondrestrom	Griffiss AFB	1320	- 1700	No usable data recorded.

(England) on 16.0 kHz, NAA (Cutler, Maine) on 14.7 and 17.8 kHz, NLK (Jim Creek, Washington) on 18.6 kHz and Forestport, New York on 36 kHz. Vertical electric fields ( $E_V$ ) and both vertical magnetic ( $H_V$ ) and horizontal magnetic ( $H_H$ ) fields were measured using the long wire and the vertical and horizontal loop antennas. The horizontal electric field ( $E_H$ ) is obtained from the vertical magnetic ( $H_V$ ) measurements.

The NELC multi-frequency sounder data were also measured aboard the aircraft by using the long wire as well as the crossed loop array. The transmitted frequencies are as follows: First, the sounder operates from a 100 kHz rubidium standard. The standard is offset to 99.631 kHz or to 99.580 kHz so that the spectral lines of the pulse-type sounder transmissions are displaced from spectral lines that are typical of operational system transmissions. The actual transmitted frequencies are then synthesized from the offset standard frequencies and are listed in Table V as frequency sets 1 through 5.

Table VI lists and identifies the experimental frequencies and antennas used for each aircraft flight as related to the NELC multi-frequency sounder.

TABLE V. FREQUENCY SETS FOR NELC MULTI-FREQUENCY SOUNDER TRANSMISSIONS (kHz)

<u>Set #1</u>	<u>Set #2</u>	<u>Set #3</u>	<u>Set #4</u>	<u>Set #5</u>
10.897	9.340	9.340	9.336	10.897
14.011	10.897	14.011	14.003	14.010
15.567	15.567	17.124	17.115	15.567
21.794	21.794	24.908	24.895	21.794
24.908	28.021	28.021	28.007	24.908
28.021	37.361	34.248	34.231	31.134
38.918	40.475	38.418	38.898	40.475
43.589	46.702	43.589	43.566	46.702
49.815	52.929	49.816	49.790	52.929
56.042	56.042	56.042	56.104	56.042
(99.631 kHz)	(99.631 kHz)	(99.631 kHz)	(99.580 kHz)	(99.631 kHz)
(Standard)	(Standard)	(Standard)	(Standard)	(Standard)

TABLE VI. IDENTIFICATION OF EXPERIMENTAL PARAMETERS FOR EACH AIRCRAFT  
FLIGHT AS RELATED TO THE NELC MULTI-FREQUENCY SOUNDER

Receive Antenna Key:	LW - Long Wire	Received Electric Field Vertical Component ( $E_V$ )
	HL - Horizontal Loop	Received Magnetic Field Vertical Component ( $H_V$ )
	VL - Vertical Loop	Horizontal Component ( $H_H$ )

Transmitted					
Aircraft	Transmitter	Frequency Set	Receive	Electric	Magnetic
<u>Flight No.</u>	<u>Site</u>	<u>(Table V)</u>	<u>Antenna</u>	<u>Field Measured</u>	<u>Field Measured</u>
1 thru 13	Sentinel	#1	LW	$E_V$	
14 thru 21	Thule	#2	LW	$E_V$	
			HL		$H_V$
22, 23	Sentinel	#3	LW	$E_V$	
			HL		$H_V$
24	Hawaii	#2	LW/VL	$E_V$	$H_H$
	Sentinel	#4	LW/VL	$E_V$	$H_H$
25 thru 28	Hawaii	#2	LW	$E_V$	
	Sentinel	#4	LW	$E_V$	
29, 30	Sentinel	#4	LW	$E_V$	
			HL		$H_V$
31, 32, 33	Thule	#5	LW	$E_V$	
			HL		$H_V$

### C. NELC Multi-frequency Sounder

#### 1. General

A detailed description of the NELC multi-frequency VLF ionospheric sounder system has been presented in a previous report (reference 11). Basically, the sounder consists of a 10-frequency, time-shared transmitter and receiver. The transmitted signal consists of pulses of ten frequencies in sequence. The pulse length at each frequency can be varied and may be as short as 80  $\mu$ sec. In normal operation, this group of ten pulses is repeated continuously, giving a 10% duty cycle for each transmitted frequency. The receiving system consists of 20 correlation-type receivers -- two for each transmitted frequency. Each correlation receiver is gated on in synchronism with the transmitted pulse at that frequency, with an appropriate delay to allow for propagation time. Both transmitter and receiver are controlled by very accurate and stable rubidium vapor frequency standards so that synchronization can be maintained over very long periods of time. The sounder system can be set up at any location where sufficient space is available at the terminators to construct the transmitting antenna and where the terrain conductivity at the transmitter terminal is sufficiently low to obtain adequate antenna efficiency.

Figure 2 shows a basic diagram of the transmitting and receiving systems; the individual systems are described in detail below.

#### C. Transmitting Antennae

##### a. Hawaii Antenna

One of the transmitting antennas used to obtain propagation data for this experiment is located on the island of Hawaii at an altitude of 7000 feet in an area of recent lava flows. This antenna is a center-fed broad-band stagger-tuned dipole (reference 17) laid directly on the lava surface. This

type of antenna requires an area of low soil conductivity for efficient operation; the Hawaiian lava beds were chosen because they have a conductivity on the order of 0.4 millimhos/meter. The physical configuration of this antenna consists of ten parallel conductors which act as a broad-band horizontal dipole. The conductors are of different lengths to give a stagger-tuned effect; thus, the antenna has a band-width which is large with respect to the specified frequency range. The conductors are approximately 15 percent successively shorter, with the longest being 11 km in length. Efficiencies of several percent are achieved with this antenna.

b. Sentinel Antenna

This NELC VLF/LF transmitting antenna is located five miles south of Sentinel, Arizona. The characteristics of this antenna are described in detail in reference 18. The physical configuration of the Sentinel VLF/LF antenna consists of five elements, each 8.85 km long, elevated to a height of 8 meters, and oriented on a magnetic north-south bearing. Also, there is a single identical element oriented on an east-west bearing. The north-south elements were used for signal transmissions during propagation measurements to the north, while the east-west element is used for measurements to the west, such as toward Hawaii.

The north-south antenna was terminated with its characteristic impedance at both the north and the south ends to allow for broad-band operation, and was operated as a center-fed dipole. The radiation efficiency below a perfect monopole varied somewhat linearly from 43 dB at 10 kHz to 24 dB at 50 kHz.

During some transmission periods, the antenna was configured as an end-fed dipole by terminating the north end with its characteristic impedance and by applying a reflection transformer at the south end. This resulted

in an increase in radiation efficiency of from 3 to 6 dB off the north end over that obtained from the center-fed transmissions. The center-fed resonant east-west single element antenna radiated 5 dB more efficiently than the terminated 5-element center-fed north-south antenna.

In general, the average ground conductivity deduced from antenna measurements (reference 18) was found to be 8 millimhos/meter in the low VLF band and 3 millimhos/meter in the high VLF band.

#### c. Thule Antenna

The antenna constructed at Thule, Greenland consists of two elements 8 km in length, elevated 3 meters above the ground surface. The direction of the antenna is such that it will radiate end-on towards Point Barrow, Alaska. This is a bearing of 300° off the west end from true north. For propagation measurements toward England, the antenna was end-fed. For transmissions to Alaska, the antenna was also end-fed but was terminated with its characteristic impedance by applying a reflection transformer at its west end. The ground conductivity at the antenna was found to range from 1.6 millimhos per meter at 10 kHz to 0.3 millimhos per meter at 40 kHz. The effective radiated power of this antenna has not been determined at this time but will be presented in a future report.

#### 3. Transmitter

A block diagram of the transmitter/receiver system is shown in figure 2. The system is controlled by a rubidium frequency standard, the (- 100-kHz) output of which is used to drive the programmer. The programmer synthesizes all transmitted VLF frequencies and provides the necessary gating. The (- 100-kHz) input to the programmer is divided by a string of binary dividers to a frequency of  $f_A = (- 100)/64$  kHz. The outputs at that frequency and at

higher multiples of it are taken from the divider chain and fed to a series of VLF synthesizers, which select and filter the proper harmonic to produce the desired VLF/LF frequency. The output frequencies from the synthesizers are then fed through a series of analog gates. The analog gates are operated by a 10-stage ring counter which uses the  $f_A$  -kHz output from the divider chain as a clock. Thus, each of the 10 gates is opened in sequence for the proper duration, each frequency being repeated at intervals of 10 times the dwell time on a given frequency. For example, if the gates are programmed to remain open for 80  $\mu$ sec, a given frequency is repeated every 800  $\mu$ sec. A patchboard in the unit enables any ring-counter output to be patched to any of the analog gates, so that the 10 frequencies can be selected in any desired sequence. Since the clock rate for the ring counter is obtained from the  $f_A$  -kHz signal and since all frequencies are harmonics of that frequency, each gate is switched on at zero crossing of the VLF synthesizer outputs. The programmer output is fed directly to the VLF power amplifier.

#### 4. Receiver

A block diagram of the receiver system is shown in figures 2 and 3. The VLF signal from the antenna is amplified by a wide-band amplifier; this unit contains a number of notch-rejection filters used to eliminate interference from VLF communications stations. The signal is then fed to 10 narrow-band filters, the outputs of which are applied in parallel to the correlation detector unit.

A block diagram of the correlation detector unit is shown in figure 4. The reference signals for the correlation detector unit are derived from a rubidium frequency standard and synthesizer-programmer. The latter is similar to the transmitter programmer, with the exception that separate output

lines are provided for each of the 10 VLF/LF frequencies generated. The 20 correlation detectors are operated in pairs, and in one element of each pair the reference signal is shifted 90° in phase so that the quadrature signal is detected. Therefore, the output of the correlation detectors for a given frequency is a pair of filtered signals corresponding to the X and Y components of the received signal and referenced in phase to the locally synthesized signal. The integrator unit of each correlator detector consists of two operational amplifiers in series. This provides the characteristic of a two-stage RC low-pass filter, thus achieving a sharp rejection of high-frequency noise components. Time constants for the integrator units are selected between 10 and 130 sec. The philosophy for optimum operation is to use the shortest time constant that will provide an adequate signal-to-noise ratio for real-time assessment of system performance. Additional digital filtering can be applied later to the recorded data as necessary to improve signal-to-noise ratios.

The outputs of the correlation detection units are recorded both on digital magnetic tape and by strip chart recorders. The digital recorder samples the output of each detector a minimum of three times with the selected integration time constant. The scan rate of the digital recorder system is set at the maximum that is consistent with equipment tolerances, so that all channels are sampled as close together in time as practicable. Typically, 40 channels can be scanned in 2 sec. Strip chart recorders are used to provide a real-time readout to assist the operator in checking equipment performance for equipment calibration and for system synchronization.

A calibration injection system for the loop receive antennas consists of a separate single-turn loop coincident with the turns of the antenna. The long wire antenna is calibrated by injecting a signal through a dummy antenna

into the receiver. The dummy antenna is contained within the receiver synthesizer-programmer unit. The 10-frequency output of the synthesizer is applied, through a calibrated attenuator, to the calibration injection point. This signal, when applied, allows a determination of the receiving system output for a known voltage input. Thus, the gain of the receiver system is determined. In addition, this signal is very useful for checking receiver operation. All 10 channels are simultaneously calibrated.

##### 5. Computer Data Processing

The sounder data that is recorded on digital magnetic tape is suitable for direct input to a digital computer for processing. The existing programs for data processing contain many useful and flexible features. The data is originally written in 7-track digital tapes in binary-coded decimal format at 200 bits per in. On the first computer pass through the data, the data is rewritten on 9-track tapes in binary format at 800 bits per inch; this speeds up the reading of the data on any subsequent passes and conserves tape. During this rewrite operation, any errors detected on the original data tape are corrected, if possible. Additional filtering can be applied to the data with any arbitrary time constant; calibration levels can be read and the data scaled to absolute field strength; and the X, Y signal components can be converted to phase and amplitude. During the calibration and scaling process, compensation can be made for any receiver gain changes or changes in transmitted power. During this gain compensation procedure, allowances are made for the finite rise or decay times caused by the analog filters in the receiver. When phase is calculated from the X and Y components of the signal, a  $360^\circ$  jump discontinuity is experienced whenever the Y component changes sign and the X component is negative. These discontinuities are automatically sensed by the computer program and re-

moved by adding or subtracting the proper multiple of  $360^\circ$ . Thus, a continuous phase record is obtained. The processed data at this point is written on magnetic tape from which it can be read back into the computer and plotted on an incremental digital plotter to any desired scale within the limitations of the plotter (an 11 inch by 120 feet plotting surface is available, and minimum step size for the plotter is 0.01 inch). The plotting portion of the program allows any portion of any data channel to be plotted independently of other channels.

## D. Aircraft Receive Antennas

### 1. Long Wire

One of the VLF/LF receiving antennas used onboard the aircraft consisted of a long wire (LW), 100 feet in length. This antenna is used to measure the vertical component of the radiated electric field. The long wire is supported between the vertical fin and a mast located on the side of the aircraft. See figure 5. This is the type of antenna normally used by the high frequency (HF) communications equipment contained aboard the aircraft. The antenna enters the aircraft through an antenna coupler. This coupler contains a lightning arrestor and a transmit-receive relay plus circuitry for properly loading the transmitter. While in the receive mode the only apparent connection to the antenna, other than a BNC connector on the coupler, is a 100 K resistor from the antenna to ground. The measured capacitance to ground of the antenna-coupler combination was about 300 pf. This capacitance and the 100 K resistor will produce a high pass filter with a cut-off frequency of about 5 kHz and should have negligible effect at frequencies of interest.

A second similar antenna is also installed on the aircraft. It is located slightly above the VLF/LF long wire and is supported between the vertical fin and a short antenna mast near the front of the aircraft. See figure 5. This antenna was used for HF communications during the flights. The reception of VLF/LF signals was severely disturbed during HF transmission periods.

### 2. Loop Assembly

A crossed-loop assembly was also designed and installed on the aircraft for measurement of VLF/LF fields. This assembly consisted of two orthogonally mounted shielded loops mounted at the rear of the aircraft on the refueling boom. See figure 6. The loops are oriented one each in the horizontal and the

vertical plane, so as to measure both the vertical and the horizontal magnetic fields respectively.

Each loop contains 40 turns and has a nominal diameter of 3 feet. The calculated effective height of such a loop is  $5.5 \times 10^{-3}$  meters at a frequency of 10 kHz. Each loop is provided with a calibrate turn. The calibrate turns are constructed from RG-188/U coax with the outer shields cut and grounded so as not to form a shorted turn. The calibrate turns are connected in series so that both loop antennas are calibrated at the same time. A 47 ohm resistor is inserted in series with the combination of the two turns.

Separate preamplifiers for each loop are contained in the loop assembly base. Each preamplifier is transformer coupled to its respective loop. The loops are tuned to about 65 kHz and loaded to give a Q of about 0.7. Each preamp has a gain of about 42 dB at mid-frequency and is capable of an output level of 0.5V rms into 100 ohms before distortion.

### 3. Antenna-Preamp-Multicoupler Calibration Measurements

Measurements were made on various portions of the equipment in an effort to provide useful calibration information. A block diagram of the front end of the receiver is contained in figure 7. The calibration system is also shown in this figure.

When the long wire antenna receiver was calibrated, the calibrate attenuator was connected to the input of the long wire dummy antenna. The low pass filter was disconnected from the antenna coupler and connected to the dummy antenna output. The calibration voltage level was read on a differential voltmeter and the attenuator sections which were switched in were noted.

When the loop receivers were calibrated the calibrate attenuator was connected to the loop calibrate cable and the calibration voltage level and

attenuator switches were noted. The loop calibration factors were determined by measuring the open-circuit loop output voltages while injecting a known calibration voltage into the single turn calibration loop. Then, by using the calculated effective height of the 40 turn loop antenna, at each frequency, the simulated field could be determined. The values are that: for a calibration voltage of 5 millivolts, the simulated field is 100 millivolts/meters for all frequencies.

During the latter portion of aircraft flight No. 21, measurements were made on the loop antennas and the long wire antenna of VLF/LF station signals. The station measurements provide a means of relating the effective height of the long wire antenna to that of the vertical loop for the frequencies measured. Both NAA, 17.8 kHz, and Forestport, 36.0 kHz, were measured. An HP 302A wave analyzer was used to make the measurements. The measurements were made at an unloaded output of the appropriate sections of the multicoupler. Most of the time NAA transmits in an FSK mode (17.8, 17.85 kHz) and accurate measurements are difficult to make on the wave analyzer; however, at about 2355 U.T., NAA was observed to be transmitting 17.8 kHz CW. The aircraft position at this time was about 48°25'N, 67°21'W which is about 225 n.m. from NAA. The aircraft heading was on a radial towards NAA. The aircraft passed over NAA about 30 minutes later. A series of measurements of the signal strength of NAA at the multicoupler outputs of the long wire and vertical loop antennas was made by switching the wave analyzer input between the two multicoupler outputs. Thirteen sets of measurements were obtained while the station was transmitting a CW signal. The average level measured on the vertical loop system was 10.8 mv, the average level measured on the long wire system was 39.5 mv and the average ratio of the long wire to vertical loop was 3.65.

The effective height of the long wire antenna can be determined

from the above measurements of the NAA signal. From characteristics of the vertical loop preamp and multicoupler response it is possible to determine that the measured vertical loop signal of 10.8 mv is equivalent to a field strength of 18.7 mv/m. To the extent that the long wire antenna was responding to the vertical component of the field, the long wire produces a multicoupler output voltage of 39.5 mv for a field strength of 18.7 mv/m. This corresponds to an effective height for the long wire antenna of 0.775 meters.

The measurements made on the Forestport transmitter (36 kHz), located at  $43^{\circ}26'41''N$ ,  $75^{\circ}05'10''W$ , were initiated sometime shortly after passing over NAA. The distance from NAA to Forestport is about 345 nm. The average ratio of the signal strength measured on the long wire antenna to that measured on the vertical loop for seven pairs of readings is 1.77. This ratio compares to that measured at 17.8 kHz,  $3.65/1.77 = 2.06$ , very nearly as the frequencies compare,  $36/17.8 = 2.08$ . This comparison is expected since the effective height of the long wire antenna should be constant with frequency while the effective height of the vertical loop should be a linear function of the signal frequency.

### III. VLF/LF PROPAGATION MODEL

The propagation model and computer program used to calculate signal levels is one that has been developed at NELC. This model, referred to as the NELC Integrated Prediction Program (IPP), obtains the full-wave solution for a waveguide whose upper boundary has arbitrary electron and ion density distributions with height and an adjustable surface conductivity. The model also allows for earth curvature, ionospheric inhomogeneity and anisotropy (resulting from the earth's magnetic field).

The basic propagation theory of the NELC model is described in reference 4. The electromagnetic waves are considered to propagate between the earth and the ionosphere as normal modes, analogous to microwave propagation in a lossy waveguide. The modal equation for propagation within the earth's ionosphere waveguide is solved for as many modes as required. The eigenvalues so obtained are then used in a modal summation to compute the total field at some distant point from the transmitter. In many instances, the earth-ionosphere waveguide can be considered to have constant propagation properties along the transmission path. The mode sum calculations made for these cases are referred to as horizontally homogeneous. In instances for which the earth-ionosphere waveguide cannot be considered as horizontally homogeneous but instead varies slowly along the propagation path, a WKB\* form of the mode sum is used (reference 19). This procedure was utilized in reference 12 to predict VLF signals as measured aboard an inflight aircraft.

\*WKB - Mathematical method for approximating the fields of a VLF/LF radio signal in regions where the propagation coefficients, such as excitation, phase velocity and attenuation, are slowly varying functions of distance.

For those cases where the changes in the propagation environment are too abrupt to be adequately simulated by the WKB procedure, mode conversion techniques must be applied. This type of computation is required for propagation through sunrise or sunset transition periods and in instances where the ground parameters change very rapidly along the propagation path. References 20 and 21 describe the NELC mode-conversion computer program and some results obtained when this model is applied to experimental data.

The NELC propagation model provides for the calculation of both vertical and horizontal electromagnetic fields and excited by dipoles of arbitrary orientation and elevation. The relevant equations and characteristic results are discussed in references 22, 23 and 24, while the computer program is discussed in references 25 and 26.

#### IV. DATA ANALYSIS - BACKGROUND AND PROCEDURE

##### A. Ionospheric Parameters

The important ionospheric parameter needed to simulate actual propagation data is the conductivity profile below which the radio waves must pass. This parameter is defined as the ratio of the ionospheric electron plasma frequency to the electron-neutral particle collision frequency and is a function of ionospheric height. Also, the plasma frequency is related to the density of free electrons at each height. That is, the ionospheric conductivity  $\omega_r$ , as a function of height  $Z$ , is given by:

$$\omega_r(Z) = \frac{\omega_p^2(Z)}{v(Z)} = \left[ \frac{N(Z)q^2}{\epsilon_0 M} \right] / v(Z) \quad (1)$$

where  $\omega_p(Z)$  is the electron plasma frequency

$N(Z)$  is the electron density in electrons per cubic centimeter

$v(Z)$  is the electron-neutral particle collision frequency

$q$  is electron charge

$M$  is electron mass

$\epsilon_0$  is the permittivity of free space.

Following Wait (reference 27) the conductivity parameter  $\omega_r(Z)$  may be considered of the exponential form  $\omega_r(Z) = \omega_0 \exp[\beta(Z-H')]$  (2)

where  $\beta$  is a gradient parameter in inverse height units

and  $H'$  is a reference height

The ionospheric parameters needed as inputs to the IPP computer program, then, are the electron density profile and the effective electron-neutral particle collision frequency profile. These terms may be assigned exponential relationships

with height and are identified by the terms  $\beta$ ,  $\text{km}^{-1}$  and  $H'$ , km. The  $\beta$ ,  $H'$  parameter combinations, for which field strength computations were carried out in this report, are given in Table VII.

The value of the electron density  $N(Z)$ , in electrons/cubic centimeter, is calculated as a function of height  $Z$ , in km, by the equation:

$$N(Z) = \{1.43 \cdot 10^7 \frac{\text{el}}{\text{cm}^3}\} \cdot \exp(-0.15 H') \cdot \{\exp[(\beta - 0.15)(Z - H')]\} \quad (3)$$

The collision-frequency profile for the computations was taken as

$$v(Z) = v_0 \exp(-\alpha Z) \quad (4)$$

where  $Z$  is the height in km,

$v_0$  is  $1.82 \times 10^{10}$  collisions/sec, and

$\alpha$  is  $0.15 \text{ km}^{-1}$ .

The exponential form of these profiles was chosen for the computations since attempts to find more complex shapes would likely require much additional effort. This is true because the state-of-the-art in analysis procedures allows for an almost infinite variety of profile shapes to be examined.

A further incentive for utilizing exponential type profiles was provided by the exceptional results obtained previously in predicting field strength with distance behavior from inflight measurements of VLF transmissions from Hawaii (see reference 12). Also, exponential profiles have been used successfully to predict multi-frequency transmissions from Hawaii to fixed receiver sites in southern California (see reference 14). It is possible that profiles of more

TABLE VII. EXPONENTIAL PROFILES FOR WHICH FIELD STRENGTH  
VALUES WERE COMPUTED

		<u>NIGHTTIME</u>					
$\beta$ (km <sup>-1</sup> )	H'(km)	<u>84.0</u>	<u>86</u>	<u>87</u>	<u>88</u>	<u>89</u>	<u>90</u>
0.2				X			
0.25							X
0.3				X	X	X	X
0.35				X			
0.4			X	X			
0.45						X	
0.5		X	X	X	X		
0.6				X	X		
0.7				X	X		
0.8				X	X		
0.9							
1.0				X	X		
1.2						X	
		<u>DAYTIME</u>					
$\beta$ (km <sup>-1</sup> )	H'(km)	<u>70</u>	<u>72</u>	<u>73</u>	<u>74</u>	<u>75</u>	
0.3			X		X	X	
0.35			X	X	X		
0.4			X		X		
0.5		X					

complex forms than the exponential could be found to produce a slightly better fit to the data in some instances but since the propagation paths being considered are quite long, any profile determined to produce a "best-fit" to the data is really an average profile for the total path.

**B. Field Strength vs. Distance Characteristics Computed from Exponential Profiles**

The field strength levels produced by IPP computations, using various values of the  $\beta$  and  $H'$  parameters of the electron density profile, are illustrated in figures 8 through 12 for the vertical electric field. All computations of field strength in this report are for an assumed horizontally homogeneous wave-guide where no ionospheric (or ground) variation along the propagation path is considered. Figure 8 shows a plot of received signal amplitude vs. propagation distance for 10.9 kHz transmissions. The variation in signal level produced by varying the gradient value,  $\beta(\text{km}^{-1})$ , while maintaining the scale height ( $H' \text{ km}$ ) at a constant value is presented. In this case,  $\beta$  was assigned values between 0.2 to  $0.7 \text{ km}^{-1}$  and  $H'$  was held at 87 km. It is observed that an increase in  $\beta$  produces an increase in mode structure. That is, the signal level is found to vary over a wider range in the regions of strong modal interference when the larger values of  $\beta$  are input to the computer program. Figures 11, 12, and 13 for 15.6 kHz, 28.0 kHz and 40.5 kHz, respectively, illustrate this same characteristic of increased variation in signal level with  $\beta$  value. There is a marked increase in fine structure of amplitude vs. propagation distance as the  $\beta$  value is increased on the higher frequencies. This is due to a greater number of wave-guide modes being effective at the higher frequencies. The larger values of  $\beta$  are found to produce the stronger mean signal level as is observed in the figures. This characteristic proves to be important in the determination of a "best fit" to the data.

Figure 12 is an example of the field strengths computed by maintaining the  $\beta$  value at some constant value and varying the  $H'$  parameter. It is determined that an increase of  $H'$  results in the field strength pattern, as a function

of propagation distance, being displaced outward away from the transmitter.

These two characteristics (i.e., increased signal level with increasing  $\beta$  and displacement of modal interference structure to larger distances with increase in  $H'$ ) prove to be very helpful in determining a "best fit" to the experimentally recorded data.

### C. Comparison of Predicted VLF/LF Signal Levels with Multi-frequency Propagation Data

Propagation data analyzed in the present report, as recorded by the NELC multi-frequency sounder, consists only of those measurements of the vertical electric field taken aboard aircraft flight numbers 24, 26, 27 and 28. Data from other flights will be presented in future reports.

These data were obtained for propagation across the Pacific Ocean between Hawaii and southern California. In particular, flights 24 and 26 were carried out while the path was in nighttime. (The total path is in darkness from 0130 U.T. until 1430 U.T.) Flights 27 and 28 were done during daytime conditions. (The total path is in daylight from 1430 U.T. until 0130 U.T.) Both the Hawaii and Sentinel, Arizona transmitters were in operation simultaneously for all flights. In general, the Hawaii transmissions were such that acceptable data were obtained on all four flights. The data recorded from the Sentinel sounder system did not prove to be of nearly as high quality. Most of the problems in the Sentinel system appear to originate from the inability of the aircraft receiver to gain and remain in synchronization with the transmitted signals. This is due to the poor signal-to-noise ratio available from the Sentinel antenna at the ranges for which data acquisition was attempted.

The propagation data used to determine ionospheric electron density profiles consists of all four flights from Hawaii transmissions, but only flight No. 27 for the Sentinel signals.

The procedure used in obtaining a "best-fit" profile to a specific data sample (i.e., 21.794 kHz on aircraft flight No. 24 using Hawaii transmissions) was to compare the vertical electric field strengths, computed as a function of distance from the transmitter to those fields recorded aboard the aircraft. The

fields were computed using a particular ( $\beta$ ,  $H'$ ) electron density profile as input to the IPP computer program. The electron density profiles described by the ( $\beta$ ,  $H'$ ) combinations, as listed in Table VII, were utilized in obtaining the "best-fit" profile for each set of recorded data.

In February 1969, multi-frequency sounder data was recorded via a nighttime aircraft flight between the Hawaii transmitter and Ontario, California. This data consisted of ten VLF frequencies between 9 and 30 kHz. Analysis of this data resulted in a choice of a "best-fit" profile for all ten frequencies of  $\beta = 0.5$ ,  $H' = 87$ . This profile has since been considered by NELC to be the "standard" nighttime low latitude profile. This profile did not, however, give an exceptional fit to the data at the lower VLF frequencies and, therefore, the recorded signal levels from this aircraft flight have been reconsidered in the present analysis.

The resulting "best-fit" electron density profiles to the 1969 multi-frequency field strength data and to that data of each of the aircraft flights, numbers 24, 26, 27 and 28, are listed in Table VIII.

The "best-fit" IPP computed fields are also compared with the recorded data in figures 13 through 18. In these figures the received signal amplitude of the vertical electric field  $E_v$ , in dB above 1  $\mu\text{V/m}$  for 1 kilowatt radiated power, are shown as a function of distance from the transmitter. In all cases only the horizontally homogeneous waveguide version of the IPP computer program was used to compute the field strength levels. The receiver height is 3 km (10,000 ft) for the 1969 data, while for the 1974 data this height is 9 km (30,000 ft). The exponential electron density profiles which were input to the IPP computer program to generate these fields are called out on the figures. The method of normalization and calibration as applied to the experimental data is discussed in the Appendix.

TABLE VIII. "BEST-FIT" EXPONENTIAL ELECTRON DENSITY PROFILES TO DATA RECORDED ABOARD AN AIRCRAFT.  
HAWAII TO SOUTHERN CALIFORNIA PROPAGATION PATH.

Aircraft Flight kHz	1969 Nighttime		No. 24 Nighttime		No. 26 Nighttime		No. 27 Daytime		No. 28 Daytime		No. 27 Daytime		
	$\beta$ ( $\text{km}^{-1}$ )	$H'$ (km)	kHz	$\beta$ ( $\text{km}^{-1}$ )	$H'$ (km)	$\beta$ ( $\text{km}^{-1}$ )	$H'$ (km)	$\beta$ ( $\text{km}^{-1}$ )	$H'$ (km)	kHz	$\beta$ ( $\text{km}^{-1}$ )	$H'$ (km)	
9.340	0.35	87	9.340	0.3	87	0.3	89	0.3	72	0.3	75	9.336	0.3
10.897	0.4	87	10.897	0.4	86	0.3	89	0.3	72	0.3	75	14.003	0.3
14.010	0.5	87	15.567	0.5	86	0.4	88	0.3	72	0.3	75	17.115	0.3
15.567	0.5	87	21.794	0.7	87	0.5	88	0.3	72	0.3	75	24.895	0.3
17.124	0.5	87	28.020	1.0	88	0.5	89	0.3	73	0.3	75	28.007	0.3
21.794	0.5	88	37.361	1.0	88	0.6	88	0.35	73	0.3	75	34.231	0.3
24.908	0.5	88	40.475	1.2	88	0.6	88	0.35	73	0.3	75	38.898	0.3
26.464	0.5	88	46.702	1.2	88	0.7	88	0.35	73	0.3	75	43.566	0.3
28.020	0.5	88	52.929	1.2	88	0.7	88	0.35	73	0.3	75	49.790	0.3
31.134	0.6	88	56.042	1.2	88	0.7	88	0.35	73	0.3	75	56.104	0.3

→ Hawaii Transmitter → Sentinel Transmitter →

An approximate relationship between  $\beta$  and propagation frequency for nighttime is given by:

$$\beta = 0.72 \times 10^3 \log_{10} (f \text{ kHz}) - 0.40 \quad (5)$$

In the case of propagation when the path is in daylight, the computed fields are shown for the best-fit profile (see Table VIII) as well as those fields computed by  $\beta = 0.5$ ,  $H' = 70$ . Observation of figures 13 and 14 illustrates that fields computed, using either the "best-fit" profile from Table VIII or ( $\beta = 0.5$ ,  $H' = 70$ ), are identical for frequencies below 15 kHz. The fact that the "best-fit" profiles for aircraft flight numbers 27 and 28 are not the same illustrates the time variability characteristic of daytime ionospheric propagation.

The result of the poor signal-to-noise ratio in the Sentinel data is very obvious in figure 15. The predictions do, however, tend to produce the general form of the field strength vs. distance curves.

In figures 16, 17, and 18, experimental nighttime data are compared with fields computed from "best-fit" profiles only. Of interest is the observation that the "best-fit" exponential profile varies with propagation frequency. As the frequency is increased, the value of the conductivity gradient,  $\beta$ , is found to increase. The scale height parameter  $H'$ , however, is found to remain somewhat constant at the higher frequencies.

The electron density profiles determined to fit both the 1969 data, figure 16, and the data from aircraft flight No. 26, figure 17, appear to follow a similar relationship between propagation frequency and the profile gradient parameter,  $\beta$ . In the case of aircraft flight No. 24, figure 18, the recorded data tends to require a larger value of  $\beta$  in order to produce an acceptable fit to the field strength levels. The explanation as to the reason for the differences in "best-fit" electron density profile between No. 24 and No. 26 data is not completely understood. The results suggest that the effective ionosphere actually changed between the nights for which the two aircraft flights recorded data.

#### D. Airborne Propagation Data from an Operational Transmitter

An example of nighttime vertical electric field ( $E_V$ ) and horizontal electric field ( $E_H$ ) excited by NAA on 17.8 kHz is illustrated in figure 19. These data are recorded at 30,000 feet altitude during a flight from Mildenhall (England) to Griffiss Air Force Base (New York) on 18-19 January 1974. The computed fields illustrated in figure 19 were obtained with the IPP computer program assuming a  $\beta = 0.5$ ,  $H' = 80$  exponential electron density profile. The "standard" nighttime low latitude profile,  $\beta = 0.5$ ,  $H' = 87$ , predicted an  $E_V$  modal interference null at 2.9 megameters, instead of the 2.2 megameter distance where it was measured, and the predicted  $E_H$  field was generally 10 dB higher than measured. The  $E_V$  and  $E_H$  fields computed with the  $\beta = 0.5$ ,  $H' = 80$  km exponential profile agree better with the measured data.

Calculations made with the propagation prediction computer program have illustrated that the amplitude of the horizontal  $E_H$  field is more sensitive to changes in the  $H'$  parameter than those of the corresponding vertical,  $E_V$ , field. It has been determined that a 1 km increase in  $H'$  results in a 1 dB increase in signal level for the  $E_H$  field.

VLF/LF propagation data recorded on other aircraft flights, during the October and January-February test series, will be analyzed in future reports.

### E. TACAMO Propagation Data

On the night of 30 January 1974, a DCA MEECN test of airborne VLF/LF range performance in the Pacific Ocean was conducted. A TACAMO aircraft was transmitting from the nominal position  $31^{\circ}\text{N}$ ,  $169^{\circ}\text{W}$ . During these airborne transmissions, the RADC KC-135 aircraft was flying at 29,000 feet from March AFB to Hickam AFB making measurements of the fields using both the vertical and horizontal loop antennas. The TACAMO  $E_H$  measured fields are plotted in figure 20 as a function of distance.

During these measurements, TACAMO alternated between orbiting and flying straight and level along the sides of a square. The altitude and orientation angle ( $\theta_T$ ) of TACAMO relative to the propagation path toward the RADC KC-135 aircraft is also indicated in figure 20. Much of the variability indicated by the data is due to the various orientations of the TACAMO aircraft and changes in inclination of the long trailing wire antenna (LTWA). The signal is particularly variable during the TACAMO orbiting periods. During these maneuvers, TACAMO transmissions alternated between FSK and CW as indicated by the dashed and solid lines respectively. Generally the signal level recorded during FSK transmissions is lower than that recorded during CW transmissions because of the reduced duty cycle within the effective bandwidth of the recording receiver. However, in figure 20, the actual dB difference in recorded signal level between FSK and CW transmissions cannot be determined because of variability in aircraft attitude and associated changes in the orientation of the LTWA.

During three periods of time, TACAMO was oriented such that CW signals were transmitted broadside from the LTWA to the receive aircraft. These field intensity data are plotted in figure 21, together with IPP computed fields.

The computed fields are for a transmitting antenna inclined 80° from the vertical (nearly horizontal) to represent straight flight conditions. The four curves are for the four azimuthal orientations relative to the propagation path (i.e.,  $\theta = 0^\circ$  and  $180^\circ$  for end-on transmission; and  $\theta = 90^\circ$  and  $270^\circ$  for broadside transmission). The predicted  $E_H$  field is higher for broadside orientation as expected and the three data points average about 3 to 4 dB above the predicted value, this is attributed to experimental uncertainty or improper ionospheric profile, (assumed to be exponential  $\beta = 0.5$ ,  $H' = 87$ ).

#### F. ABNCP Window Antenna Data

Other airborne measurements of horizontal fields of interest were made of Airborne Command Post (ABNCP) transmissions from nominally 36°N, 74°W on 30 November 1973. The data were recorded aboard a United Air Lines 727 commercial passenger flight about 350 to 500 kilometers west of Chicago enroute to San Jose, California. The receiving system consisted of the battery-operated equipment shown in the block diagram of figure 22, most of which was in a briefcase at the operator's feet. The antenna system consisted of wire mesh placed against the inside surface of the two windows directly opposite each other across the cabin. A battery-operated preamplifier, just beneath each window, converted the high impedance "plate antenna" signal source to a low impedance signal for mixing in the "combiner" shown in figure 22. A switch on the "combiner" allowed the VLF/LF signal voltage from each preamplifier to be monitored separately or the voltage sum or difference to be monitored. Measurements and analysis have indicated that for the most part, the voltage sum is proportional to the  $E_y$  field and the voltage difference is proportional to the  $E_H$  field when the aircraft is level and flying toward or away from the signal source.

The daytime data, recorded about 1603 to 1700 Z (1130 to 1200 EST), are plotted in figure 23, along with predicted fields. The effective height ( $h_e$ ) and length ( $l_e$ ) of the window antenna system, needed to normalize the data to absolute field intensity, was determined by monitoring during this flight the fields excited by the Air Force 37.2 kHz transmissions from Hawes, California, located nominably at 35°N, 117.5°W. Since reliable daytime prediction of  $E_y$  fields within CONUS can be made, the relative  $E_y$  37.2 kHz and ABNCP signals measured aboard the United 727 airplane were used to obtain  $h_e$ . When the aircraft banks at low altitude as it approaches or departs an airport, the window antenna

difference voltage is proportional to  $E_V \cdot \sin b$ , where  $b$  is the airplane bank angle.

The agreement between the ABNCP data and the prediction illustrated in figure 23 appears better than the expected experimental uncertainty but indicates the validity of  $E_H$  as well as  $E_V$  fields computed with the NELC VLF/LF IPP computer program.

#### G. Continuous Ground Recording of VLF/LF Sounder Signals

During October 1973, while airborne measurements of VLF/LF signal levels were being conducted, ground-based receiver systems were also installed at Glasgow AFB, Montana and Saskatoon, Saskatchewan, Canada. The transmitted signals originated from the NELC multi-frequency sounder located at Sentinel, Arizona.

The propagation distances involved were approximately 1800 km from Sentinel to Glasgow, and 2300 km from Sentinel to Saskatoon. The sounder was operated continuously for a period of three weeks and specific examples of the recorded signal levels are shown in figures 24, 25, and 26.

Figure 24 shows signal amplitudes recorded at Saskatoon on October 3, 4, and 5 in the frequency range from 10.9 kHz to 55.0 kHz. These data are calibrated in dB above  $1\mu\text{V/m}$ ; however, they have not been normalized to 1 KW of radiated power. At the receiver site, sunset occurs near 0100 U.T., while sunrise occurs close to 1300 U.T. These time periods are easily discernible on several frequencies in that the signal level becomes very weak and then recovers at a slightly later time. A relatively stable and repeatable daytime signal level is apparent at all frequencies whereas the nighttime signal level is rather variable, particularly on 15.6, 28.0 and 49.8 kHz. Relatively slight changes in the ionospheric profile properties, such as its height, may cause changes in the position of a signal minimum along the propagation path. This effect can produce large changes in the signal amplitude as the signal null moves through the receiver site. This phenomenon was illustrated in figure 12 where it is observed that, at 4 Mm, the signal level may vary by 30 dB as the ionosphere changes in height by 2 km. The stability of the daytime data in figure 24 indicates that no significant modal interference minima occur in the sounder frequency band at the

Saskatoon receiver site. Figure 25 presents sounder data recorded at Saskatoon on 12, 14 and 15 October. These data indicate that the ionospheric properties may have changed since the earlier time period. The signal levels at 15.6 and 43.6 kHz show increased variability.

Figure 26 shows sounder data recorded at Glasgow AFB on 12, 14 and 15 October. These data were obtained simultaneously with that of figure 26. It is observed that at this shorter propagation distance (1800 km), as compared to that for Saskatoon (2300 km), the signal amplitudes at 15.6 and 43.6 kHz show much less amplitude variability during nighttime. This result is typical of the modal interference nulls which exist as a function of propagation distance in that the phasing between the individual waveguide modes changes with propagation distance. This property leads to regions of constructive modal interference and regions of destructive modal interference (nulls) along the propagation path.

All data recorded at the fixed site receivers were obtained jointly for the DCA-Tri-Service propagation program to obtain time variability propagation data and for the Office of Naval Research to examine solar particle precipitation events.

## V. CONCLUSION

The ability of the propagation prediction computer program "IPP", (reference 25), to predict realistic VLF/LF signal levels is illustrated very distinctively in this report. Comparisons between predicted and measured values of electric field strength, as presented in the figures, show that the complicated interference structure characteristic of radio wave propagation at these frequencies may be stimulated very closely if the effective ionospheric propagation parameters are known with sufficient accuracy.

For propagation at midlatitudes in a winter daytime environment, the use of approximately identical exponential electron density profiles at frequencies between 9 and 56 kHz will adequately predict the measured signal levels. The values of the "best-fit" exponential electron density profiles were  $\beta = 0.3 \text{ km}^{-1}$  and  $H' = 72=75 \text{ km}$ .

In order to best-fit the winter nighttime fields, it was found necessary that the value of the exponential electron density gradient parameter  $\beta (\text{km}^{-1})$  increase with frequency. The ranges of this parameter varied from 0.3 at 9.4 kHz to 0.7 or 1.2 at 56 kHz. The value of the  $H'$  parameter was determined to vary between 86 and 89 km, depending on frequency and the aircraft flight from which the experimental data were recorded. The variations in  $\beta$  from 0.7 to 1.2 at the higher frequencies on two different nights illustrate changes in the ionosphere for the two nights. The fact that different best-fit exponential profiles are obtained over the VLF/LF band at night suggests the possibility that a more general multi-parameter profile is needed to represent VLF/LF propagation rather than the two parameter exponential representation.

Based on the field strength levels recorded over the midlatitude Hawaii to Southern California transmission path the following exponential profiles most accurately describe the propagation data.

**Table IX:**  
RECOMMENDED ELECTRON DENSITY  
PROFILES FOR USE IN PROPAGATION  
PREDICTIONS (midlatitude)

DAYTIME Winter		NIGHTTIME Winter	
Frequency (kHz)	Profile $\beta$ ( $\text{km}^{-1}$ ), $H'$ (km)	Frequency (kHz)	Profile $\beta$ ( $\text{km}^{-1}$ ), $H'$ (km)
9-60	$\beta=0.3$ , $H'=74$	below 10	$\beta=0.3$ , $H'=87$
		10 - 15	$\beta=0.4$ , $H'=87$
		15 - 25	$\beta=0.5$ , $H'=87$
		25 - 30	$\beta=0.6$ , $H'=88$
		30 - 40	$\beta=0.7$ , $H'=88$
		40 - 60	$\beta=0.8$ , $H'=88$

These ionospheric profiles result in predictions of signal amplitudes which on the average are within 2 dB for daytime and within 3 dB for nighttime of those amplitudes recorded aboard the inflight aircraft.

Horizontally polarized (TE) as well as vertically polarized (TM) electric fields are important for meeting the MEECN requirement for a viable communication system involving the airborne assets. Calculations made with the propagation

prediction computer program, (reference 25), and which agree with measured data, indicate that stronger signal levels can be obtained for the horizontal electric field than for the vertical electric field at operational aircraft altitudes. Broadside transmission from an airborne horizontal radiator during nighttime is an example. Calculations made with the propagation prediction computer program have also illustrated that the amplitude of the horizontal electric field,  $E_H$ , is more sensitive to changes in the  $H'$  parameter than those of the corresponding vertical electric field,  $E_V$ . It has been determined that a 1 km increase in  $H'$  results in a 1 dB increase in signal level for the  $E_H$  field. The validity of the computations and the utility of polarization diversity reception systems aboard aircraft should be investigated thoroughly to quantify the dB improvement possible for 99% time availability of operational VLF/LF propagation links.

## VI. RECOMMENDATIONS

The use of exponential electron density profiles, as presented in Table IX, is recommended in analyses of deployment, operation and evaluation of VLF/LF MECN assets involving mid-latitude propagation paths in the winter.

In a previous report, (reference 16), the profile  $\beta = 0.5 \text{ km}^{-1}$ ,  $H' = 87$  was determined to produce acceptable nighttime TM signal levels throughout the 10-30 kHz frequency band and its use was suggested for frequencies up to 60 kHz. Utilization of the nighttime profiles, as presented in Table IX, results in an improvement in predicting signal amplitudes. These improvements are a function of propagation range and the average improvement over the 4 Mn path from Hawaii to Southern California are shown in Table X.

Table X:  
IMPROVEMENTS IN THE ACCURACY  
OF PREDICTED SIGNAL LEVELS OVER  
THAT OBTAINED FROM PREVIOUSLY  
RECOMMENDED PROFILE  
(midlatitude - winter)

Frequency (kHz)	dB
28.0	1
37.4	3
40.5	4
46.7	5
52.9	9
56.0	9

As suggested earlier both seasonal and latitudinal variations occur in the ionospheric parameters and hence the value of  $\beta$  and  $H'$  as presented in Table IX apply only to propagation during the winter months for midlatitudes. Application to other conditions may yield as much as 6 dB variance in predicted performance. Therefore, the accuracy of the VLF/LF propagation procedure for other seasons of the year and for other geographical latitudes needs to be examined.

## VII. APPENDIX A- Notes on Calibration and Normalization Procedures

The electric field intensity  $E$  of a radio wave is typically determined from the relationship:

$$E = V/h_e \quad (A-1)$$

where ( $V$ ) is the voltage available at a receive antenna, ( $h_e$ ) is the "effective height" in meters of the antenna and ( $E$ ) is then in volts/meter.

The open circuit "effective height" of a vertical monopole, which is short compared to the wavelength of the radio wave, is  $1/2$  the physical length of the antenna. For a loop antenna, whose dimensions are small compared to a wavelength, the open circuit "effective height" is given by:

$$h_e = \frac{2\pi N A}{\lambda} \sin \phi \quad (A-2)$$

where  $N$  is the number of turns in the winding of the loop,  $A$  is the area of the plane of the loop,  $\lambda$  is the wavelength of the radio wave, and  $\phi$  is the angle between the plane of the loop and the direction of the magnetic component of the electromagnetic field.

The usual procedure for determining the electric field intensity ( $E$ ) of the radio wave is to receive the propagated signal with a loop antenna. The reason for this is that the output voltage of the loop is at a lower impedance than that of a whip antenna. Also, an exact knowledge of the load impedance is generally not as critical for a loop measurement as would be required for measurements made using the whip antenna.

The "effective height" of a long wire receiving antenna system may be determined by measuring the voltage ( $V$ ), available at the terminals of the antenna, when the antenna is located in a known field ( $E$ ). The "effective height" ( $h_e$ ) is computed by using these measurements in equation A-1. With the assumption that ( $h_e$ ) remains constant for a given time period over which data is recorded, voltage meas-

urements can be converted to field strengths.

Propagation data recorded aboard an inflight aircraft can be normalized to an absolute field intensity for an assumed radiated power. This may be done without knowing the "effective height" of the aircraft receive antenna or the actual radiated power of the transmitter. The procedure makes use of the relation that the vertical electric field at ground level produced by a vertical transmitting antenna, which is short compared to a wavelength, is given by

$$E(\mu\text{V/m}) = \frac{3.0 \times 10^5 \cdot P_r^{1/2} [\text{KW}]}{d[\text{km}]} \quad (\text{A-3})$$

where  $P_r$  is the radiated power and  $d$  is the propagation distance.

Under the assumption that the vertical electric fields radiated off the ends of long horizontal antennas will be described by equation A-3, the aircraft data described in this report are normalized to dB above 1 $\mu\text{V/m}$  for 1 KW radiated power.

On many of the data acquisition flights, which were carried out for the Tri-Service propagation program, it was possible to record signal levels continuously as the aircraft passed over the transmitter and proceeded on to its destination. These radial flights, together with navigation data, are used to obtain plots of field intensity vs. distance from the signal source. The data reduction computer program, which operates on the raw data as obtained from the digital recording system, allows for the field strength levels to be plotted in units of relative dB. When plots of the received signal level in dB (i.e., 20 $\log V$ ) vs. log distance are obtained, the near radiation field is generally a straight line with a slope of 20 dB per decade of distance. A "best-fit" straight line through these voltage levels (in dB), recorded in the (ground wave only) region of the propagation data, provides a technique for averaging the measured

values.

From equation A-3, the field at 30 km is 10 millivolts/meter for 1 kilo-watt radiated power. This corresponds to a value of 80 dB above  $1\mu\text{V}/\text{m}$  for 1 KW radiated power. To normalize the propagation data recorded aboard the aircraft to 1 KW of radiated power, the data plots of received signal in relative dB (i.e.,  $20 \cdot \log V$ ) vs. distance are adjusted by a constant dB value so that the "best-fit" straight line field has a defined value of 80 dB above  $1\mu\text{V}/\text{m}$  at 30 km.

Results presented in reference 28 show that the near radiation field of a transmitting antenna does not vary inversely with distance for all conditions of aircraft altitude, ground conductivity, and frequency. Under these circumstances, the inverse distance variation assumed to average the close in radial data would be replaced with the actual functional variation expected for 1 KW radiated power.

VIII. APPENDIX B - Figures 1 through 26

<u>Figure</u>	<u>Title</u>	<u>Page</u>
1.	Aircraft Flight Paths	
2.	Block Diagram of Transmit/Receive Systems	
3.	Block Diagram of Receiver System	
4.	Block Diagram of Correlation Receiver Unit	
5.	KC-135 Longwire Antennas	
6.	KC-135 Aircraft Showing Crossed Loop Assembly	
7.	VLF/LF Antenna Subsystem	
8.	A Comparison of Computed Field Strength as a Function of $\beta$ for Constant $H'$ . (10.9 kHz)	
9.	A Comparison of Computed Field Strength as a Function of $\beta$ for Constant $H'$ . (15.6 kHz)	
10.	A Comparison of Computed Field Strength as a Function of $\beta$ for Constant $H'$ . (28.0 kHz)	
11.	A Comparison of Computed Field Strength as a Function of $\beta$ for Constant $H'$ . (40.5 kHz)	
12.	A Comparison of Computed Field Strength as a Function of $H'$ for Constant $\beta$ (15.6 kHz)	
13.	Measured and Computed Daytime Signal Levels on the Hawaii to Sentinel Path. Hawaii Transmitter, Aircraft Flight No. 27, February 2, 1974	
14.	Measured and Computed Daytime Signal Levels on the Hawaii to Sentinel Path. Hawaii Transmitter, Aircraft Flight No. 28, February 3, 1974	
15.	Measured and Computed Daytime Signal Levels on the Hawaii to Sentinel Path. Sentinel Transmitter, Aircraft Flight No. 27, February 2, 1974.	
16.	Measured and Computed Nighttime Signal Levels on the Hawaii to Ontario, California Path. Hawaii Transmitter, February 1969.	
17.	Measured and Computed Nighttime Signal Levels on the Hawaii to Sentinel Path. Hawaii Transmitter, Aircraft Flight No. 26, February 1, 1974.	

<u>Figure</u>	<u>Title</u>	<u>Page</u>
18.	Measured and Computed Nighttime Signal Levels on the Hawaii to Sentinel Path. Hawaii Transmitter, Aircraft Flight No. 24, January 30, 1974.	
19.	NAA 17.8 kHz Nighttime $E_Y$ and $E_H$ Data Recorded on 18-19 January Aboard the RADC DC-135 Airplane. The Data are Compared with IPP-Computed Fields.	
20.	Tacamo, 27.0 kHz Nighttime $E_H$ Data Recorded on 30 January 1974 Aboard the RADC KC-135 Airplane.	
21.	Tacamo, 27.0 kHz CW Transmission $E_H$ Data Recorded Aboard the RADC Airplane When Tacamo was flying straight and Oriented for Broadside Radiation Toward the Receiver. The IPP-Computed $E_H$ Fields are Shown for Comparison.	
22.	Block Diagram of VLF/LF Window Antenna Receiving System.	
23.	Comparison of Measured 44 kHz ABNCp Signal with Predicted Values. The Predicted Fields are for $\theta = 90^\circ$ , i.e., Broadside Radiation From ABNCp. Variability with ABNCp Orientation is Indicated by the Bars at 1.6 Mm and 1.8 Mm Where the $E_Y(0)$ and $E_H(0)$ Data Were Recorded.	
24.	Sentinel Sounder Relative Amplitude Variation Recorded at Saskatoon, Canada, October 3, 4, 5, 1974.	
25.	Sentinel Sounder Relative Amplitude Variation Recorded at Saskatoon, Canada, October 12, 14, 15, 1974.	
26.	Sentinel Sounder Relative Amplitude Variation Recorded at Glasgow, Montana, October 12, 14, 15, 1974.	

## IX. TABLES

- I. Locations and Coordinates of Air Bases and Other Sites Related to Aircraft Flight and Data Acquisition.
- II. Location, Coordinates and Frequency of VLF/LF Transmitter Sites Used on Aircraft Flights.
- III. Aircraft Flight Paths for October 1973.
- IV. Aircraft Flight Paths for January - February 1974.
- V. Frequency Sets for NELC Multi-Frequency Sounder Transmissions.
- VI. Identification of Experimental Parameters for Each Aircraft Flight as Related to the Multi-Frequency Sounder.
- VII. Exponential Profiles for Which Field Strength Values Were Computed.
- VIII. "Best-Fit" Exponential Electron Density Profiles to Data Recorded Aboard an Aircraft.
- IX. Recommended Electron Density Profiles For Use in Propagation Predictions (midlatitudes).
- X. Improvements in the Accuracy of Predicted Signal Levels Over That Obtained From Previously Recommended Profiles (midlatitude - winter).

X. REFERENCES

1. Budden, K. G., Radio Waves in the Ionosphere, Cambridge University Press, 1961.
2. Budden, K. G., The Waveguide Mode Theory of Wave Propagation, Prentice Hall, Inc., Englewood Cliffs, New Jersey, 1961.
3. Wait, J. R., Electromagnetic Waves in a Stratified Media, Pergamon Press, Inc., Elmsford, New York. 1962.
4. Pappert, R. A., E. E. Gossard, and I. J. Rothmuller, "A Numerical Investigation of Classical Approximations Used in VLF Propagation," Radio Science, v. 2, p. 387-400, April 1967.
5. Office of Telecommunications, Institute for Telecommunication Sciences, OT/ITS RR 11, A Wave Hop Propagation Program for an Anisotropic Ionosphere, by L. A. Berry and J. E. Herman, April 1971.
6. Naval Weapons Center TP 4856, An Automatic Method for Deducing D-Region Electron Densities from VLF Sounder Data, by J. N. Martin, January 1970.
7. Naval Electronics Laboratory Center Report 1773, Variations in OMEGA Propagation Parameters, by R. J. Gallenberger and E. R. Swanson, 25 June 1971.
8. Naval Electronics Laboratory Center Technical Document 139, Propagation Analysis of Diversity for VLF Communication Systems, by J. E. Bickel, D. G. Morfitt, I. J. Rothmuller and W. F. Moler, 24 September 1971.
9. Naval Electronics Laboratory Center Report 1833, Measurements of Vertical and Horizontal VLF Fields Excited by an Elevated Arbitrarily Oriented Antenna, by J. E. Bickel, 21 July 1972.
10. Naval Electronics Laboratory Center Report 1834, Effect of the VLF Propagation Channel on Spread Spectrum Communication Systems, by I. J. Rothmuller, July 1972.

11. Naval Ordnance Laboratory Corona Report 722, Multiple-Frequency Oblique-Incidence VLF Ionospheric Sounder, by D. A. Wulffing and V. E. Hildebrand, 5 May 1967.
12. Bickel, J. E., J. A. Ferguson and G. V. Stanley, "Experimental Observation of Magnetic Field Effects on VLF Propagation at Night," Radio Science, p. 19-25, January 1970.
13. Naval Electronics Laboratory Report 1798, Analysis of a Multimode Propagation Concept for Predicting VLF Signal Strengths at Night, by D. G. Morfitt, 9 December 1971.
14. Naval Electronics Laboratory Center Technical Report TR 1854, Computer Techniques for Fitting Electron Density Profiles to Oblique-Path VLF Propagation Data, by D. G. Morfitt, 16 January 1973.
15. Naval Research Laboratory Report 6359, An Investigation of the Modal Interference of Very-Low-Frequency Radio Waves, by F. J. Rhoads and W. E. Garner, 27 October 1965.
16. Defense Communications Agency, 960-TP-74-5, Comparison of Predicted VLF/LF Signal Levels with Propagation Data.
17. Naval Electronics Laboratory Center Report 653, Broad-B and VLF Transmitting Staggerer-Tuned Dipole, by E. W. Seeley and D. A. Wulffing, 18 May 1966.
18. Naval Electronics Laboratory Center Report, VLF Transmitting Antennas at Sentinel, Arizona, by E. W. Seeley and J. F. Theisen, in publication.
19. Wait, J. R., "Two-Dimensional Treatment of the Mode Theory of the Propagation of VLF Radio Waves," Radio Science, v. 68D, p. 81-95, January 1964.
20. Naval Electronics Laboratory Center Interim Report 722, Mode Conversion Program for an Inhomogeneous Anisotropic Ionosphere, by R. A. Pappert and L. R. Shockley, 1 May 1972.

21. Pappert, R. A. and F. P. Snyder, "Some Results of a Mode-Conversion Program for VLF," Radio Science, v. 7, p. 913-923, October 1972.
22. Pappert, R. A. "Effects of Elevation and Ground Conductivity on Horizontal Dipole Excitation of the Earth-Ionosphere Waveguide," Radio Science, v. 5, p. 579-590, March 1970.
23. Pappert, R. A. and J. E. Bickel, "Vertical and Horizontal VLF Fields Excited by Dipoles of Arbitrary Orientation and Elevation," Radio Science, v. 5, p. 1445-1452, December 1970.
24. Naval Electronics Laboratory Center Technical Report 1833, Measurements of Vertical and Horizontal VLF Fields Excited by an Elevated, Arbitrarily Oriented Antenna, by J. E. Bickel, 21 July 1972.
25. Naval Electronics Laboratory Center Interim Report 702, A Fortran Program for Waveguide Propagation Which Allows for Both Vertical and Horizontal Dipole Excitation, by R. A. Pappert and L. R. Shockley, 15 June 1970.
26. Naval Electronics Laboratory Center Interim Report 713, WKB Mode Summing Program for VLF/ELF Antennas of Arbitrary Length, Shape and Elevation, by R. A. Pappert and L. R. Shockley, 2 June 1971.
27. Wait, J. R. and K. P. Spies, Characteristics of the Earth-Ionosphere Waveguide for VLF Radio Waves, National Bureau of Standards Technical Note 300, 30 December 1964.
28. Defense Communications Agency Report, Horizontal Antenna Transmitting characteristics at VLF/LF by R. A. Pappert, and E. W. Seeley in Publication.

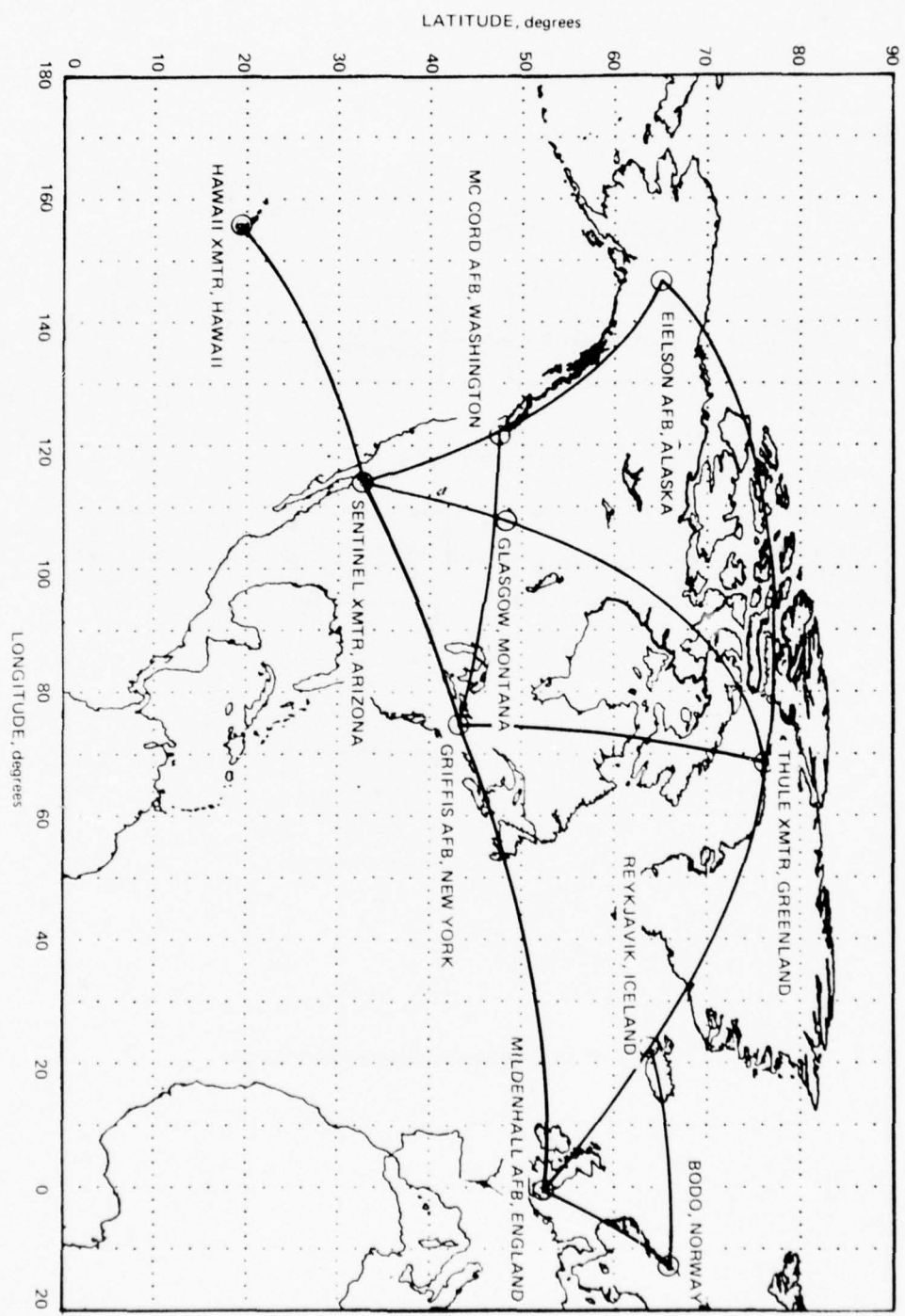


Figure 1. Aircraft flight paths.

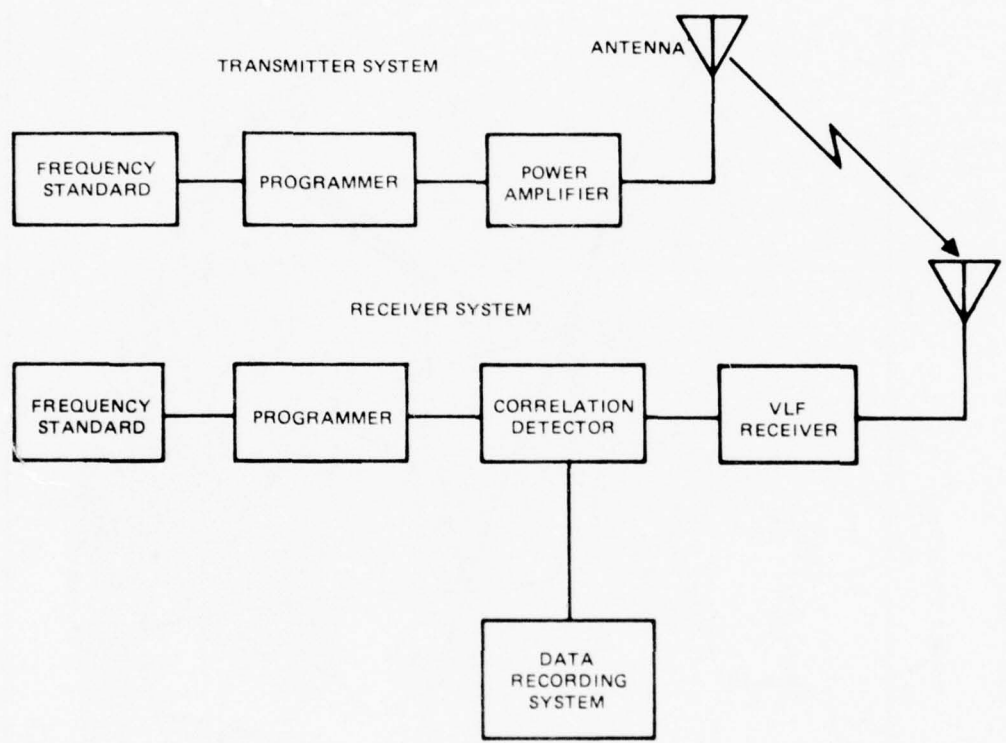


Figure 2. Block diagram of transmit/receive systems.

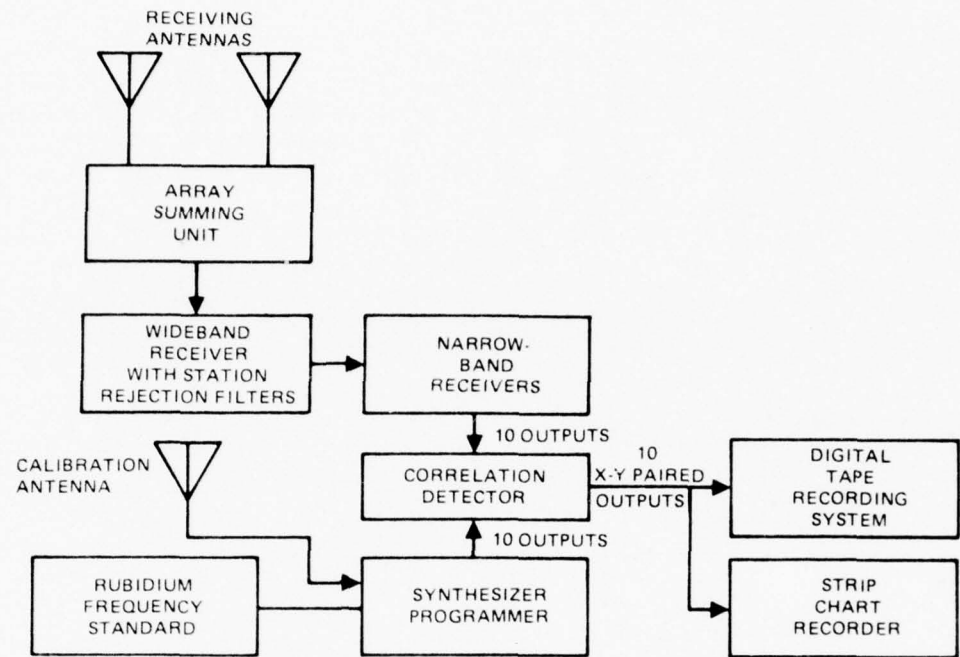


Figure 3. Block diagram of receiver system.

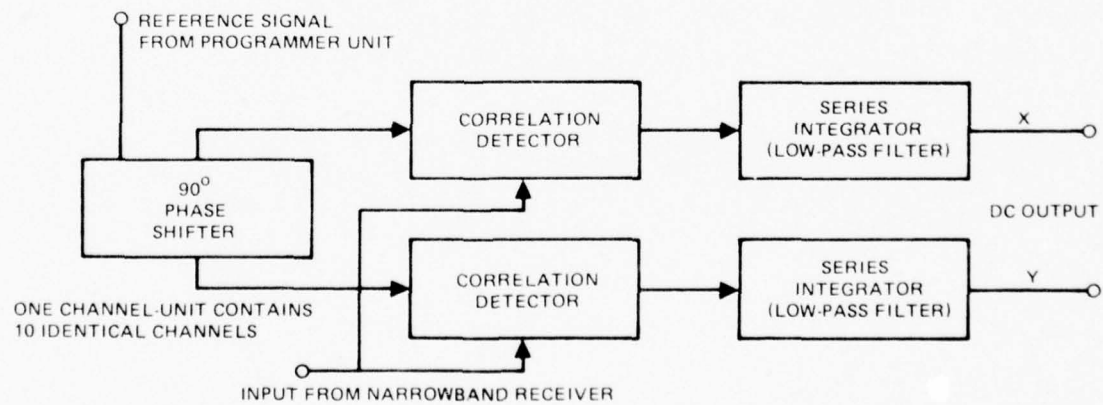


Figure 4. Block diagram of correlation receiver unit.

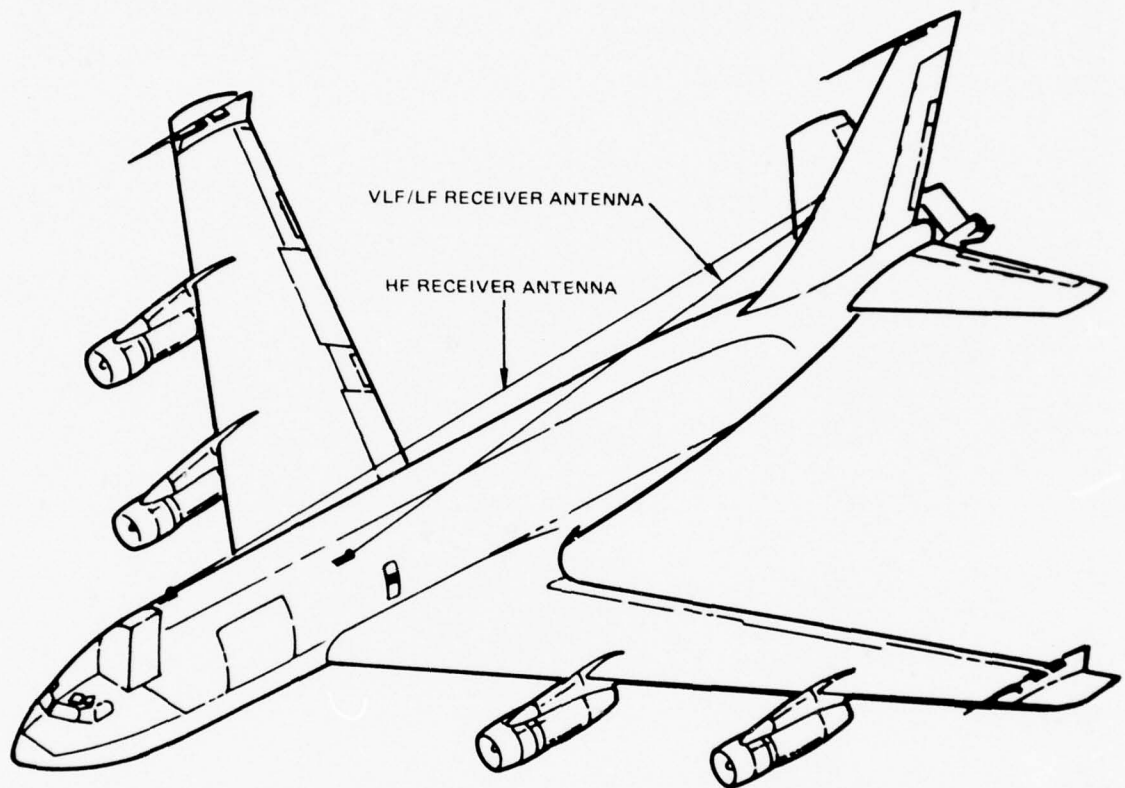


Figure 5. KC-135 longwire antennas.

**Figure 6. KC-135 Aircraft Showing Crossed Loop Assembly**



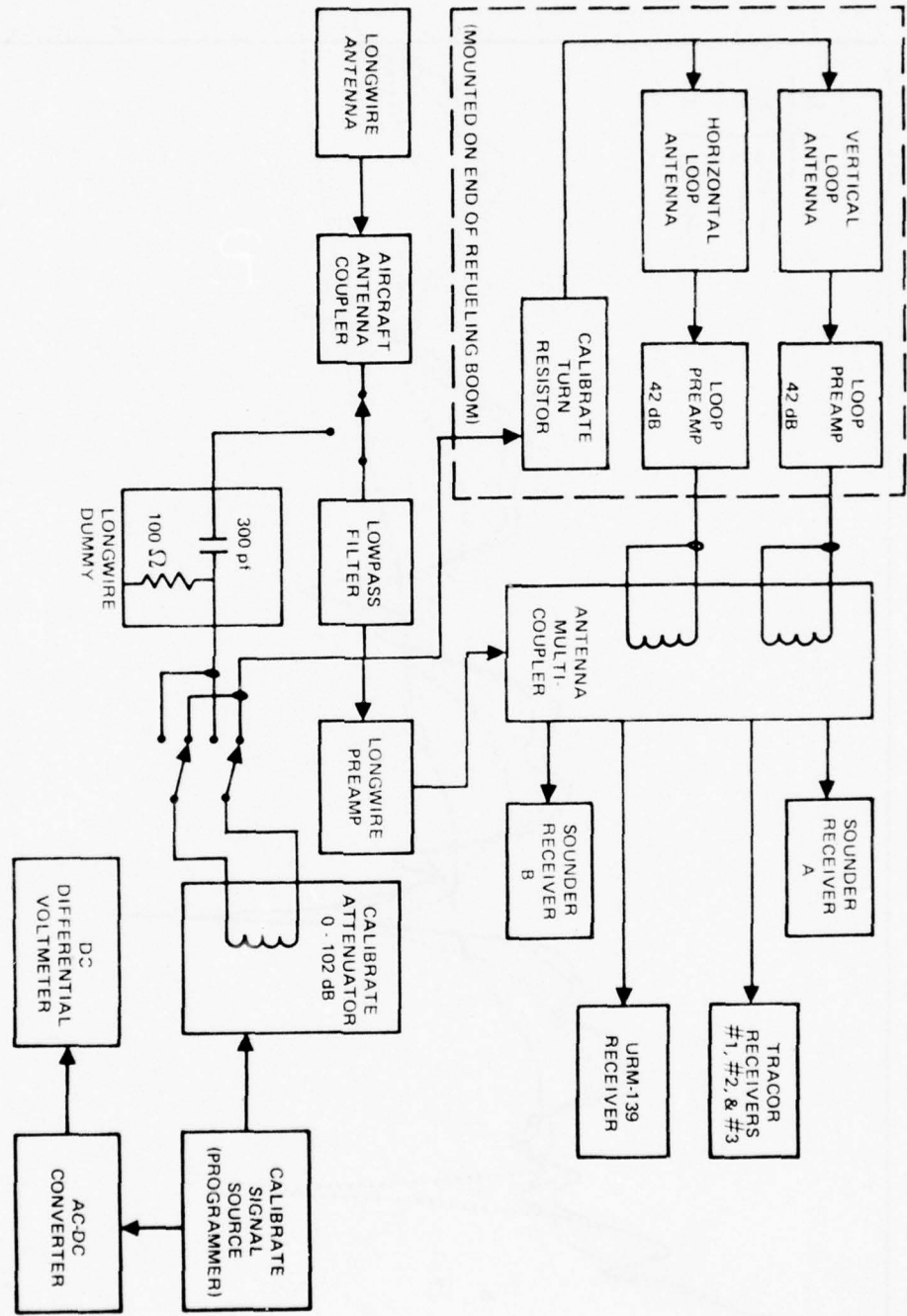


Figure 7. VLF/LF antenna subsystem.

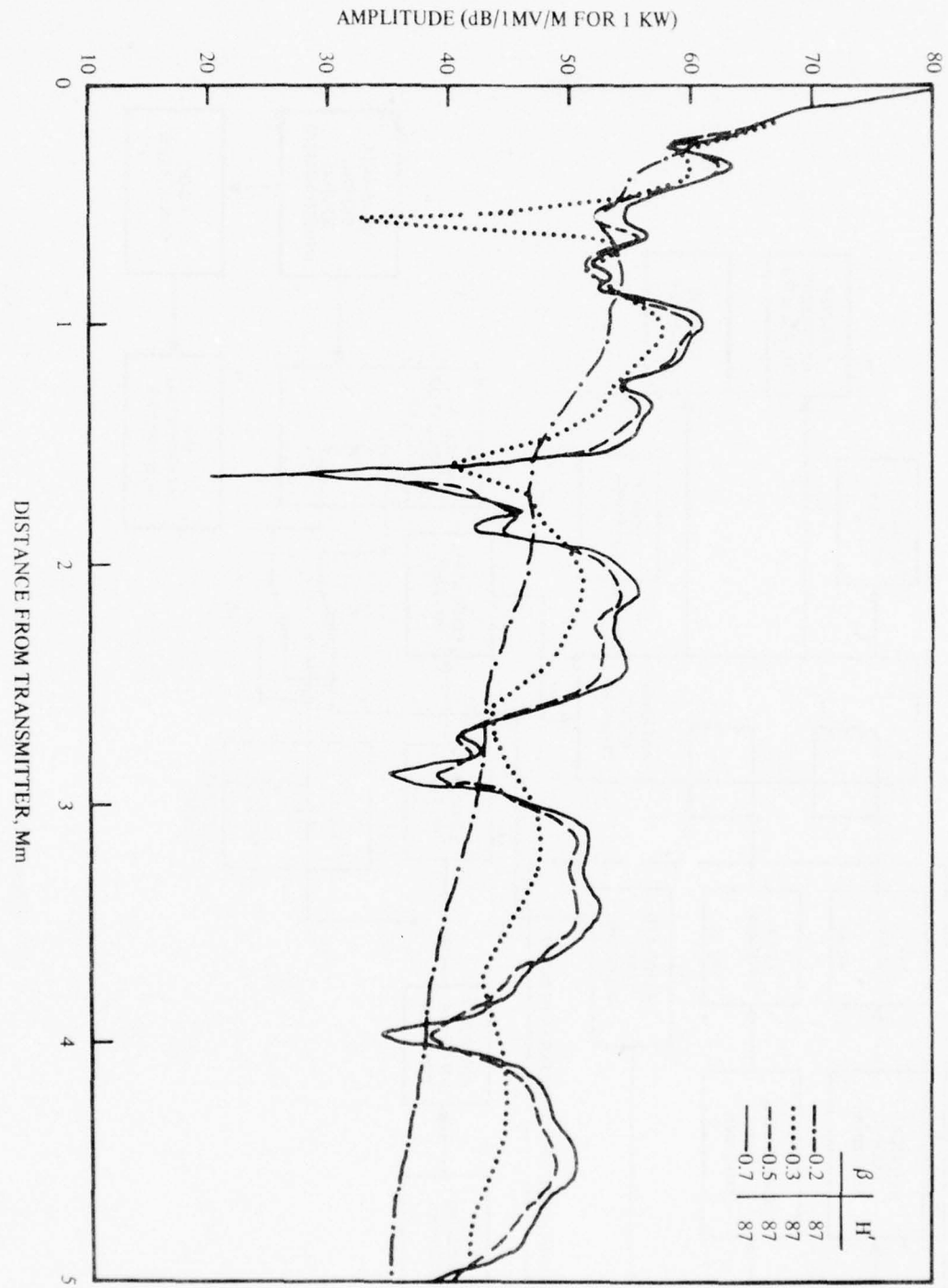


Figure 8. A comparison of computed field strength as a function of  $\beta$  for constant  $H'$ . (10.9 kHz).

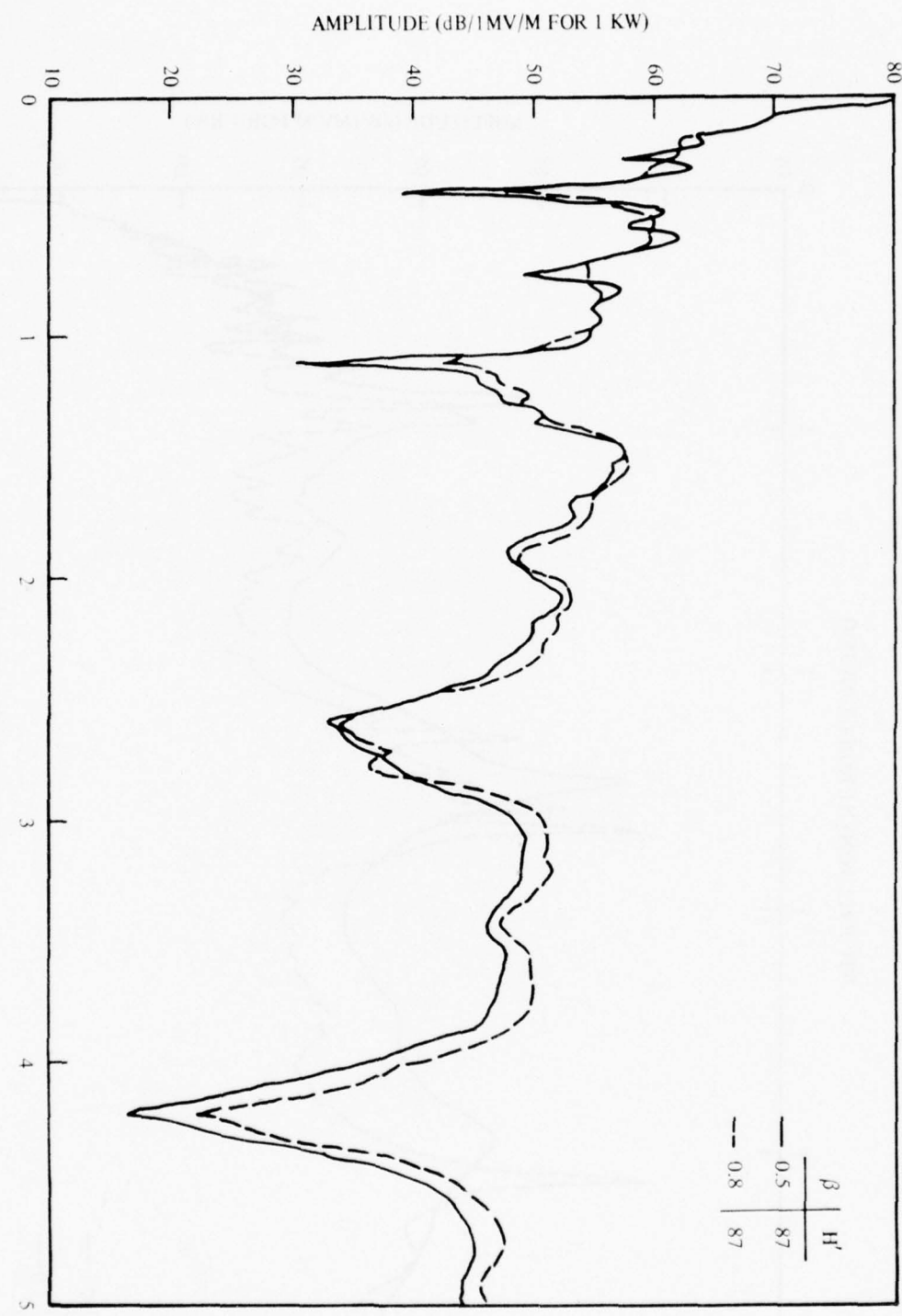


Figure 9. A comparison of computed field strength as a function of  $\beta$  for constant  $H'$ . (15.6 kHz)

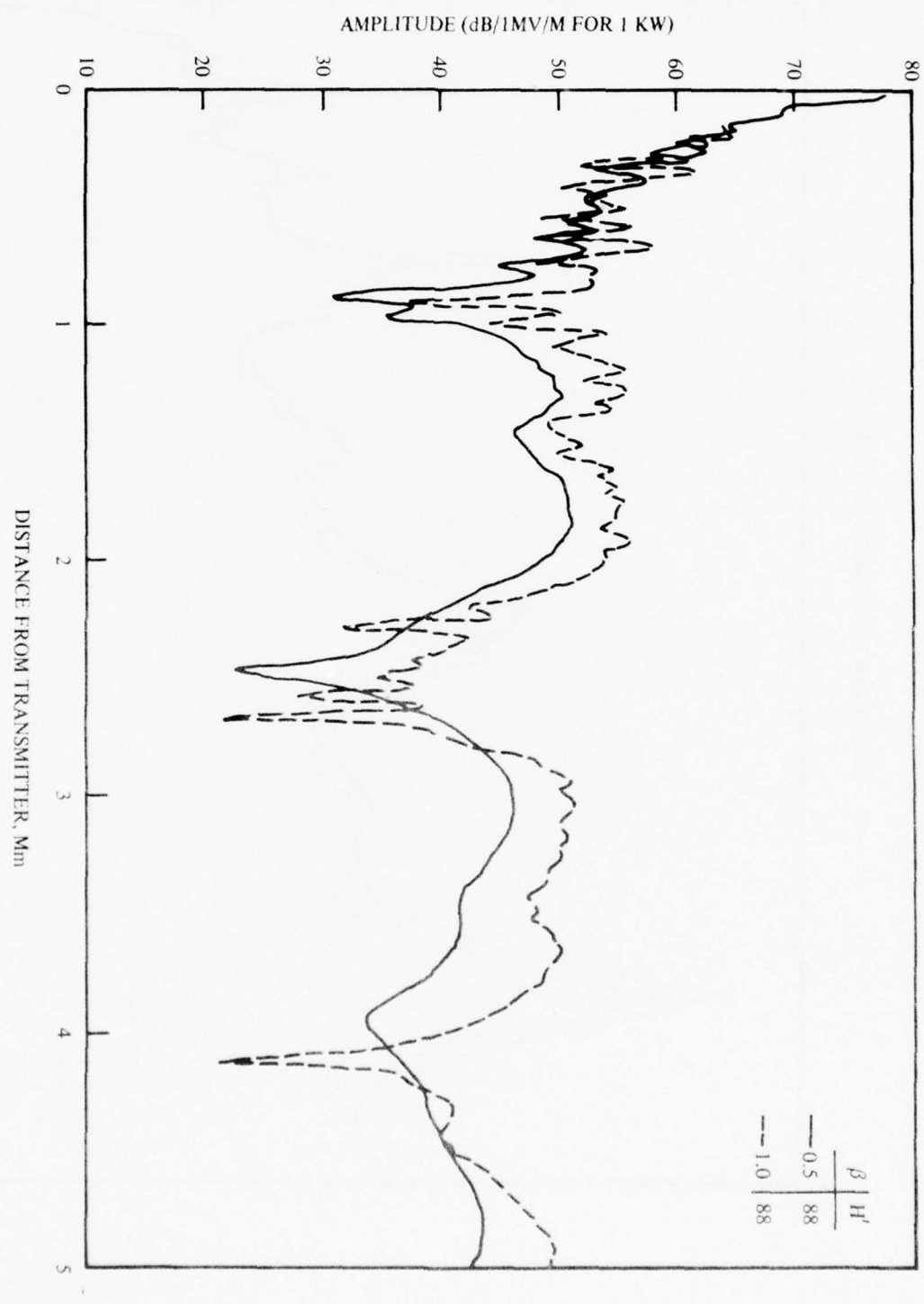


Figure 10. A comparison of computed field strength as a function of  $\beta$  for constant  $H'$  (28.0 kHz).

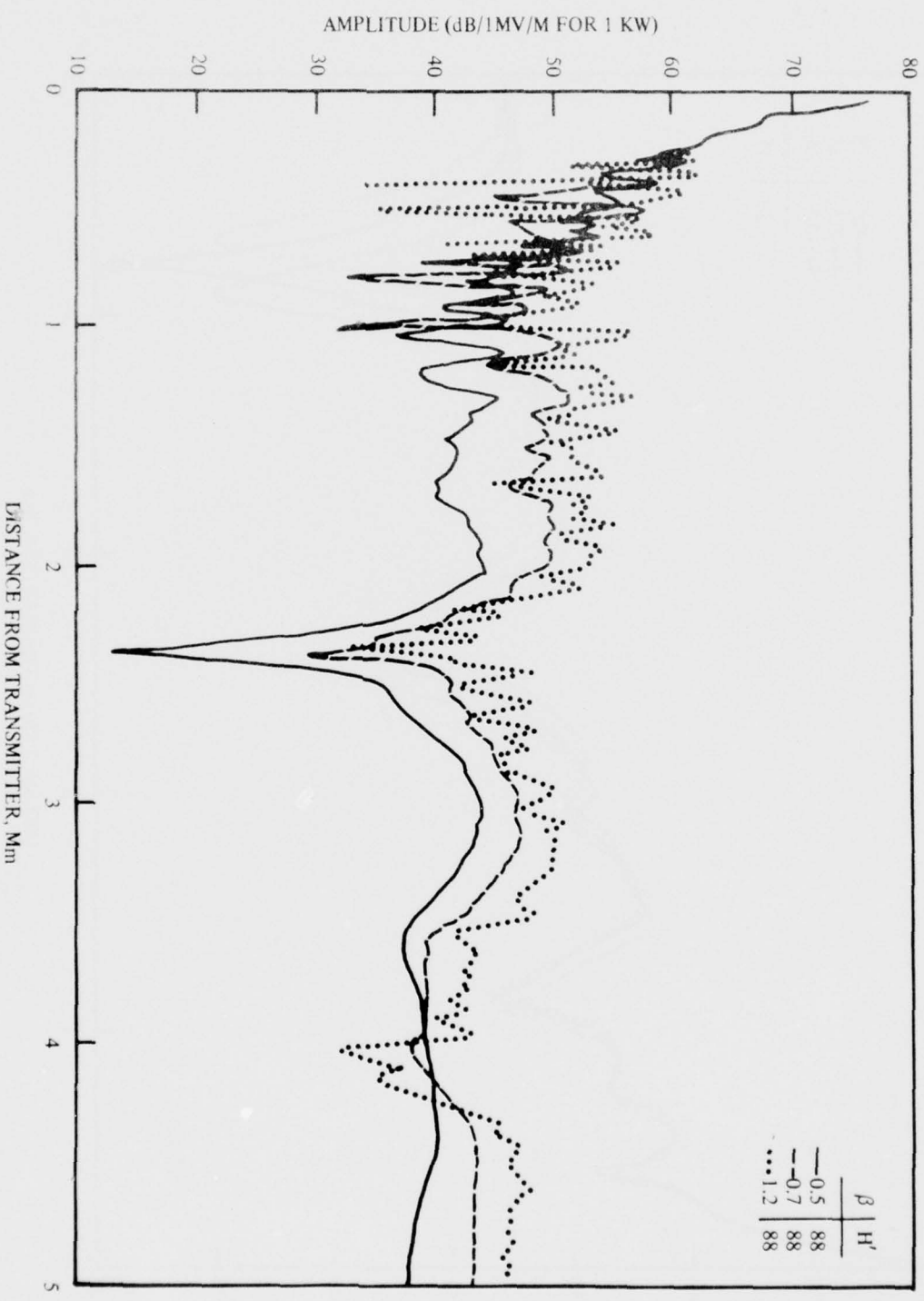


Figure 11. A comparison of computed field strength as a function of  $\beta$  for constant  $H'$ . (40.5 kHz).

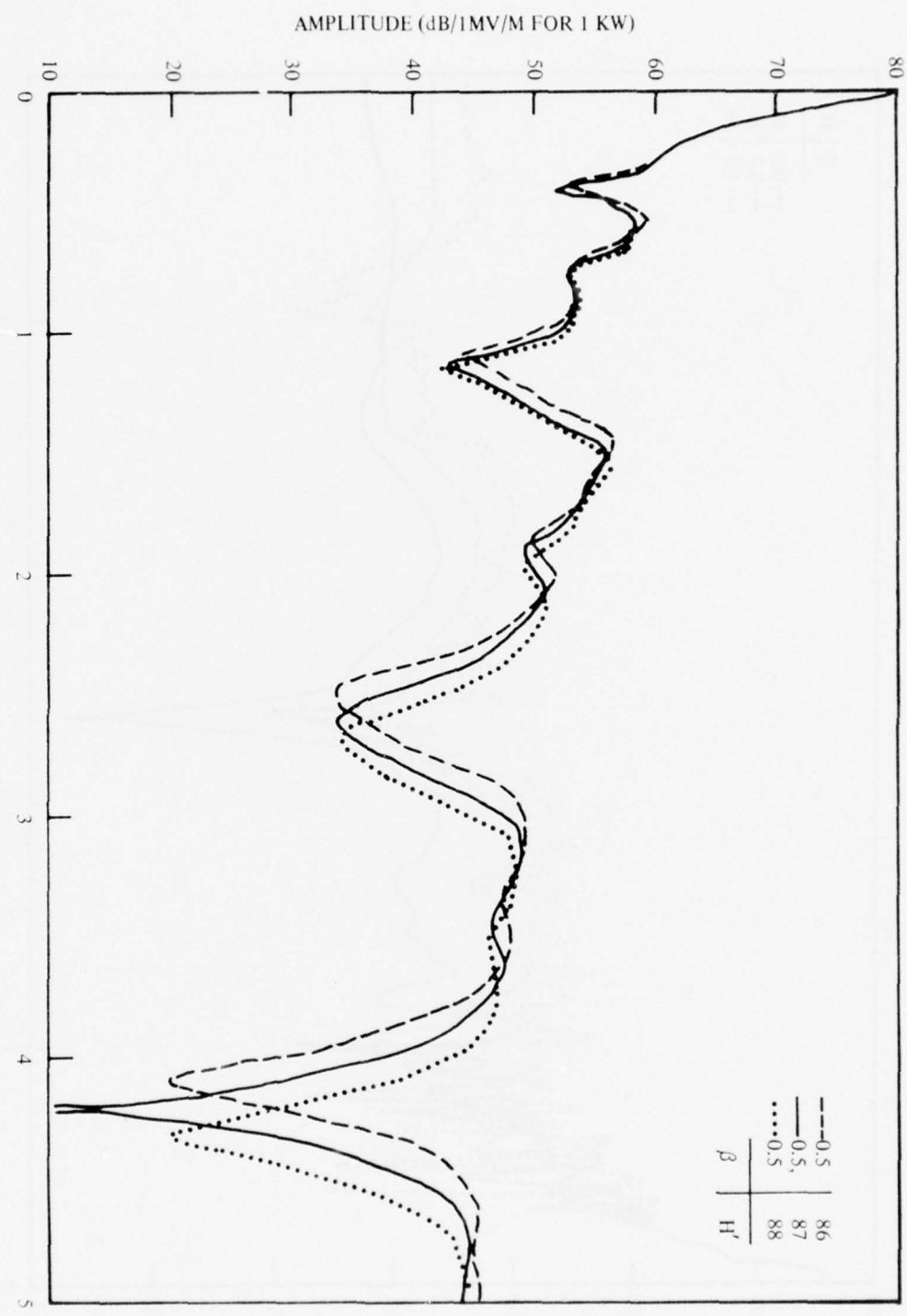


Figure 12. A comparison of computed field strength as a function of  $H'$  for constant  $\beta$ . (15.6 kHz).

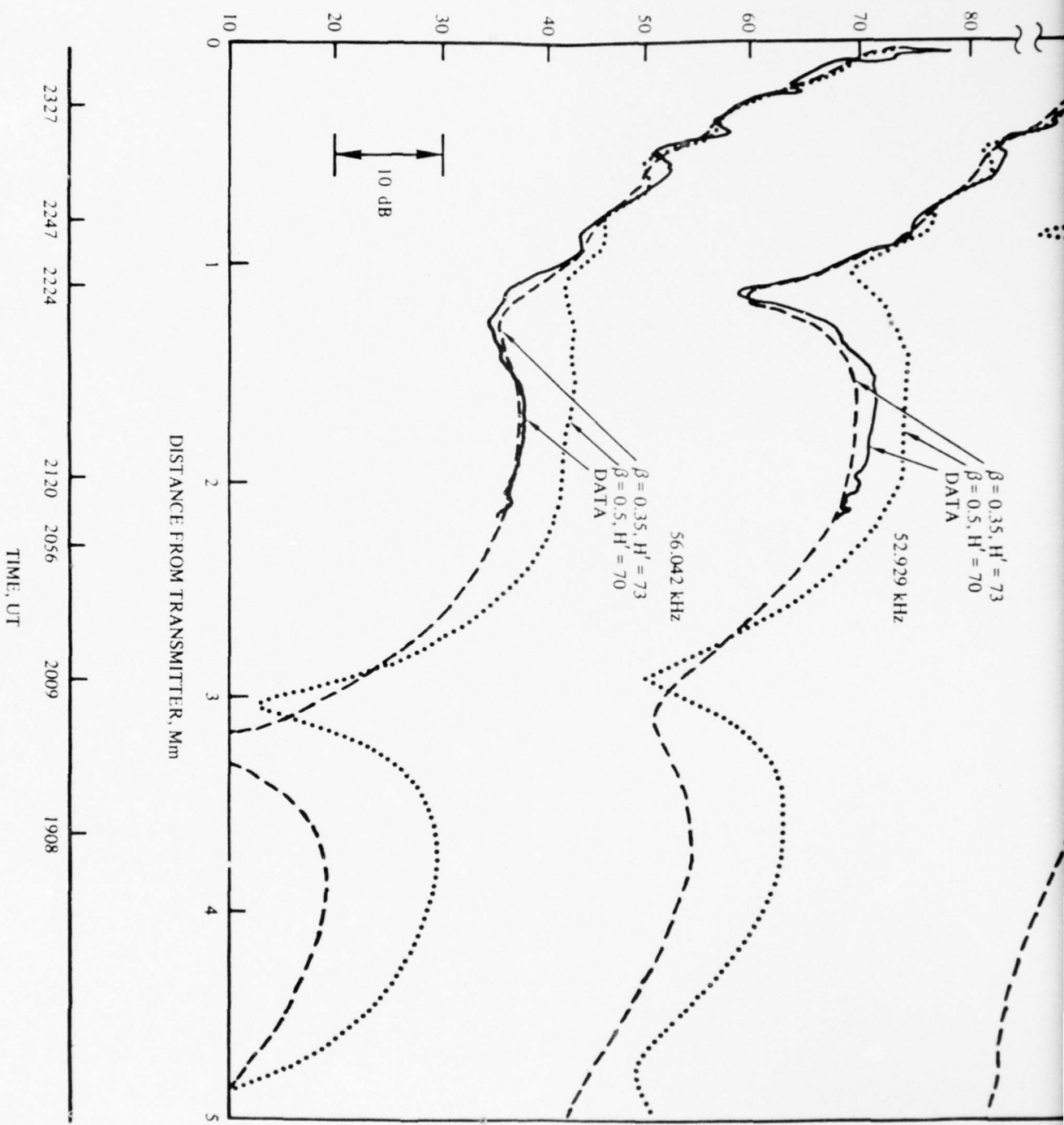
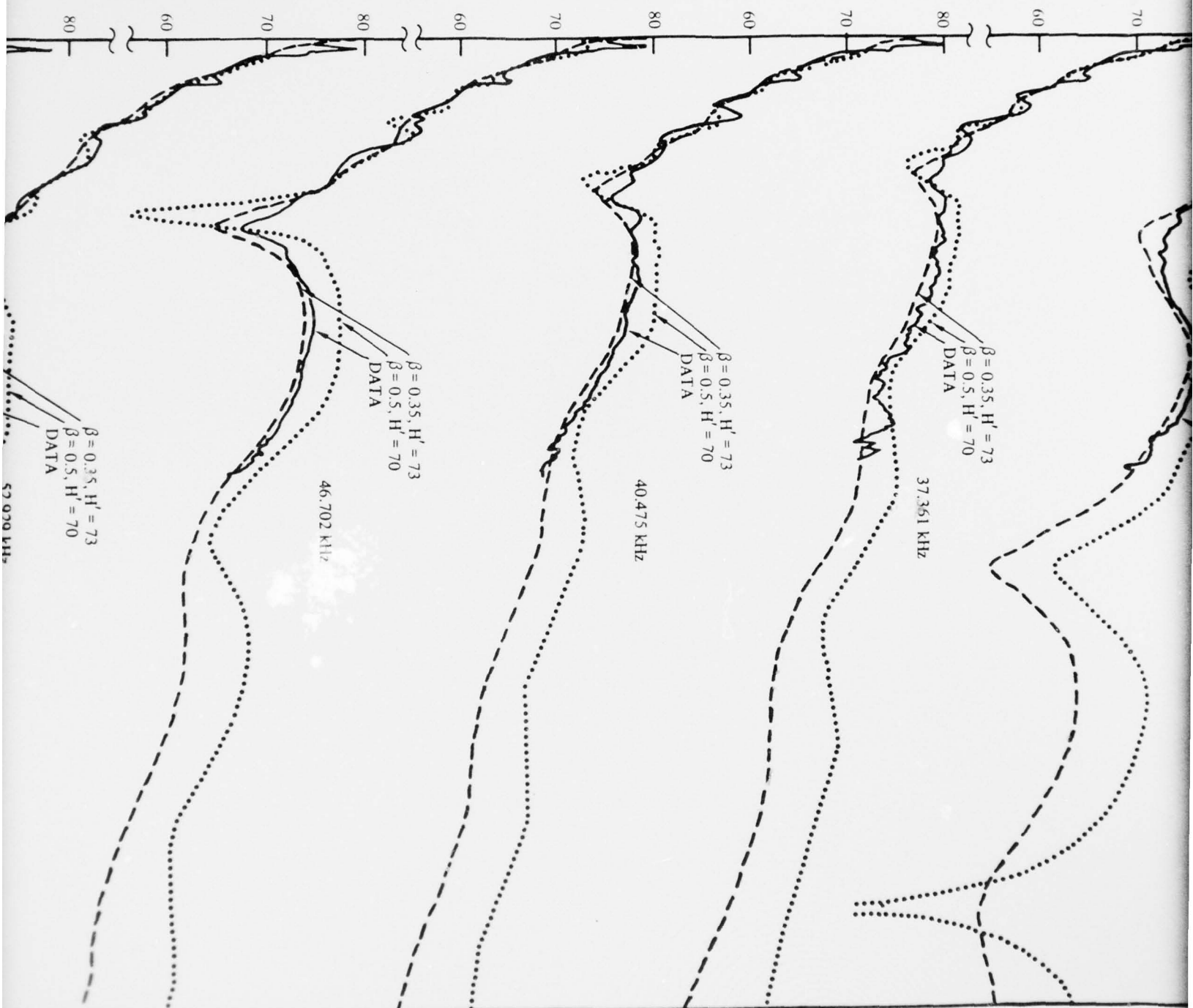


Figure 13. Measured and computed daytime signal levels on the Hawaii to Sentinel path.  
Hawaii transmitter, aircraft flight No. 27, February 2, 1974.

AMPLITUDE, dB ABOVE  $1\mu V$



TUDE, dB ABOVE  $1\mu\text{V/m}$  FOR 1 kW



3



AC 27

4

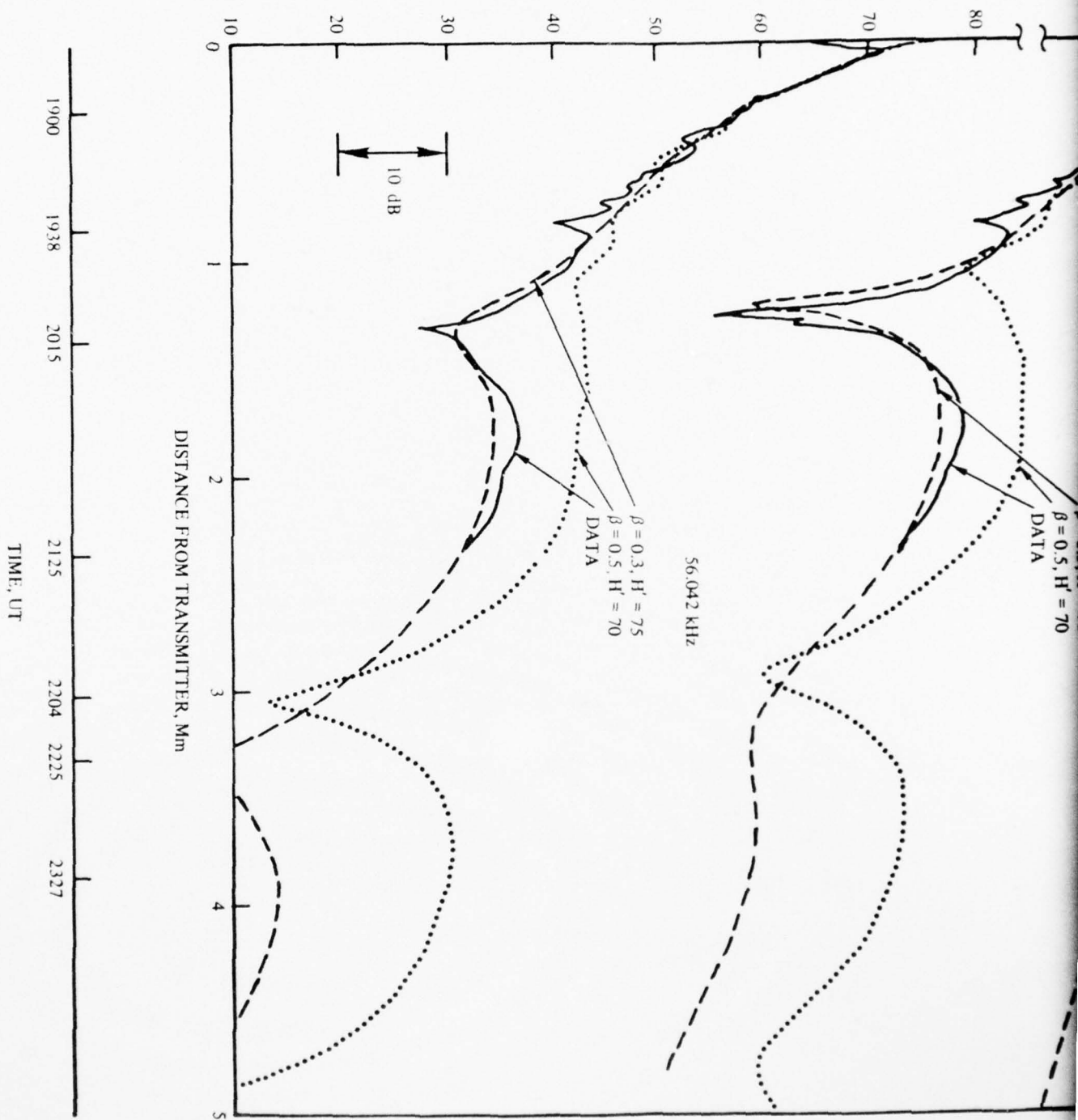


Figure 14. Measured and computed daytime signal levels on the Hawaii to Sentinel path.  
Hawaii transmitter, aircraft flight No. 28, February 3, 1974.



AMPLITUDE, dB ABOVE  $1\mu\text{V/m}$  FOR 1 kW



32

9.340 kHz

AC 28

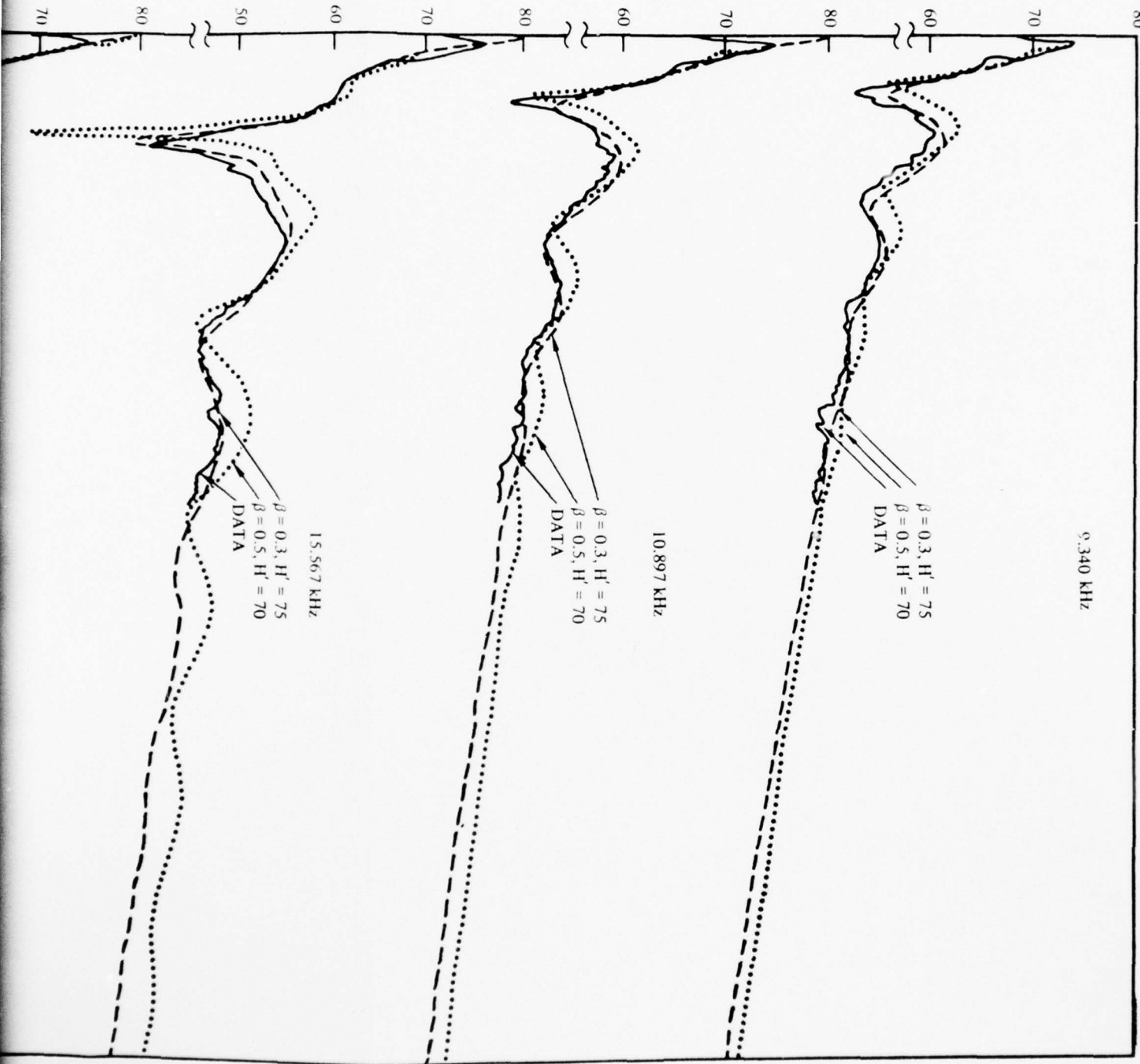
$\beta = 0.3, H' = 75$   
 $\beta = 0.5, H' = 70$   
DATA

10.897 kHz

$\beta = 0.3, H' = 75$   
 $\beta = 0.5, H' = 70$   
DATA

15.567 kHz

$\beta = 0.3, H' = 75$   
 $\beta = 0.5, H' = 70$   
DATA



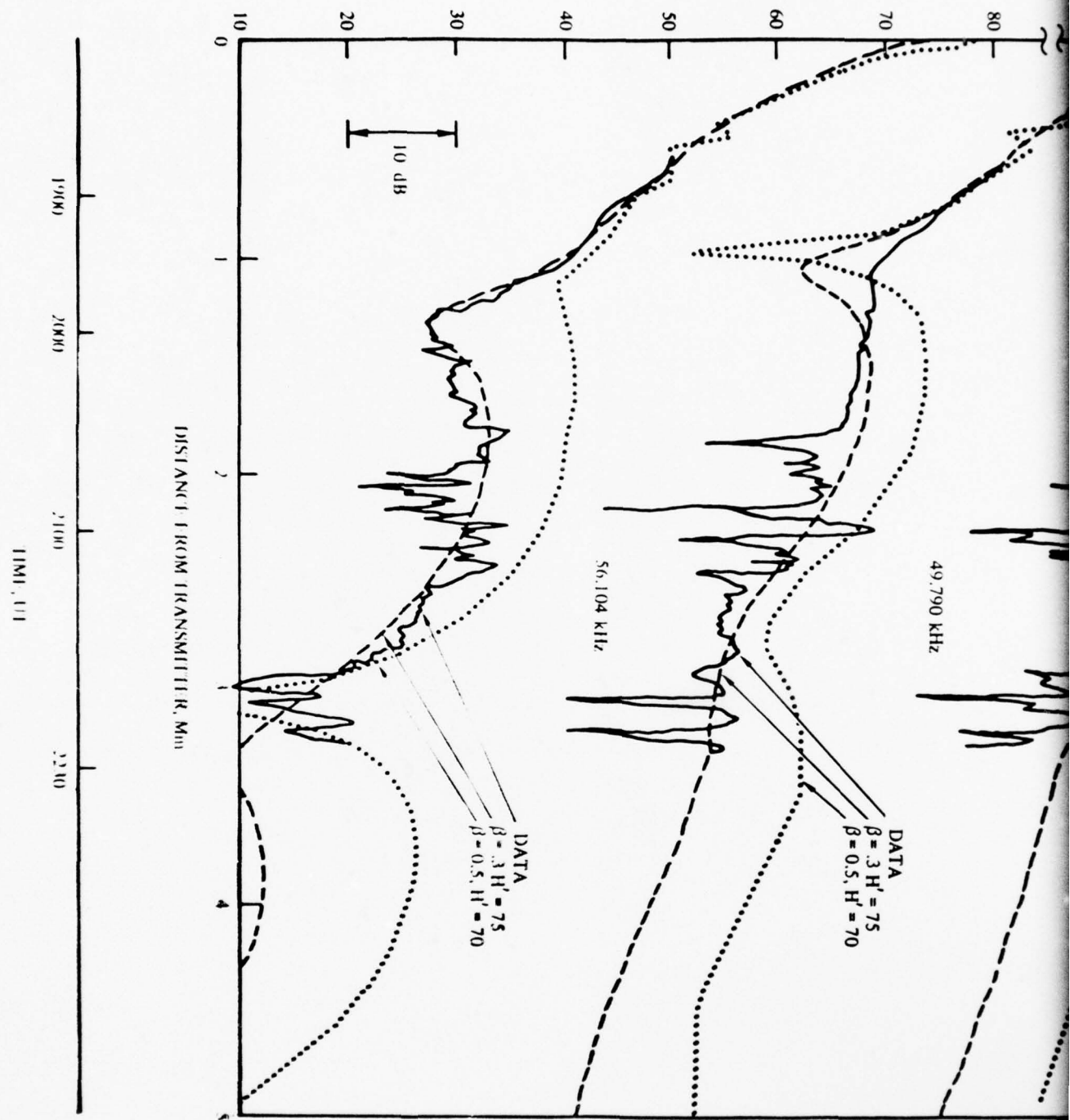
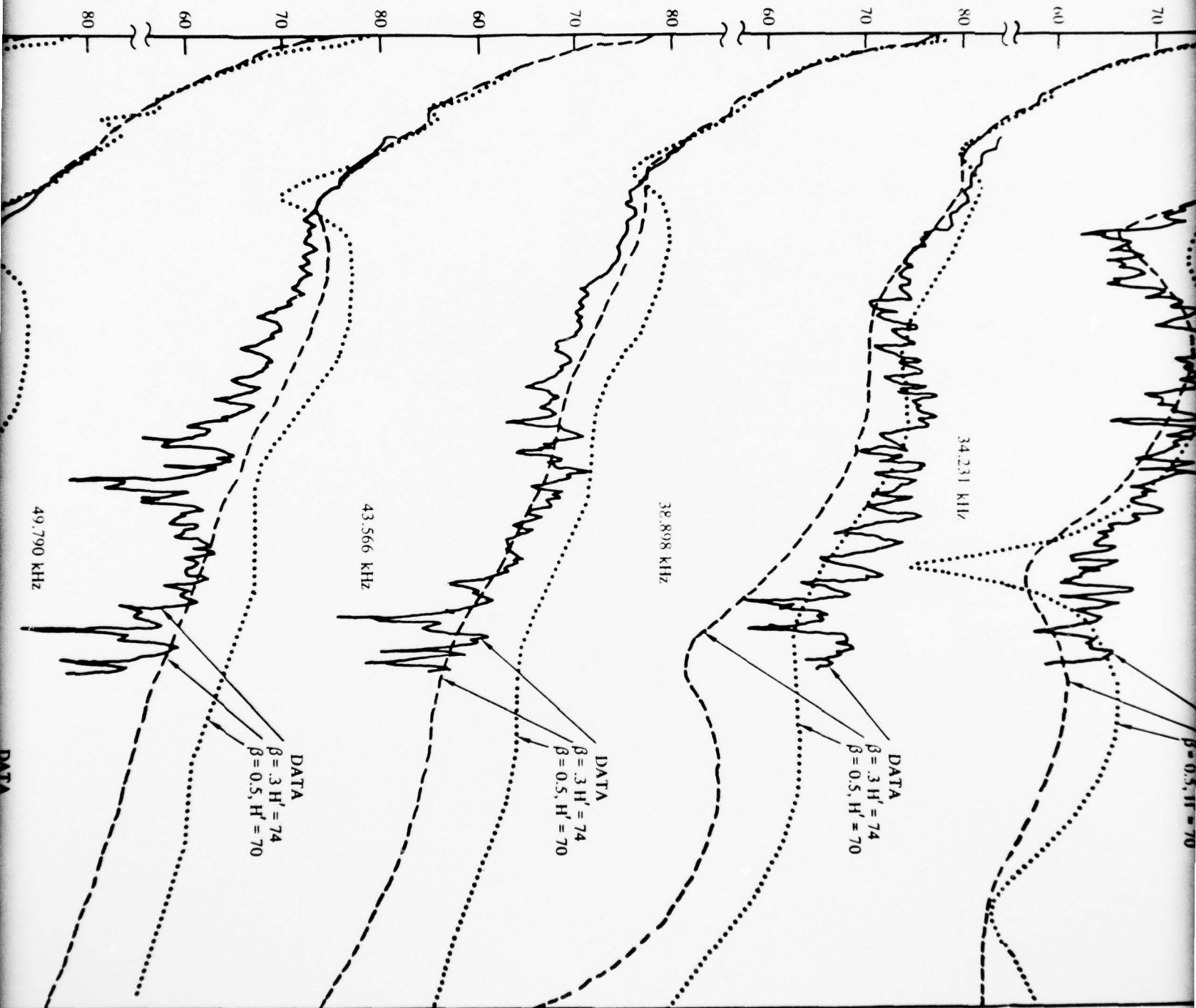
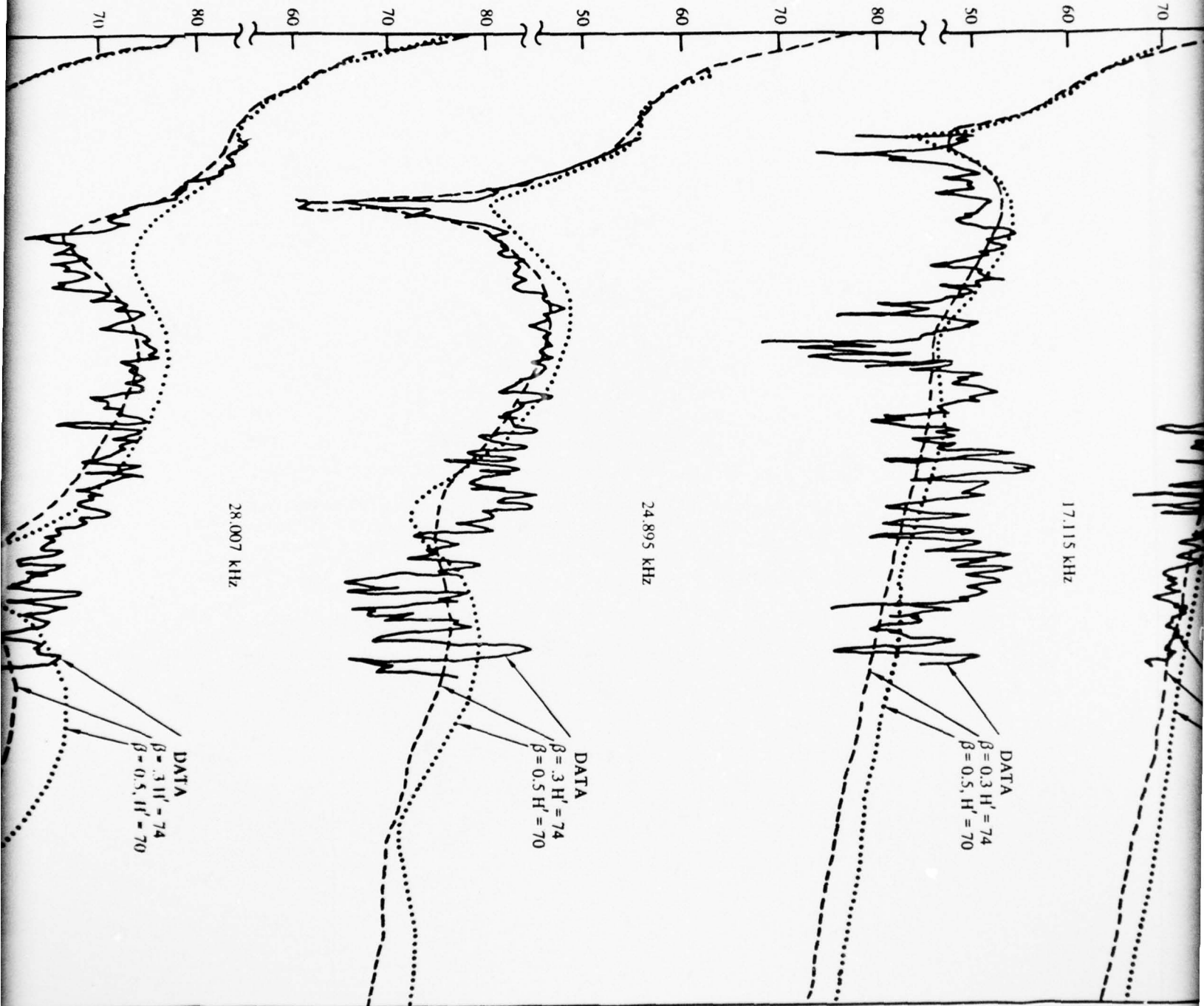


Figure 15. Measured and computed daytime signal levels on the Hawaii to Sentinel Path  
Sentinel transmitter, aircraft flight No. 1, February 5, 1974.

AMPLITUD



AMPLITUDE, dB ABOVE  $1\mu\text{V/m}$  FOR 1 kW



80

AC 27

9.336 kHz

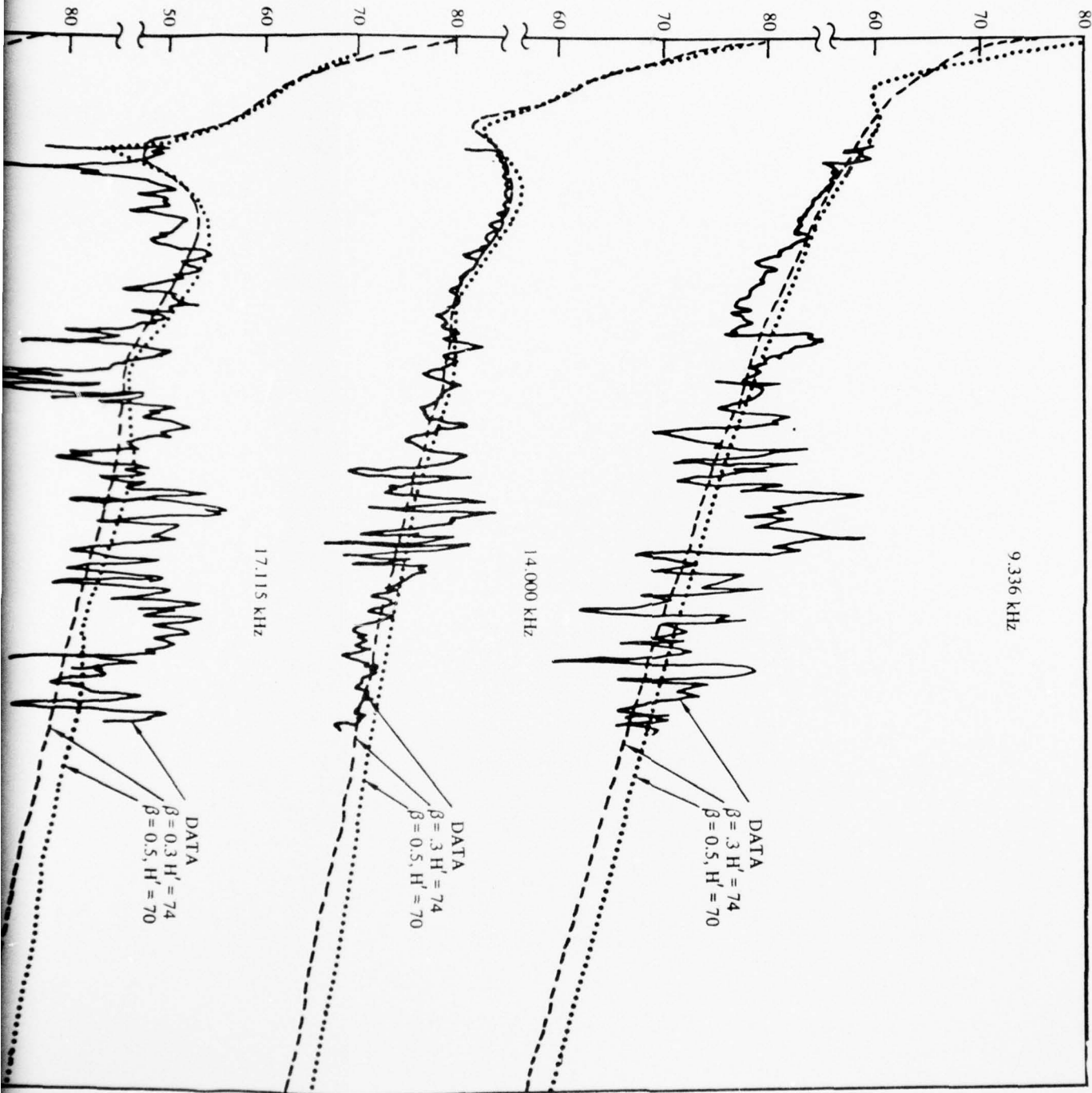
DATA  
 $\beta = .3, H' = 74$   
 $\beta = 0.5, H' = 70$

14.000 kHz

DATA  
 $\beta = .3, H' = 74$   
 $\beta = 0.5, H' = 70$

17.115 kHz

DATA  
 $\beta = 0.3, H' = 74$   
 $\beta = 0.5, H' = 70$



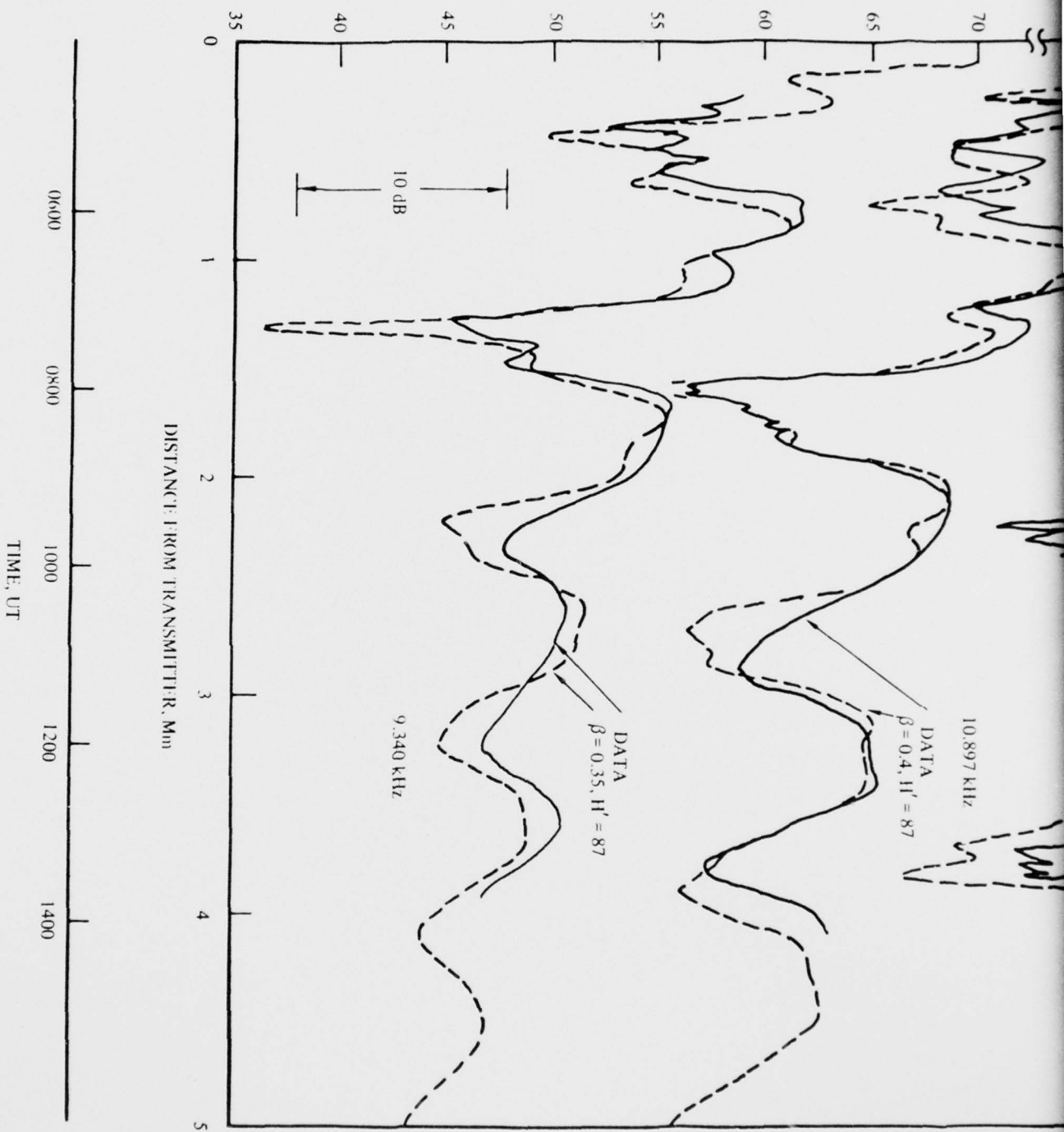
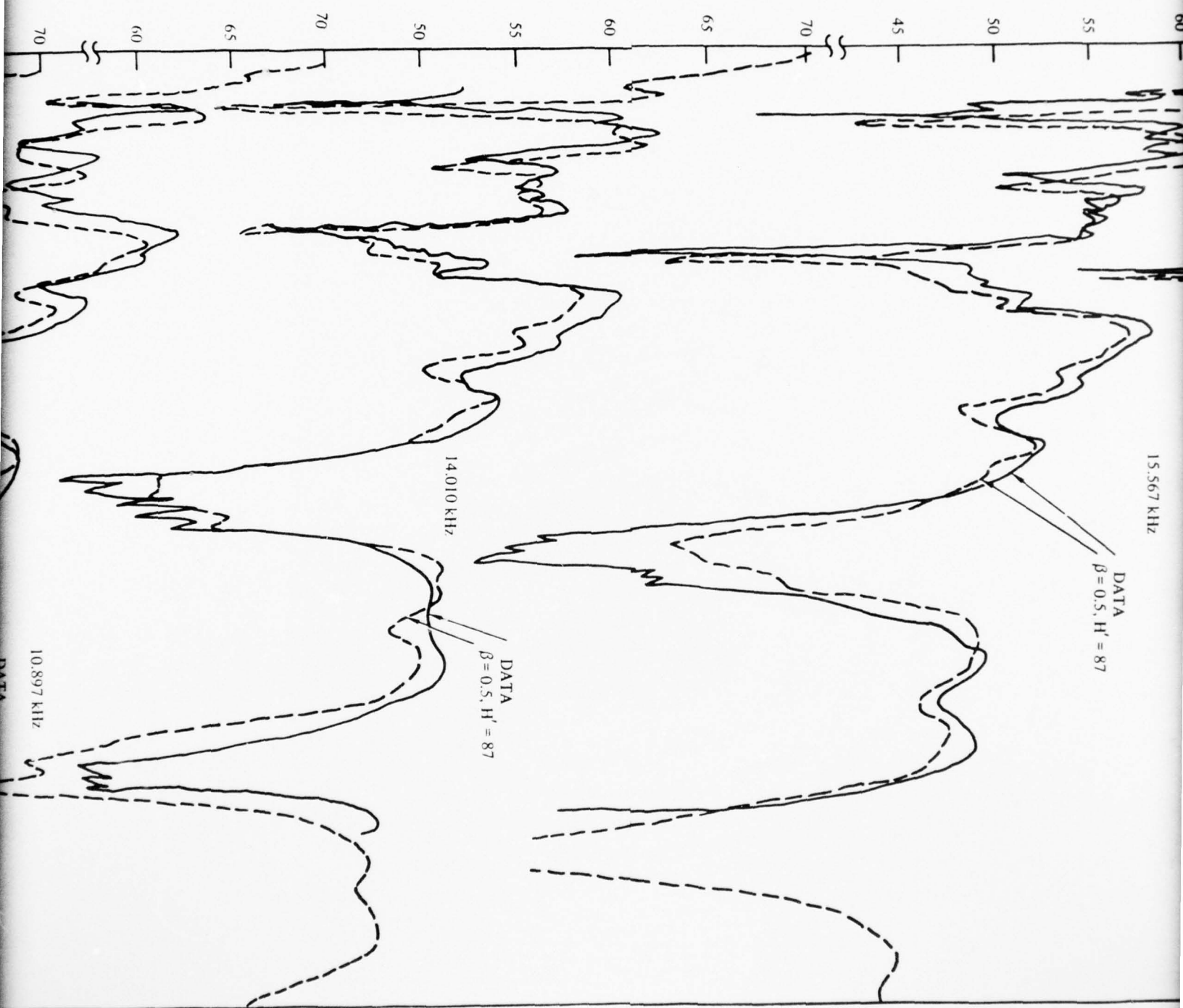
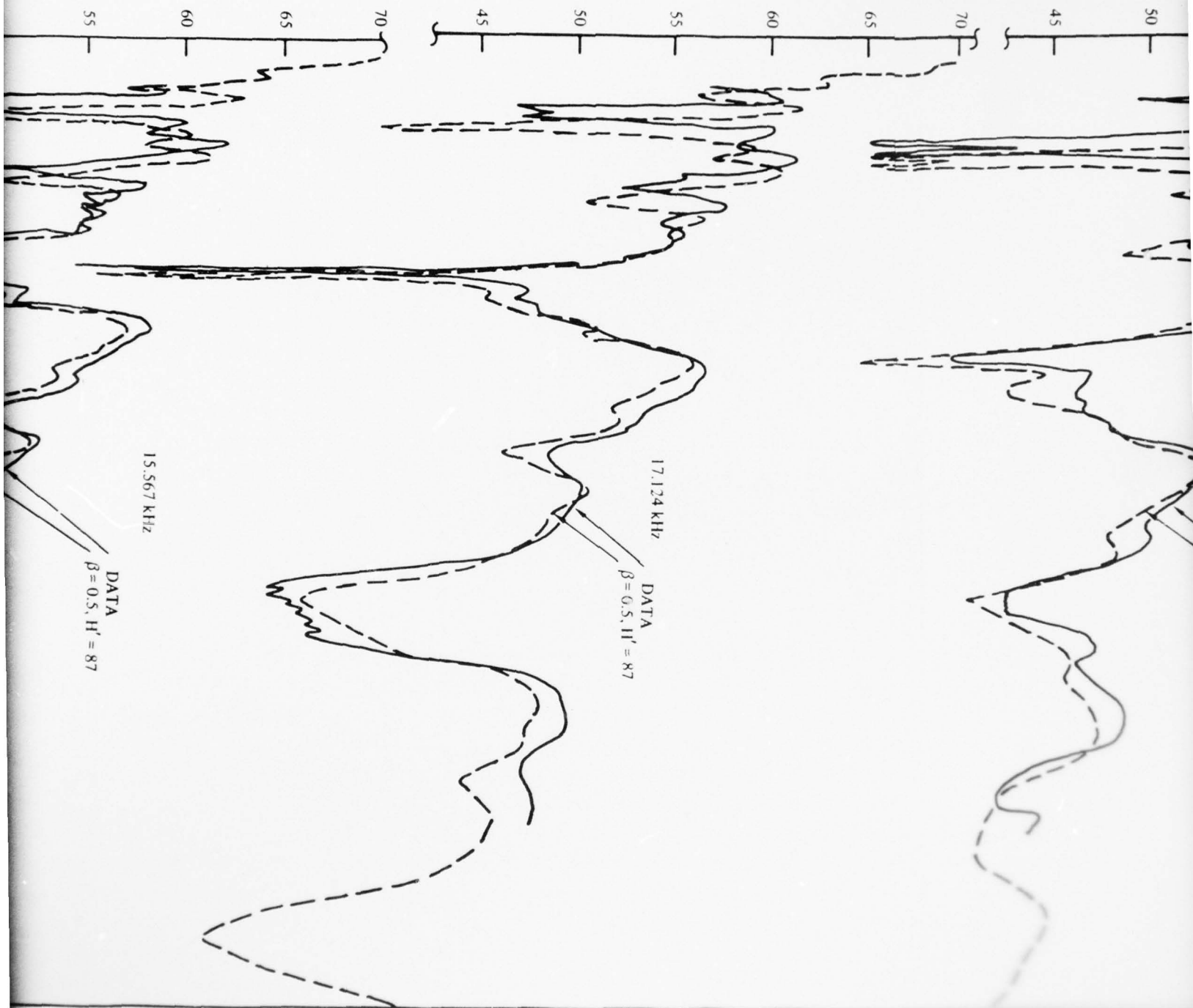


Figure 16. Measured and computed nighttime signal levels on the Hawaii to Ontario California path.  
Hawaii transmitter, February 1969.



2

AM



AD-A047 958

DEFENSE COMMUNICATIONS AGENCY ARLINGTON VA  
DETERMINATION OF EFFECTIVE IONOSPHERIC ELECTRON DENSITY PROFILE--ETC(U)  
JAN 76

F/G 17/2.1

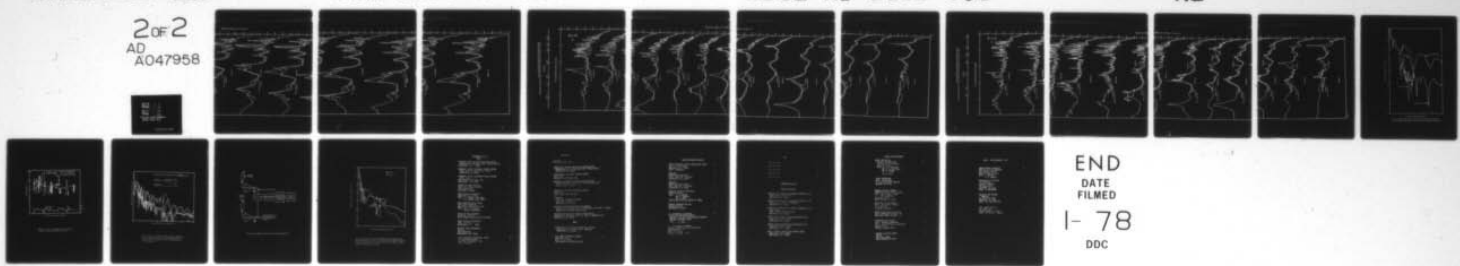
UNCLASSIFIED

DCA-C650-TP-76-4

SBIE-AD-E100 008

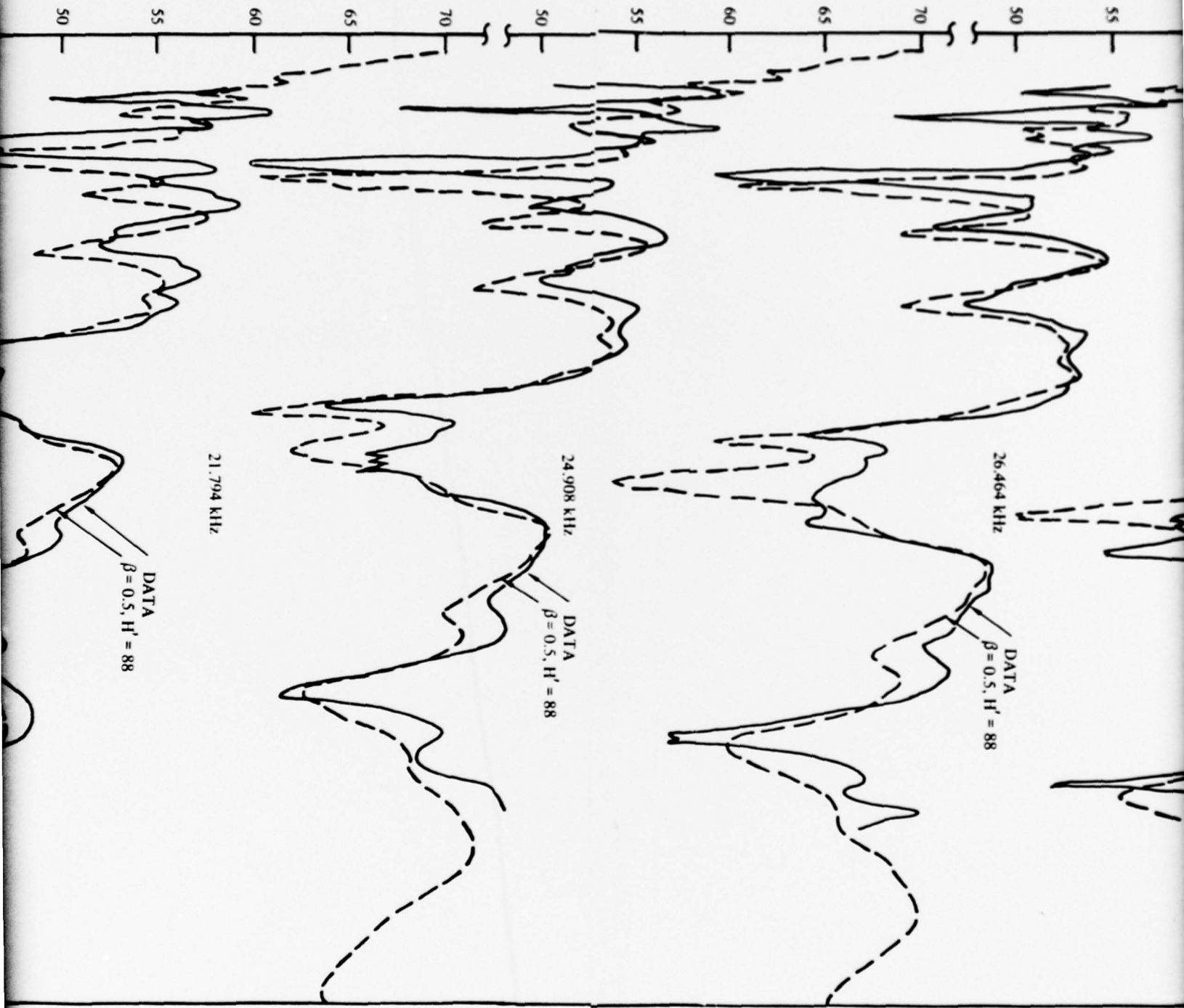
NL

2 of 2  
AD  
A047958

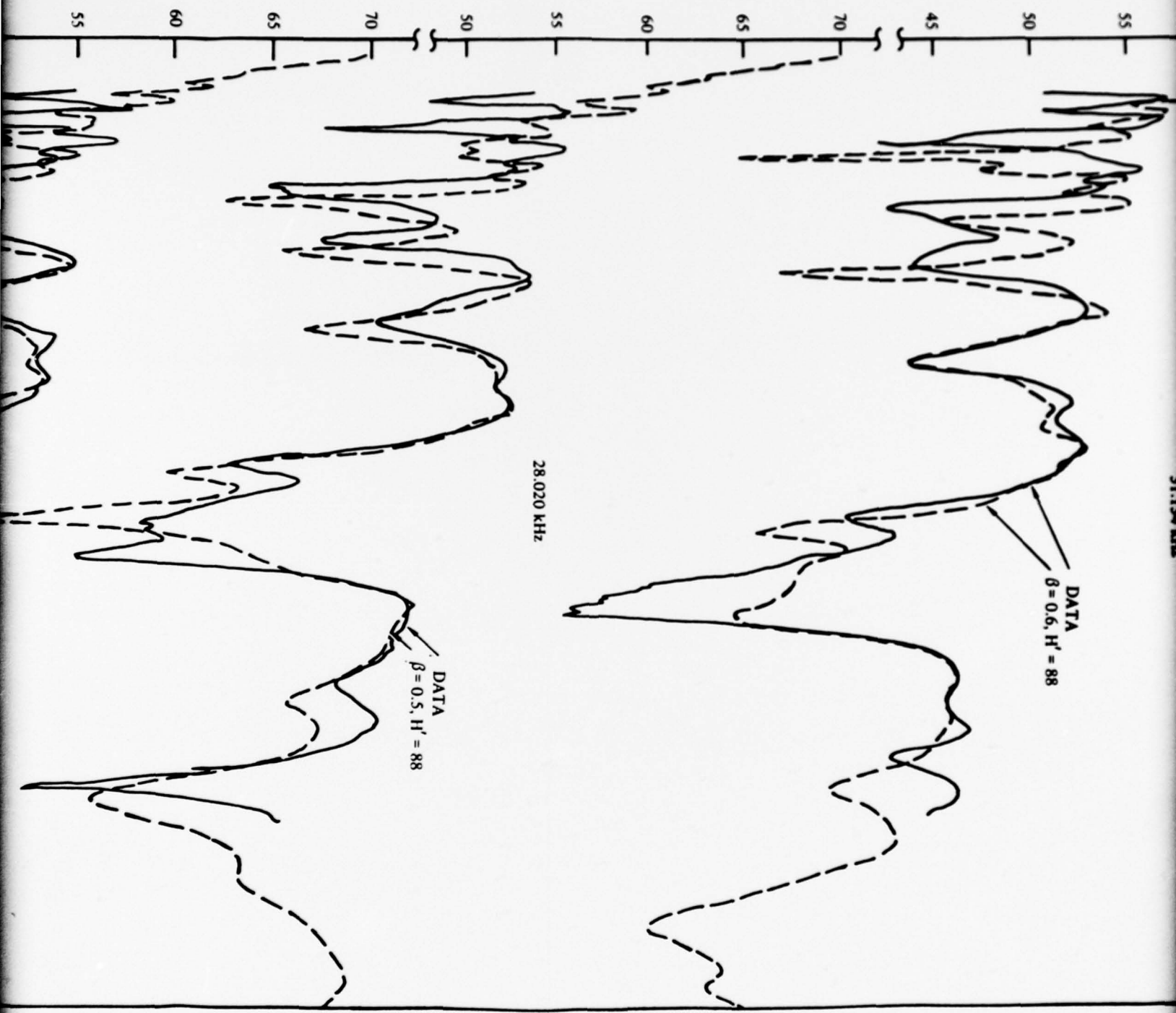


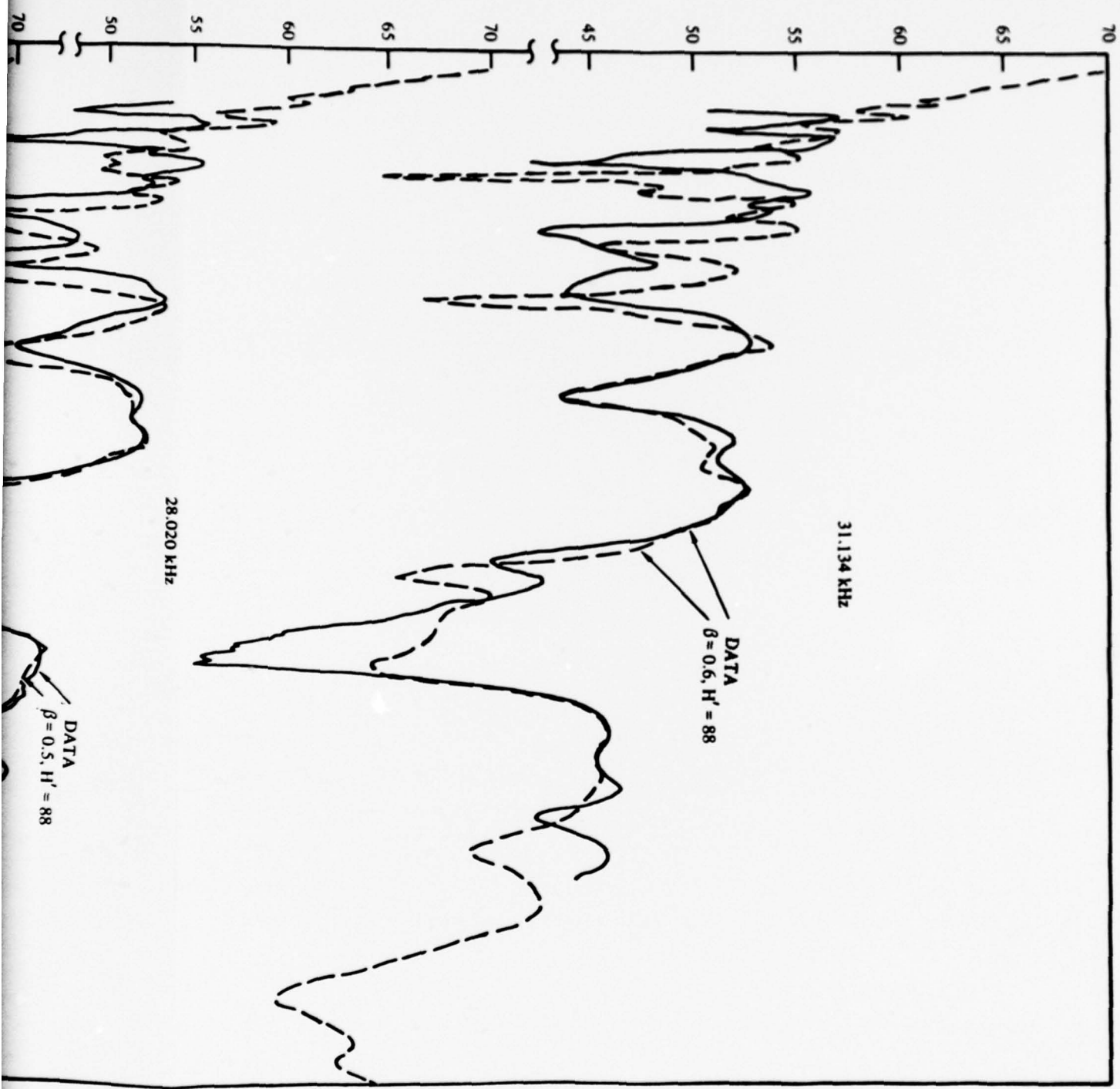
END  
DATE  
FILMED  
I- 78  
DDC

AMPLITUDE, dB ABOVE  $1\mu\text{V/m}$  FOR 1 kW



✓ A





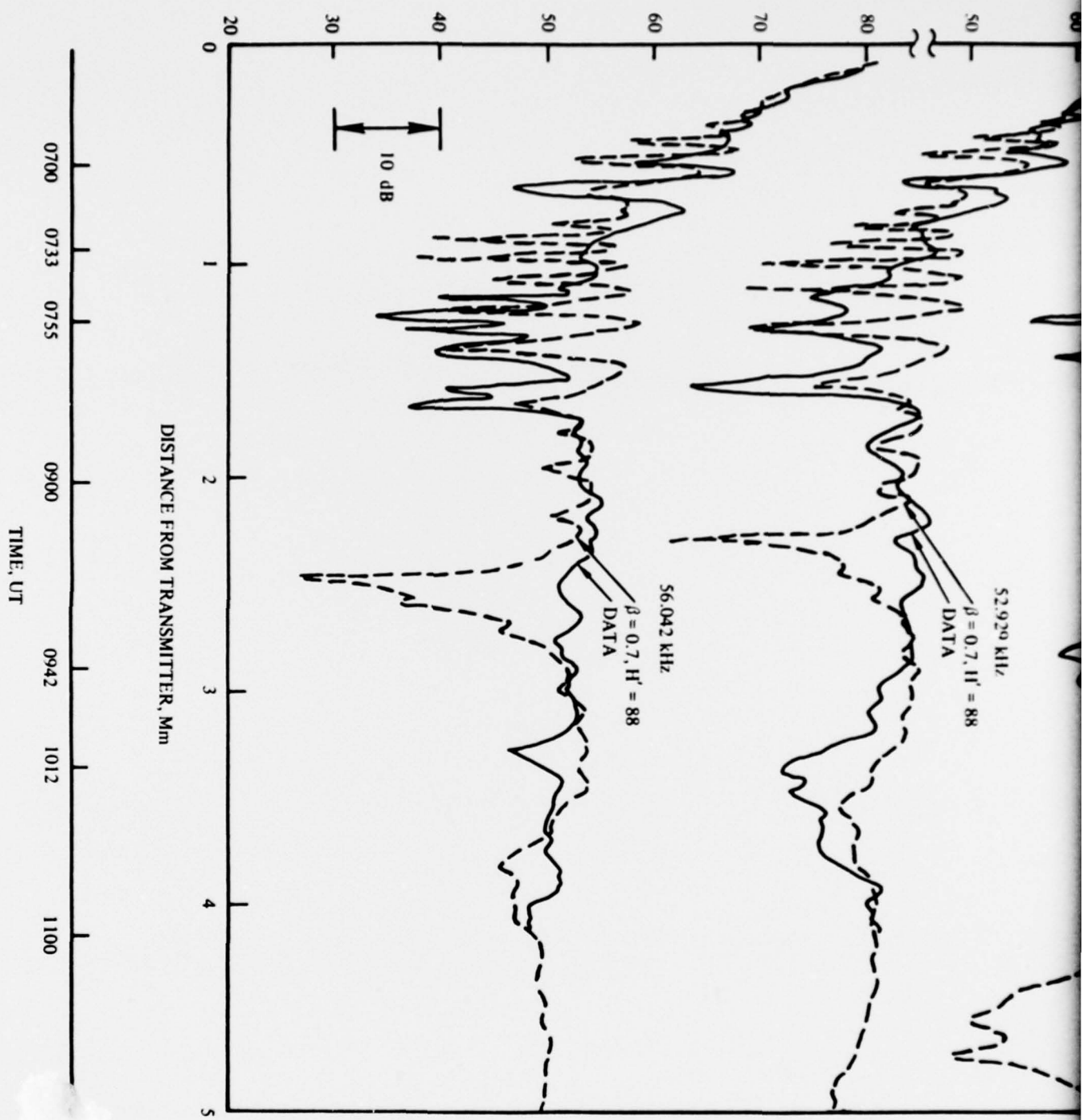
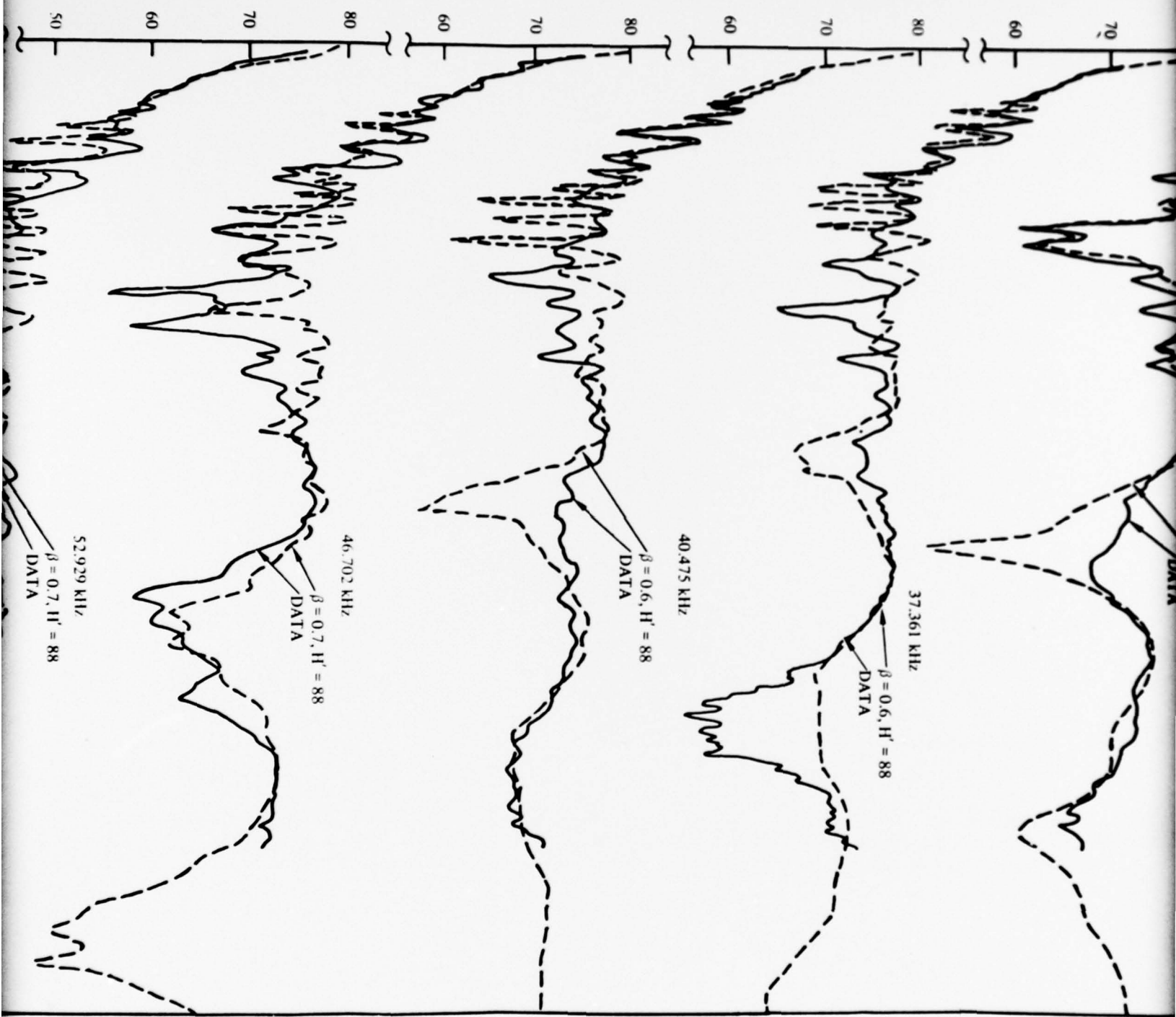
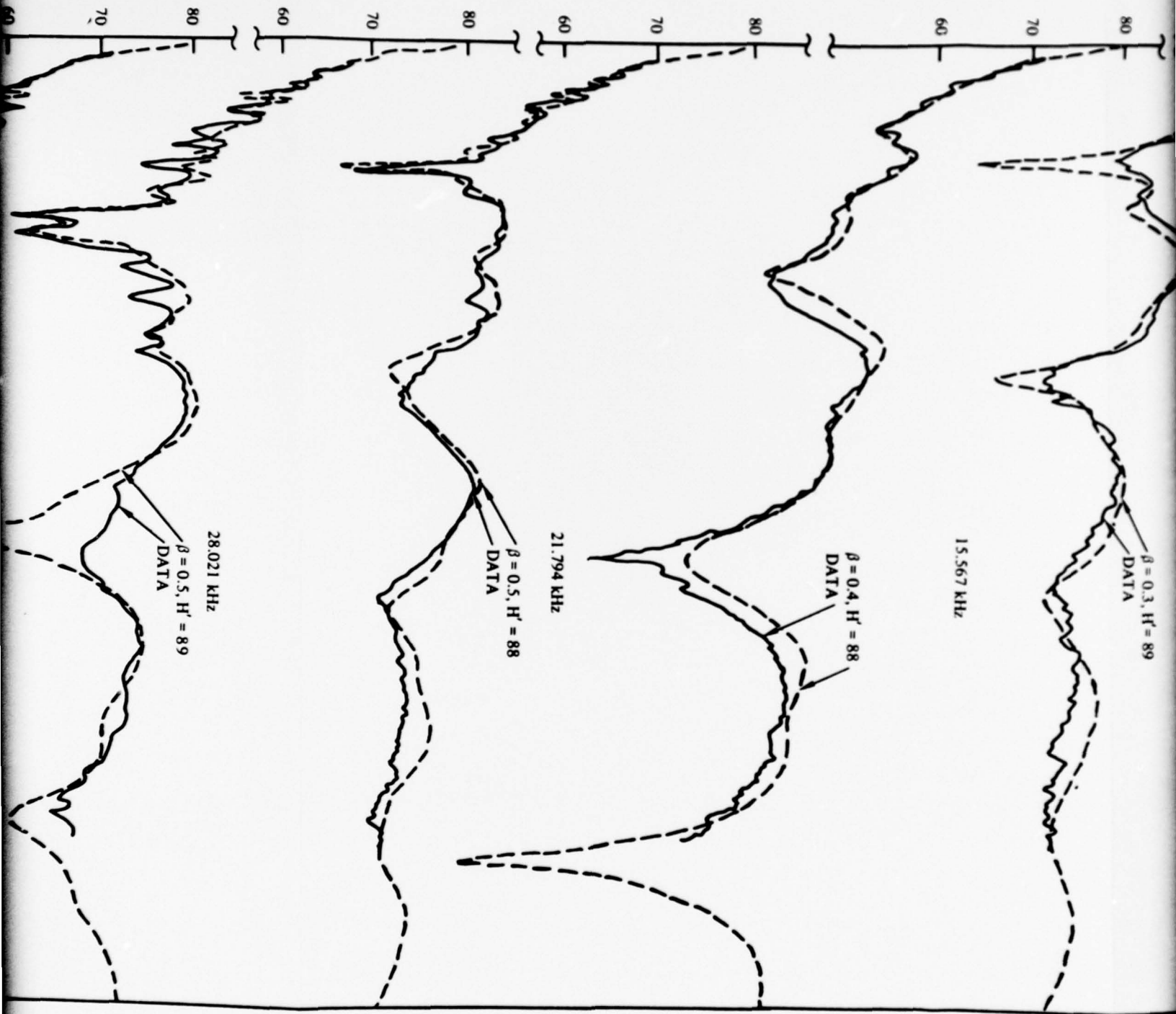


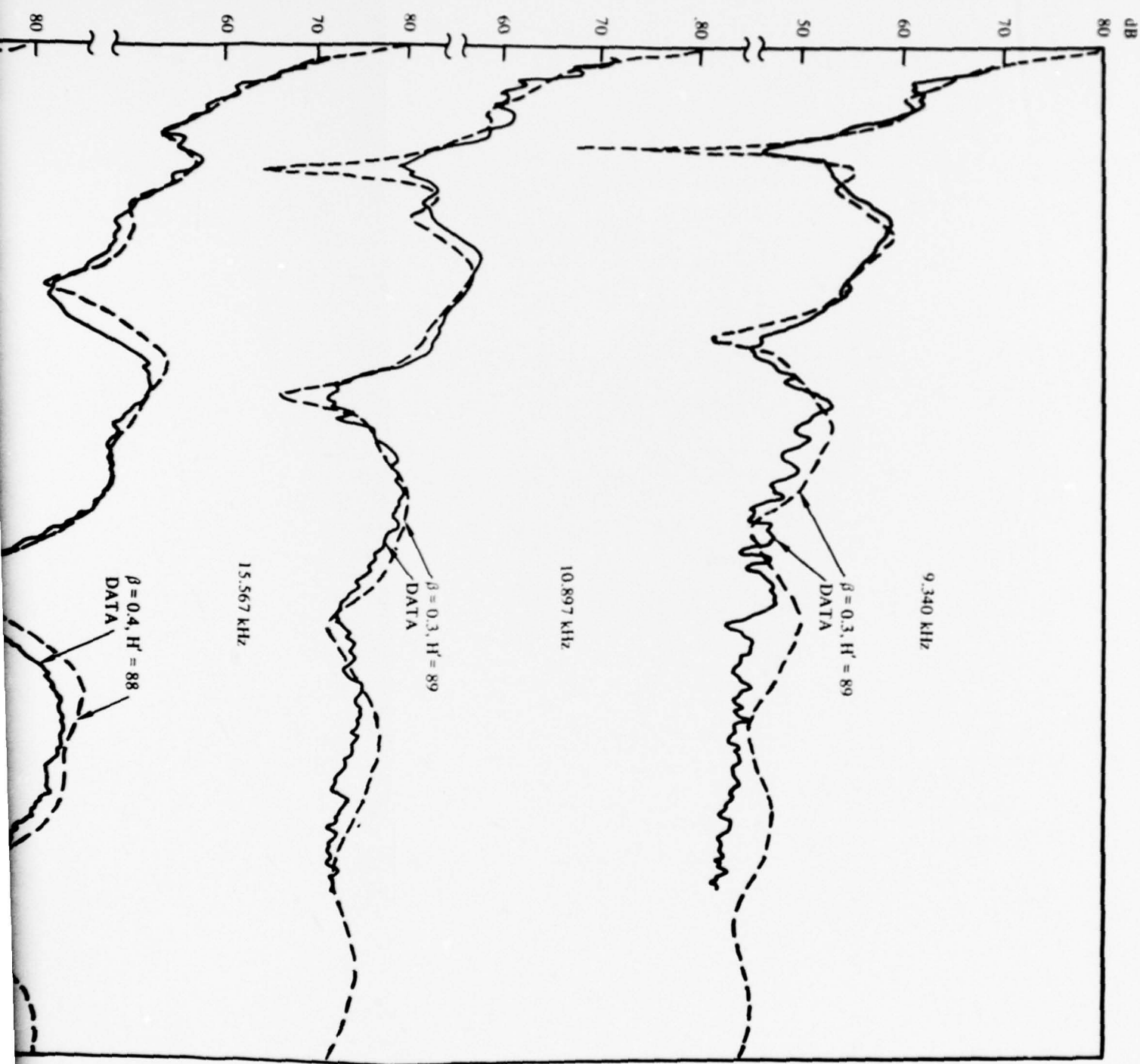
Figure 17. Measured and computed nighttime signal levels on the Hawaii to Sentinel path.  
 Hawaii transmitter, aircraft flight No. 26, February 1, 1974.

AMPLITUDE, dB ABOVE  $1\mu\text{V/m}$  FOR 1



ABOVE  $1\mu\text{V/m}$  FOR 1 kW





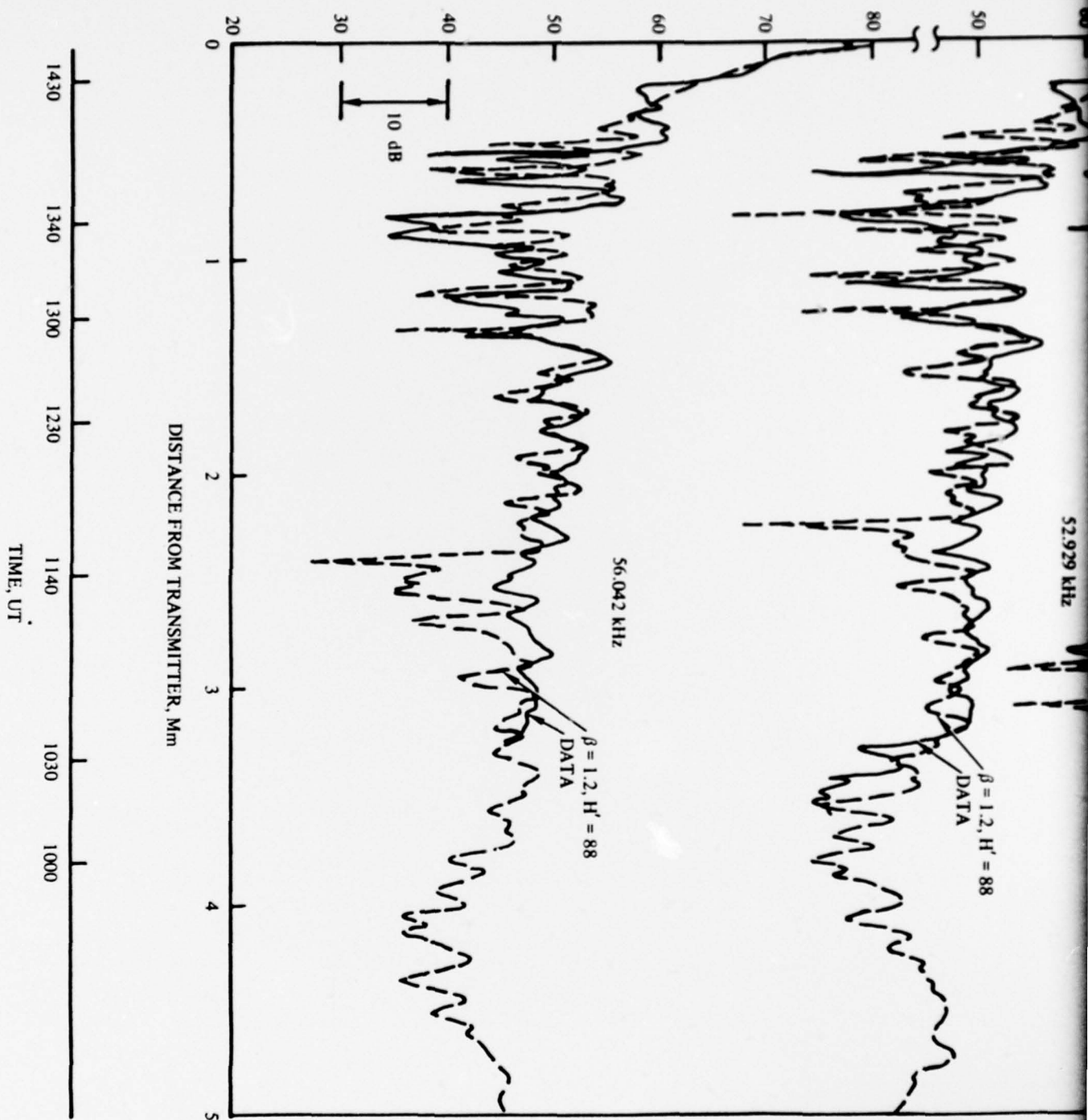
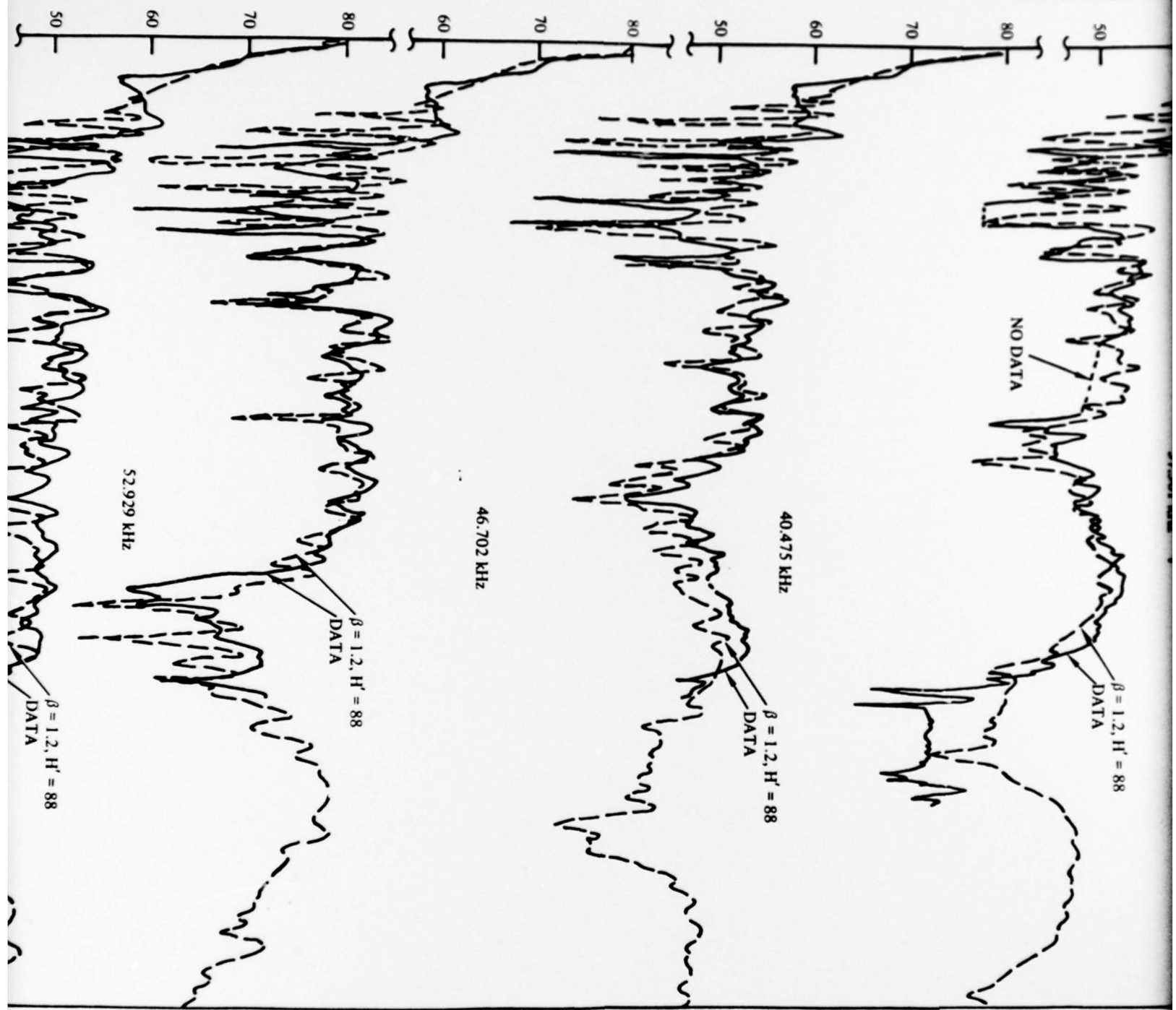
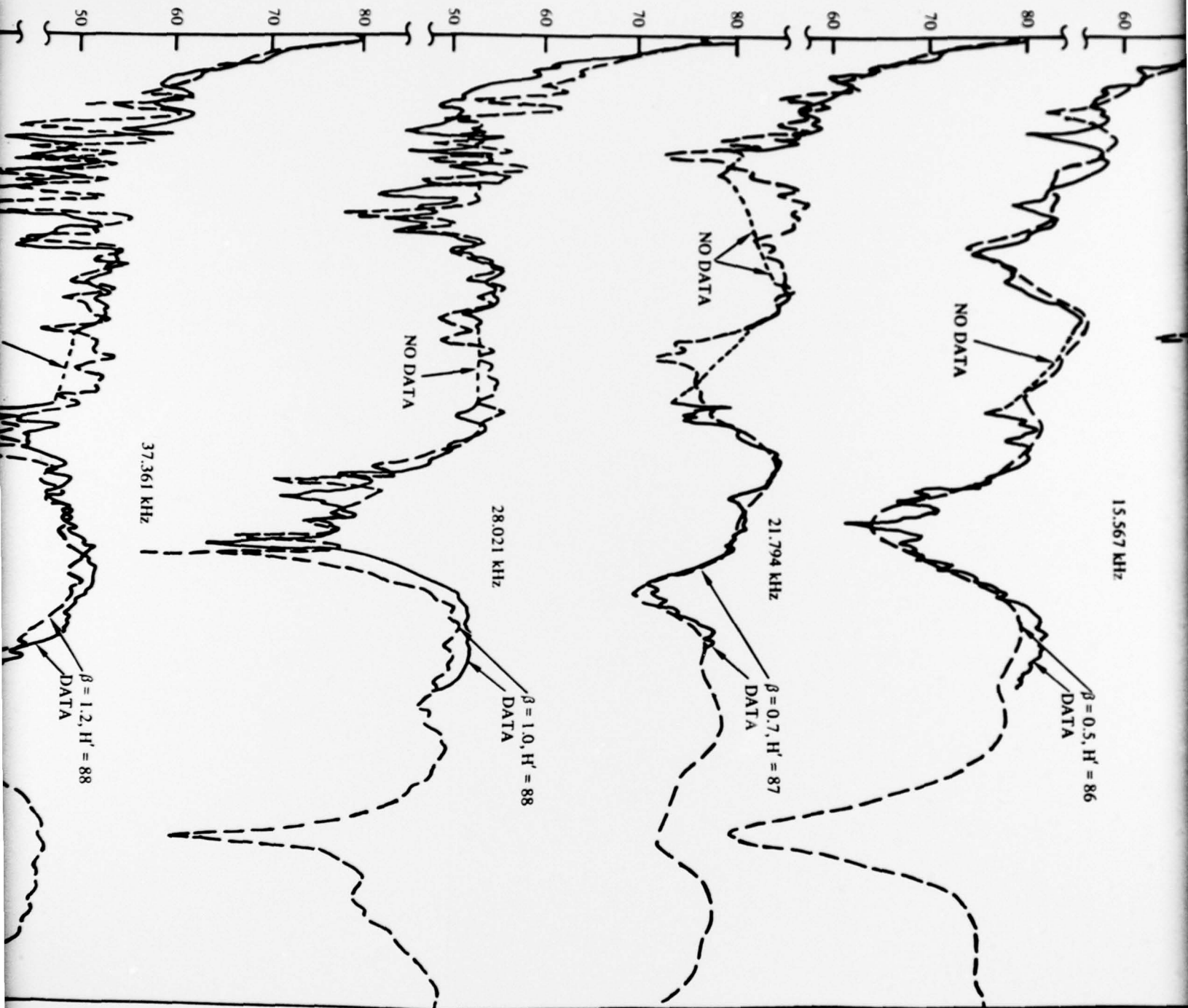


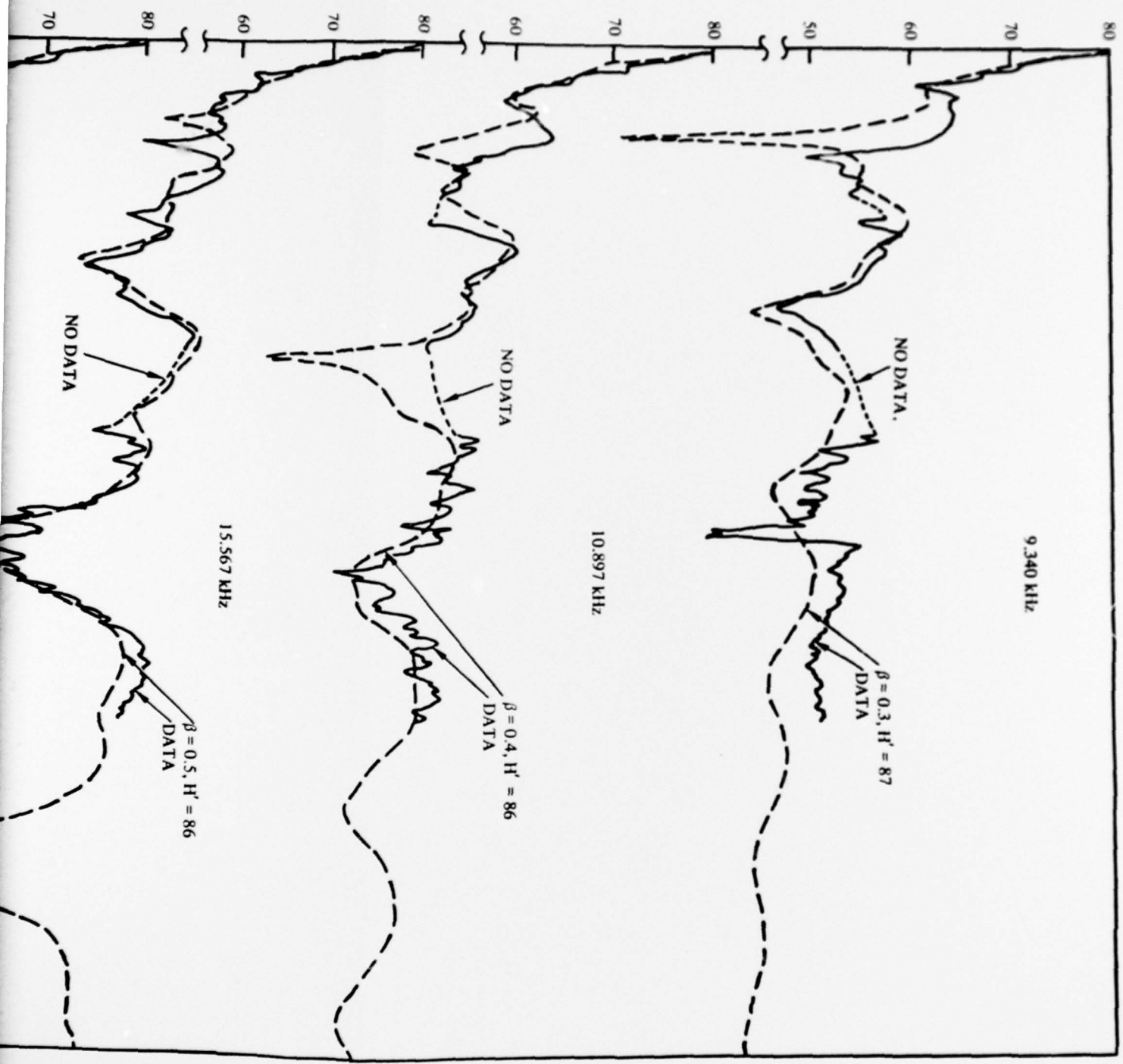
Figure 18. Measured and computed night-time signal levels on the Hawaii to Sentinel path.  
Hawaii transmitter, aircraft flight No. 24, January 30, 1974.

AMPLITUDE, dB ABC



AMPLITUDE, dB ABOVE  $I_{\mu}/V/m$  FOR 1 kW





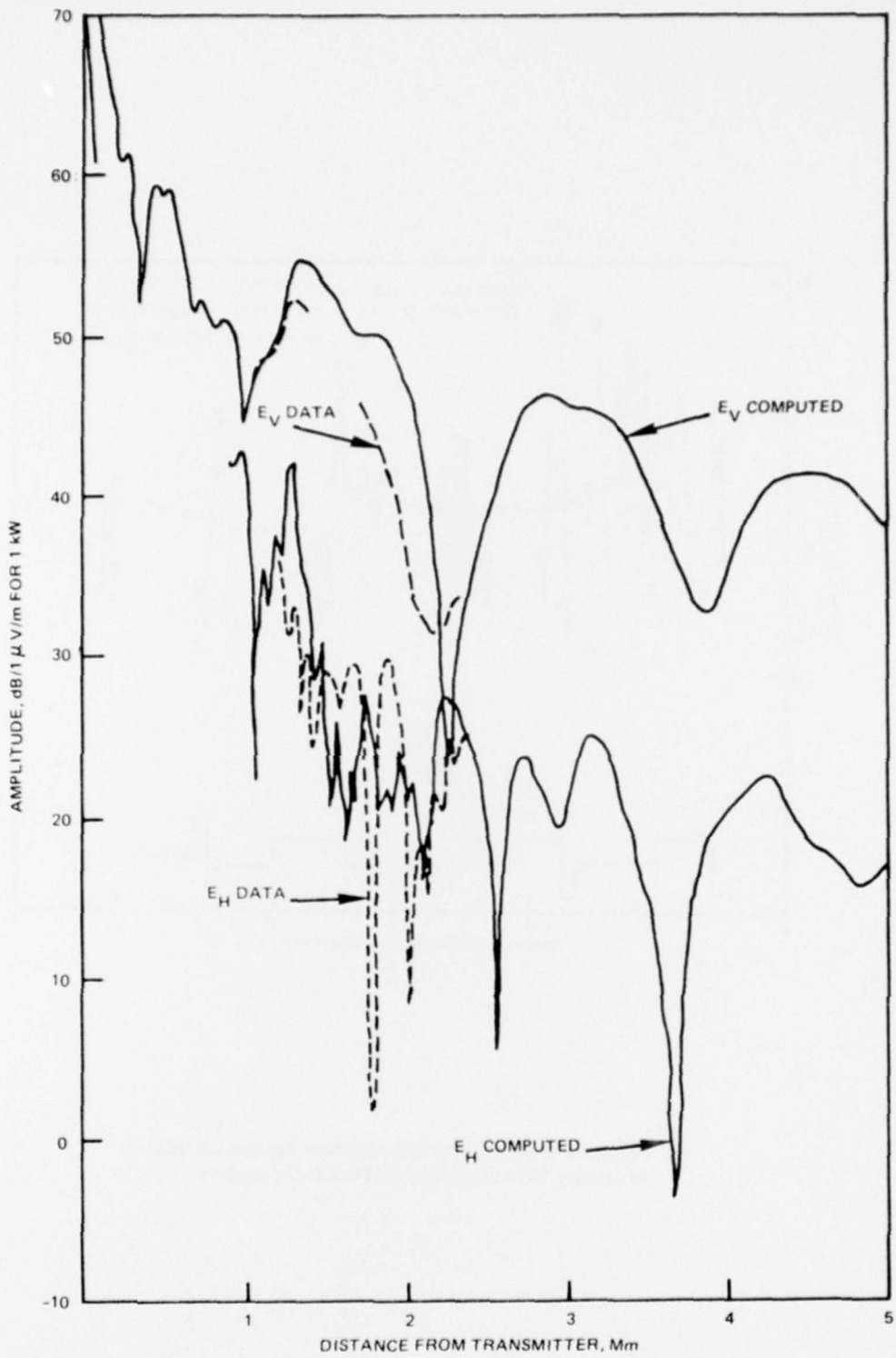


Figure 19. NAA 17.8 kHz nighttime  $E_V$  and  $E_H$  data recorded on 18-19 January aboard the RADC KC-135 airplane. The data are compared with IPP-computed fields.

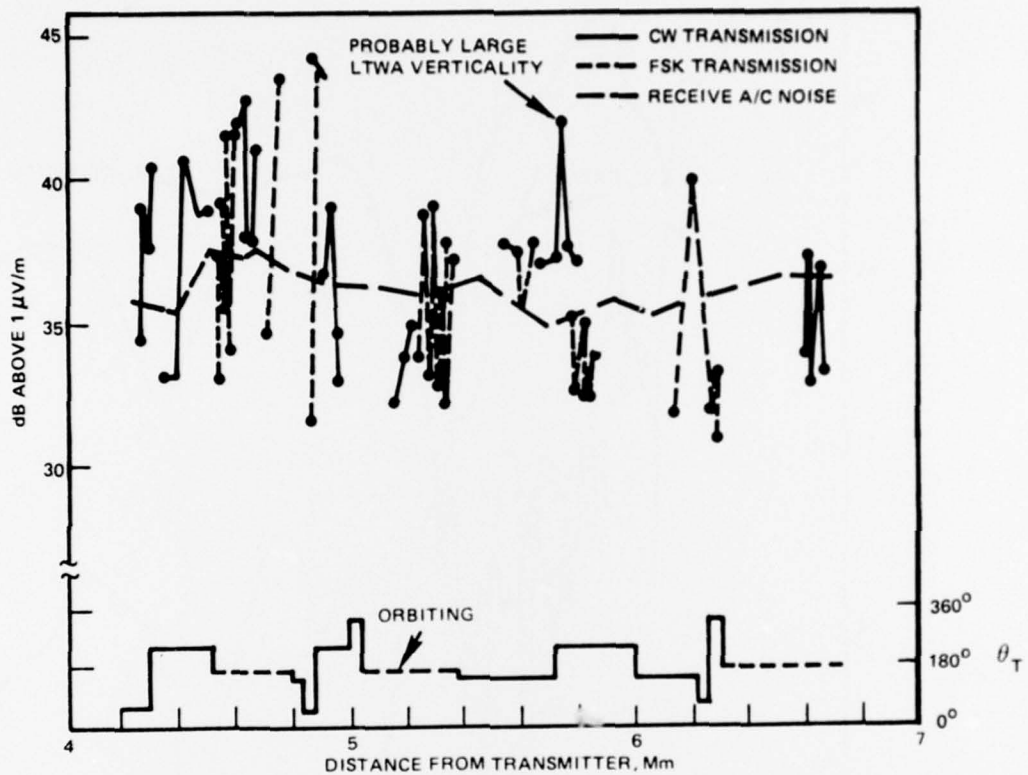


Figure 20. Tacamo, 27.0 kHz nighttime  $E_H$  data recorded on 30 January 1974 aboard the RADC KC-135 airplane.

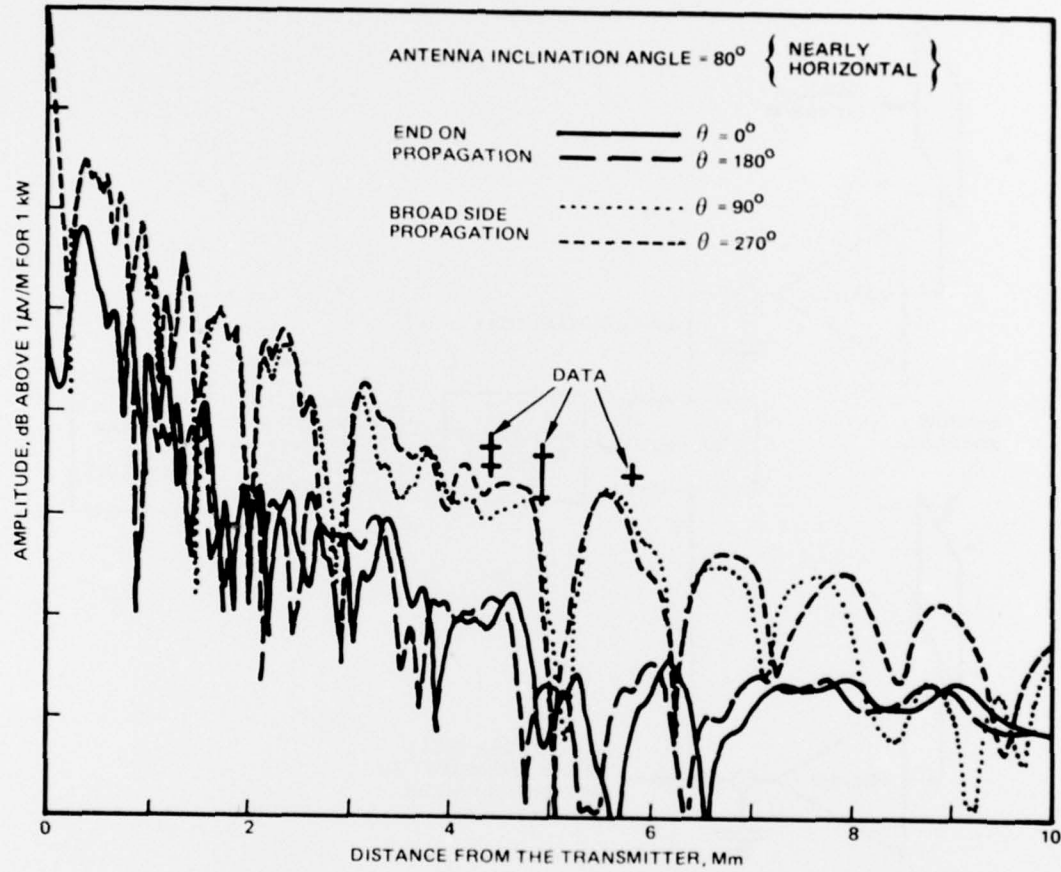


Figure 21. Tacamo, 27.0 kHz CW transmission  $E_H$  data recorded aboard the RADC airplane when Tacamo was flying straight and oriented for broadside radiation toward the receiver. The computed  $E_H$  fields are shown for comparison.

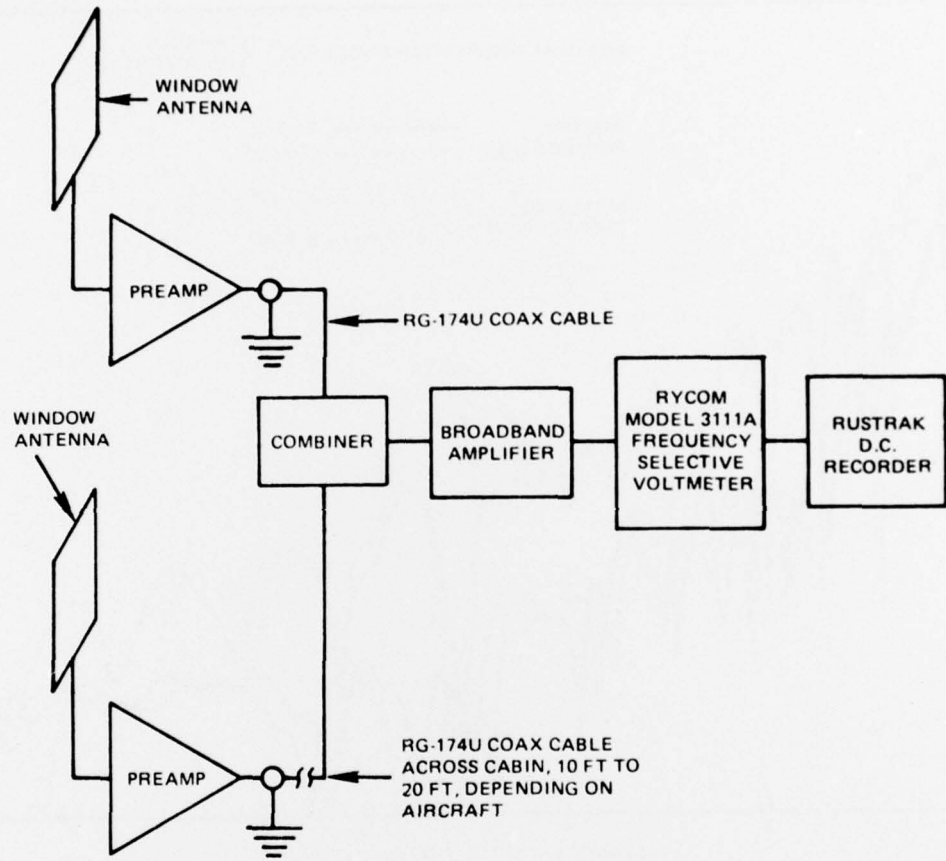


Figure 22. Block diagram of VLF/LF window antenna receiving system.

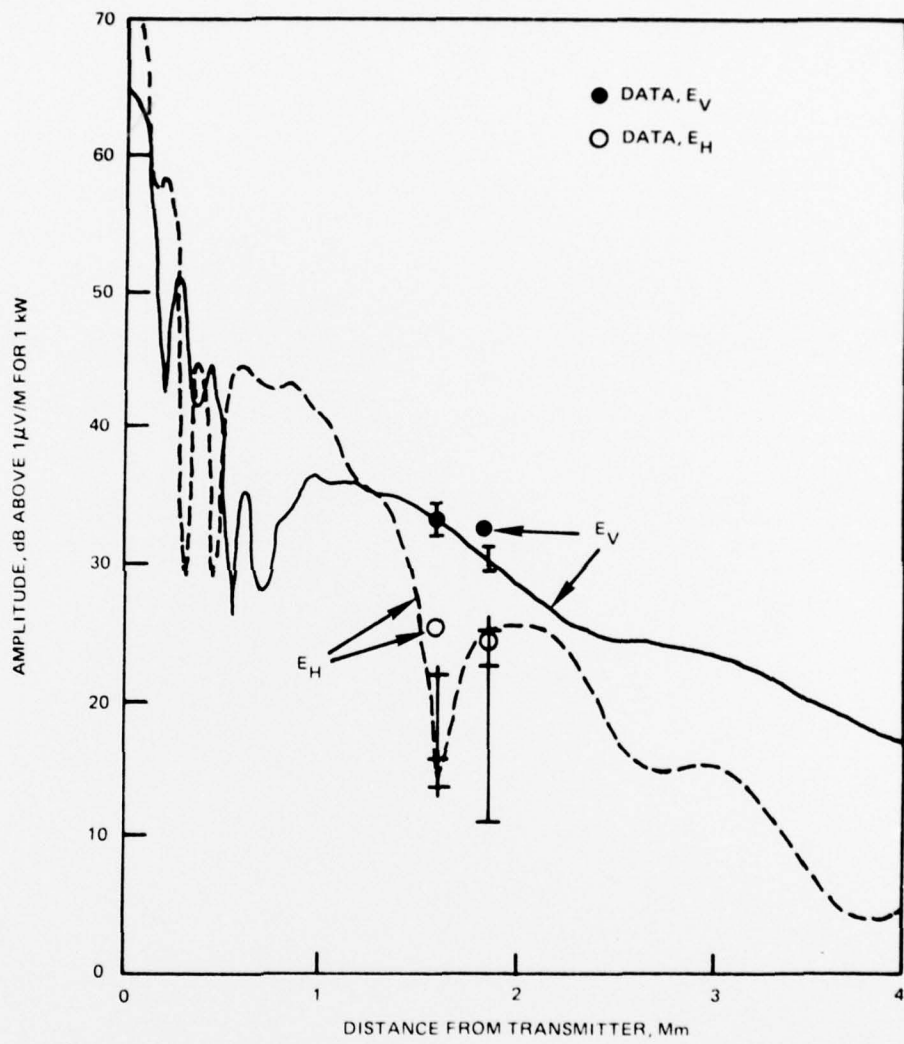


Figure 23. Comparison of measured 44 kHz ABNCP signal with predicted values. The predicted fields are for  $\theta = 90^\circ$  i.e., broadside radiation from ABNCP. Computed variability with ABNCP orientation is indicated by the bars at 1.6 Mm and 1.8 Mm where the  $E_V$  and  $E_H$  data were recorded.

DISTRIBUTION LIST  
NAVY

DIRECTOR, NAVAL TELECOMMUNICATIONS DIVISION DEPARTMENT OF THE NAVY, ATTN: NOP-941D OP 94 WASHINGTON, D. C. 20350	1
COMMANDER, NAVAL ELECTRONIC SYSTEMS COMMAND ATTN: PME-117 PME-117-22, 117-21 WASHINGTON, D.C.20360	3
COMMANDER, NAVAL TELECOMMUNICATIONS COMMAND ATTN: O3P 4401 MASSACHUSETTS AVE. N.W. WASHINGTON, D.C. 20390	1
CENTER FOR NAVAL ANALYSIS (ATTN: MR. CHARLES GARRETT) 1401 WILSON BLVD ARLINGTON, VA 22209	1
NAVAL RESEARCH LABORATORY WASHINGTON, D.C. 20390 ATTN: F. RHODES (CODE 5465) W. E. GARNER (CODE 5460)	2
NAVAL UNDERWATER SYS CENTER NEW LONDON LABORATORY NEW LONDON, CONNECTICUT 06320 ATTN: DR. D. A. MILLER PETER R. BANNISTER	2
OFFICE OF NAVAL RESEARCH ARLINGTON, VA 22217 ATTN: (CODES '402,418,420,421,427,464)	6
CHIEF OF NAVAL OPERATIONS ATTN: OP-94 PE WASHINGTON, D. C. 20350	1
CHIEF OF NAVAL OPERATIONS OP 941P NAVY DEPARTMENT WASHINGTON, D.C. 20350	1
NAVAL ELECTRONICS LABORATORY CENTER 271 CATALINA BOULEVARD SAN DIEGO, CALIFORNIA 92152 ATTN: Code 2230	30

AIR FORCE

SAC/DOKS  
OFFUTT AFB, NEB 68113

1

DIRECTOR OF COMMAND CONTROL AND COMMUNICATIONS 2  
HEADQUARTERS, U.S. AIR FORCE ATTN: PRCCW & PRCCS  
WASHINGTON, D.C. 20330

HEADQUARTERS, AIR FORCE SYSTEMS COMMAND 1  
ATTN: SDED  
ANDREWS AFB, MARYLAND 20331

COMMANDER, ELECTRONICS SYSTEMS DIVISION (AFSC) 5  
HANSOM AFB ATTN: YSEC, YSEV, XRT AND DCKS, DCKE.  
BEDFORD, MASS 01730

COMMANDER, ROME AIR DEVELOPMENT CENTER 1  
ATTN: DCCL  
GRIFFIS AFB, NEW YORK 13441

COMMANDER 1  
AIR FORCE WEAPONS LABORATORY  
ATTN: SAS J. KAMM  
KIRTLAND AFB, NM 87117

AIR FORCE CAMBRIDGE RESEARCH LABORATORIES 3  
ATTN: LIE (E. LEWIS), CRU (S. HOROWITZ), LAK (JOHN P. TURTLE)  
HANSOM AFB, BEDFORD, MASS, 01730

HEADQUARTERS AIR FORCE SUPPORT COMMUNICATION 1  
(STUDIES AND ANALYSIS) (ATTN: LT. COL. A. DAYTON, USAF)  
WASHINGTON, D.C. 20330

ARMY

DEPUTY CHIEF OF STAFF FOR OPERATIONS & PLANS 1  
DEPARTMENT OF THE ARMY, ATTN: DAMO-TCW  
WASHINGTON, D.C. 20310

U.S. ARMY ELECTRONICS COMMAND 1  
CODE AMSEC-TL-A  
ATTN: F. H. REDER  
FORT MONMOUTH, NEW JERSEY 07703

OTHER GOVERNMENT AGENCIES

OMEGA NAVIGATION SYSTEMS OPERATIONAL DETAIL  
HQ, U.S. COAST GUARD  
WASHINGTON, D.C. 20590  
ATTN: G-ONSOD/43

1

DIRECTOR,  
DEFENSE NUCLEAR AGENCY  
ATTN: RAAE, MR. D. EVELYN  
WASHINGTON, D.C. 20305

1

DIRECTOR  
DEFENSE NUCLEAR AGENCY  
ATTN: DDST, MR. W. BERNING  
WASHINGTON, D.C. 20305

1

DIRECTOR, ADVANCED REASEARCH  
PROJECTS AGENCY  
ATTN: F. A. KOETHER  
DR. P. TAMARKIN  
DR. D. MANN  
1400 WILSON BLVD, ARLINGTON VA 22209

3

DEFENSE DOCUMENTATION CTR  
CAMERON STATION  
ALEXANDRIA VA 22314

1

U.S. DEPARTMENT OF COMMERCE  
OFFICE OF TELECOMMUNICATIONS  
INSTITUTE FOR TELECOMMUNICATIONS SCIENCES  
BOULDER, COLORADO 80302  
ATTN: L. A. BERRY

1

U.S. DEPARTMENT OF COMMERCE  
NATIONAL OCEANOGRAPHIC AND ATMOSPHERIC  
ADMINISTRATION  
ATTN: J. R. WAIT  
BOULDER, COLORADO 80302

1

DCA

DCEC CODE R100	1
DCEC CODE R150	1
DCEC CODE R400	1
DCEC CODE C600	1
DCEC CODE 650	10

**DISTRIBUTION LIST**

**JOINT ACTIVITIES**

DIRECTOR FOR OPERATIONS (COMMAND & CONTROL) (J-3) JOINT STAFF: ATTN: J-32 WASHINGTON D.C. 20301	1
DIRECTOR FOR OPERATIONS (COMMAND & CONTROL) (J-3) JOINT STAFF, ATTN: EA DIVISION WASHINGTON D.C. 20301	1
DIRECTOR FOR OPERATIONS (COMMAND & CONTROL) (J-3) JOINT STAFF ATTN: WWMCCS PLANS DIVISION WASHINGTON, D.C. 20301	1
DIRECTOR FOR COMMUNICATIONS-ELECTRONICS (J-6) JOINT STAFF, ATTN: OPD-1 WASHINGTON, D.C. 20301	1
DIRECTOR FOR COMMUNICATIONS-ELECTRONICS (J-6) JOINT STAFF, ATTN: PLD-1 WASHINGTON, D.C. 20301	1
CHIEF, STUDIES, ANALYSIS AND GAMING AGENCY ROOM 1D936, THE PENTAGON WASHINGTON, D.C. 20301	1

OTHER: NON GOVERNMENT

MITRE CORPORATION  
WESTGATE RESEARCH PARK  
1820 DOLLEY MADISON BLVD.  
MCLEAN, VA 22101  
ATTN: MR. ALAN SCHNEIDER  
MR. R. W. CHITTENDEN  
MR. H. FRANKEL  
MR. R. PESCI

4

MITRE CORPORATION  
ATTN: SUSAN MORIN  
RT. 62 & MIDDLESEX TURNPIKE  
BEDFORD, MA 01731

1

GENERAL ELECTRIC COMPANY  
TEMPO-CENTER FOR ADVANCED STUDY  
ATTN: MR. WARREN S. KNAPP  
MR. B. GAMBILL  
816 STATE STREET  
SANTA BARBARA, CA 93102

1

UNIVERSITY OF CALIFORNIA  
ATTN: DR. HENRY G. BOOKER  
P. O. BOX 109  
LA JOLLA, CA 92038

1

PENNSYLVANIA STATE UNIVERSITY  
ATTN: IONOSPHERIC RESEARCH LAB.  
UNIVERSITY PARK, PA 16802

1

UNIVERSITY OF ILLINOIS  
ATTN: AERONOMY LABORATORY  
DEPT. OF ELECTRONICS ENGINEERING  
URBANA CAMPUS  
URBANA, ILLINOIS 61801

1

GENERAL ELECTRIC COMPANY  
DASIA  
816 STATE STREET  
SANTA BARBARA CA 93102

1

OTHER: NON-GOVERNMENT, CON'T

JOHNS HOPKINS UNIVERSITY  
APPLIED PHYSICS LABORATORY  
8621 GEORGIA AVENUE  
SILVER SPRING MD 20910  
ATTN: J. NEWLAND  
P. T. KOMISKE

1

MASSACHUSETTS INSTITUTE  
OF TECHNOLOGY  
LINCOLN LABORATORY  
244 WOOD STREET  
LEXINGTON, MA 02173  
ATTN: R. ENTICKNAPP

1

INSTITUTE FOR DEFENSE  
ANALYSIS  
400 ARMY-NAVY DRIVE  
ARLINGTON, VA 22202  
ATTN: DR. JOEL BENGSTON

1

TRW: MECN STUDY GP  
ONE SPACE PARK  
REDONDO BEACH, CA 90278  
ATTN: MR. DAVID D. MCNELIS

1